Nano Research
2023, 16(4): 4821–4854
ISSN 1998-0124 CN 11-5974/O4
https://doi.org/10.1007/s12274-021-3820-2

Review Article

Recent advances in flexible batteries: From materials to applications

Fuwei Xiang[1,2], Fang Cheng[1,2], Yongjiang Sun[1,2], Xiaoping Yang[1,2], Wen Lu[1,2] (✉), Rose Amal[3], and Liming Dai[3] (✉)

[1] College of Chemical Science and Engineering, Yunnan University, Kunming 650091, China
[2] Institute of Energy Storage Technologies, Yunnan University, Kunming 650091, China
[3] Australian Carbon Materials Centre (A-CMC), School of Chemical Engineering, University of New South Wales, Sydney, NSW 2052, Australia

Received: 4 May 2021 / **Revised:** 29 July 2021 / **Accepted:** 16 August 2021

ABSTRACT

Along with the rapid development of flexible and wearable electronic devices, there have been a strong demand for flexible power sources, which has in turn triggered considerable efforts on the research and development of flexible batteries. An ideal flexible battery would have not only just high electrochemical performance but also excellent mechanical deformabilities. Therefore, battery constituent components, chemistry systems, device configurations, and practical applications are all pivotal aspects that should be thoroughly considered. Herein, we systematically and comprehensively review the fundamentals and recent progresses of flexible batteries in terms of these important aspects. Specifically, we first discuss the requirements for constituent components, including the current collector, electrolyte, and separator, in flexible batteries. We then elucidate battery chemistry systems that have been studied for various flexible batteries, including lithium-ion batteries, non-lithium-ion batteries, and high-energy metal batteries. This is followed by discussions on the device configurations for flexible batteries, including one-dimensional fiber-shaped, two-dimensional film-shaped, and three-dimensional structural batteries. Finally, we summarize recent efforts in exploring practical applications for flexible batteries. Current challenges and future opportunities for the research and development of flexible batteries are also discussed.

KEYWORDS

flexible batteries, flexible power sources, wearable electronics, electrochemistries, battery applications

1 Instruction

Flexible and wearable electronic devices, such as roll-up displays, touch screens, smart watches, smart cards, wearable sensors, and knitted wristbands, have been deeply penetrating into our daily lives and will continuously change our lifestyles [1–4]. The rapid development of these emerging electronic devices has triggered a strong demand for the flexible power sources, which has in turn facilitated the research and development of flexible batteries [5, 6]. As for conventional batteries, flexible batteries require a high energy, high power, good safety, and long cycle life [7, 8]. Besides, flexible batteries should also possess excellent deformabilities, including bendability, foldability, stretchability, compressibility, and twistability, to accommodate possible mechanical deformations [9, 10]. For practical applications, therefore, careful considerations need to be taken for all four pivotal aspects of a flexible battery, including battery constituent components, battery chemistry systems, battery device configurations, and property–performance optimization for specific applications.

Of particular importance, flexible batteries must possess a high flexibility and deformability for all the four essential constituent components, namely the cathode, anode, electrolyte, and separator, to ensure their stable power supply even under mechanical deformations [11]. Although lithium-ion batteries (LIBs) with a high nominal operating voltage, high energy/power density, and long cycle life have been dominantly used in flexible and wearable electronics [12–14], other battery chemistry systems, including those with a relatively low cost and wide availability (e.g., sodium-ion batteries (SIBs) and potassium-ion batteries (PIBs) [15, 16]) and those with a relatively high energy density (e.g., lithium-metal batteries (LMBs) [17–22], lithium-sulfur batteries (LSBs) [23–25], and metal-air batteries (MABs) [26, 27]) have been actively researched to expand the landscape of flexible batteries in recent years. Furthermore, flexible batteries have been realized in different device configurations, including one-dimensional (1D) fiber-shaped [28], two-dimensional (2D) film-shaped [29], and three-dimensional (3D) structures [30]. Although flexible batteries are still in their early stage of development with many unsolved commercialization issues, extensive efforts have already been made to explore their practical applications.

During the past decade, considerable research and development efforts with numerous related publications have focused on each of the aforementioned aspects of flexible batteries [31]. Nevertheless, since all the control factors of a battery interacting and even restricting each other to jointly influence and determine the overall property and performance of flexible batteries [31], it is highly desirable to take all of them into careful consideration simultaneously. The present article aims to provide a systematic and comprehensive review on the fundamentals and recent

Address correspondence to Wen Lu, wenlu@ynu.edu.cn; Liming Dai, l.dai@unsw.edu.au

progresses of flexible batteries from materials to applications. As schematically shown in Fig. 1, our review covers all aspects of flexible batteries, ranging from battery constituent components/materials, including electrode materials, current collectors, electrolytes, and separators, through battery chemistry systems, including LIBs, non-lithium-ion batteries, and high-energy metal batteries, to battery device configurations, including 1D, 2D, and 3D batteries. Practical applications, along with current challenges and future perspectives for the research and development of flexible batteries, are also discussed.

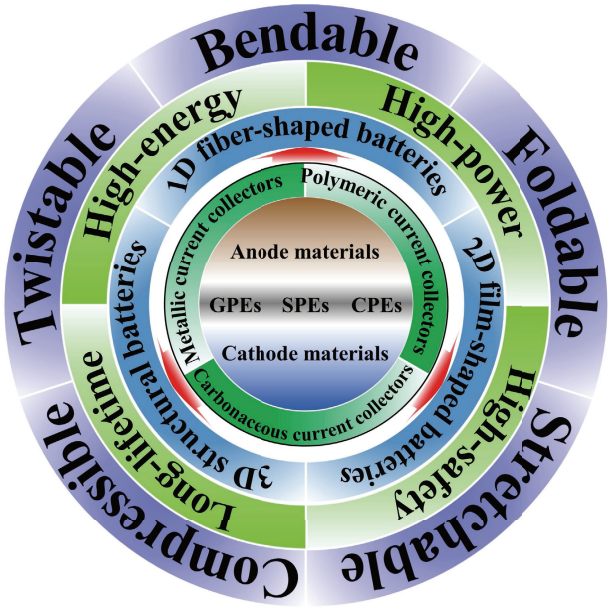

Figure 1 Schematic outline of major contents discussed in the present review.

2 Battery constituent components

Like conventional batteries, a flexible battery is also composed of four essential constituent components, i.e., a cathode, an anode, an electrolyte, and a separator. However, the rigid and fragile nature of these components for conventional batteries would cause failure and even safety issues under mechanical deformations [11], making them unsuitable for flexible batteries. Thus, fabricating flexible constituent components is of great importance to ensure the deformable properties for flexible batteries. This requires the development of flexible electrodes (cathode and anode), flexible electrolytes and separators, as reviewed in detail below.

2.1 Current collectors

Serving as both the substrate to support electrode materials and the electrical conductor to connect the electrodes with the external circuit, current collectors play an important role in the fabrication of flexible electrodes. An ideal current collector for flexible electrodes should have a high flexibility, high electrical conductivity, low weight, and strong surface adhesion with electrode materials. So far, metals, polymers and carbonaceous materials have been studied as current collectors for flexible batteries [32].

2.1.1 Metallic current collectors

Largely due to their high electrical conductivity, metal foils have been employed as current collectors for fabricating electrodes in conventional batteries for a long time. It is then the most straightforward approach to use these metallic current collectors to fabricate electrodes for flexible batteries. Indeed, a variety of metals, such as Al [33], Cu [28, 34, 35], Ti [36], stainless steel [37], and Li [38], have been adopted to construct flexible electrodes. Under deformation stresses, however, electrodes thus fabricated are the most vulnerable part among the major battery components due to the rigidity and fragility of these metallic current collectors, leading to possible delamination of electrode materials from the current collectors.

To address this issue, roughing the surfaces of metallic current collectors to create more contact points and surface areas to enhance their adhesion with active material layers has been demonstrated to be a good strategy. Towards this purpose, many technologies have been developed, including sandpaper grinding [39], chemical etching [40], and special morphology designing [40, 41]. For instance, Jeon et al. [35] compared the performance of a silicon anode coated on a highly roughed copper current collector (roughness = 3 mm) (Fig. 2(a)) versus that on a flat one (roughness = 1 mm). The roughed Cu current collector showed a higher interface adhesion strength (135.7 $N \cdot m^{-1}$) than that of the flat one (89.7 $N \cdot m^{-1}$). As a result, when tested in a half cell using a Li foil counter electrode and an electrolyte of 1.15 M $LiPF_6$ in ethylene carbonate (EC)/ethyl methyl carbonate (EMC) (3/7 by vol.) containing 5 wt.% fluoroethylene carbonate (FEC), the electrode with the roughed Cu current collector exhibited a high discharge capacity of 1,500 $mAh \cdot g^{-1}$ after 200 cycles in comparison with that of 900 $mAh \cdot g^{-1}$ for its flat counterpart. At a bending radius of 6.5 mm, a pouch-type battery fabricated from the roughed Cu current collector and a Li foil counter electrode showed a better cycling performance (a discharge capacity of 1,400 $mAh \cdot g^{-1}$ after 50 cycles) than that from the flat one (about 700 $mAh \cdot g^{-1}$). These results indicate the effectiveness of surface roughing in providing a facile, but efficient, way to fabricate flexible batteries based on a roughed metal current collector. Nevertheless, the mismatch in volume change between the active material layer and metal current collector during charge/discharge processes can exacerbate the delamination of active layer materials from the metal substrate, especially under repeated battery deformations. In addition, the heavy weight with a reduced gravimetric performance as well as rigidity and fragility for the metal substrates could inevitably restrict their practical applications in flexible batteries [32]. As a result, recent research has extended to the development of other substrate materials that are flexible and lightweight of an improved adhesion with electrode materials. In this context, polymeric and carbonaceous materials have been investigated towards this goal.

2.1.2 Polymeric current collectors

The inherent flexibility and lightweight of polymers make them attractive as current collector materials for flexible batteries [32, 42]. Indeed, both insulating and conducting polymers have been investigated as current collectors for flexible batteries.

A large number of insulating polymers, such as poly(ethylene naphthalate) (PEN), poly(ethylene terephthalate) (PET), polyimide (PI), polypropylene (PP), and poly(ether sulfone) (PES), can accommodate deformations without obvious fractures. However, their low electrical conductivity limits the direct use of them as current collectors. To overcome this limitation, insulating polymers have been metallized as current collectors [43, 44]. Of particular interest, Yun et al. used a radio-frequency magnetron sputtering method to coat Cu on polymers (PEN, PET, PI, and PES) to produce flexible polymer current collectors [43]. With the coating of a thin Cu layer, the as-prepared metallized polymer current collectors showed a surface resistance down to the level of 1 $\Omega \cdot sq^{-1}$. Similarly, Choi et al. coated Cu on a porous PI membrane to fabricate current collectors for flexible LIBs [44]. Specifically, the current collector was prepared by sputter coating a

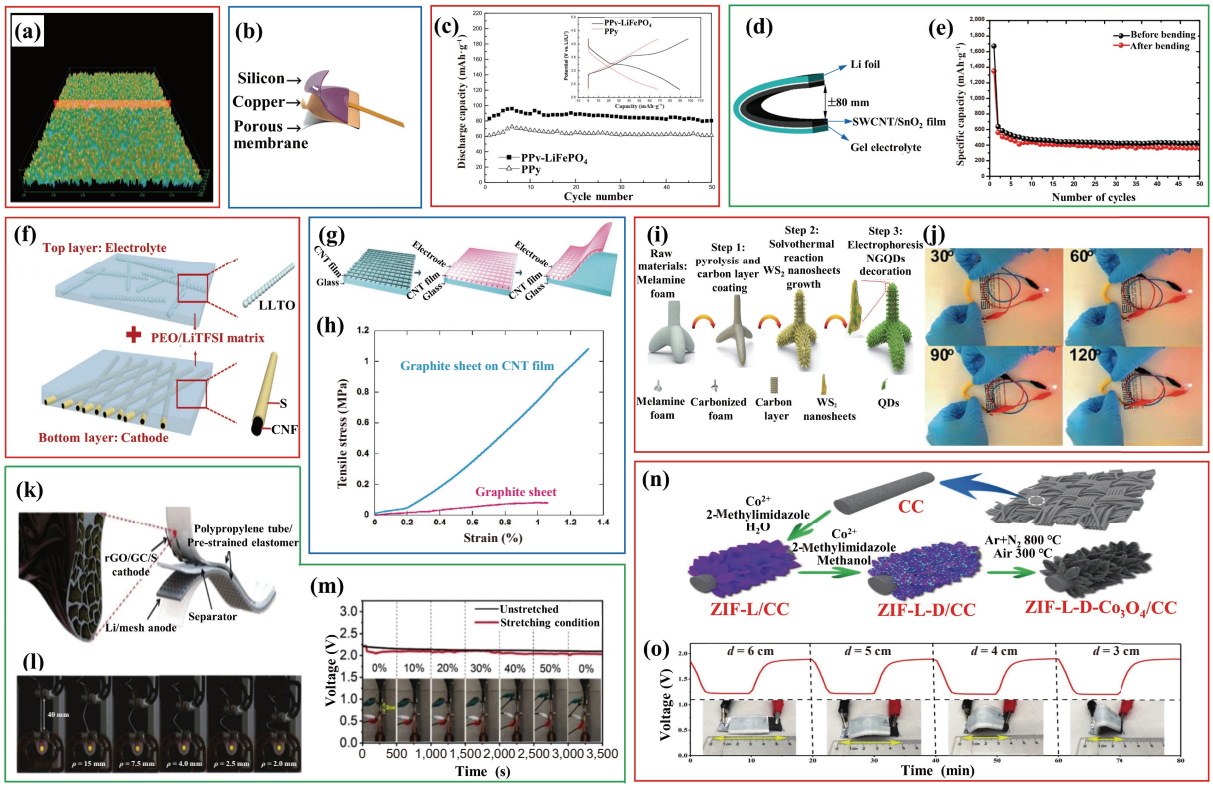

Figure 2 (a) Surface morphology of a rough Cu current collector (reproduced with permission from Ref. [35], © The Royal Society of Chemistry 2017). (b) Illustration of a multilayered silicon electrode (reproduced with permission from Ref. [44], © Wiley-VCH Verlag GmbH & Co. KGaA, Weinheim 2013). (c) Cycle performances of PPy and PPy-LiFePO$_4$ films, inset shows the discharge/charge curves of the 10th cycle (reproduced with permission from Ref. [45], © Elsevier B.V. 2008). (d) Schematic of a Li//SWCNT/SnO$_2$ cell bent inwards at 180° and (e) cycling stability of the cell before and after inward bending (reproduced with permission from Ref. [65], © Elsevier Ltd. 2011). (f) Schematic illustration of a CNF/S-PEO/LLTO bilayer structure design (reproduced with permission from Ref. [66], © Elsevier B.V. 2018). (g) Schematic illustration of the fabrication of a flexible electrode on a CNT film current collector and (h) tensile stress–strain curves of graphite sheets with and without a CNT film current collector (reproduced with permission from Ref. [67], © Wiley-VCH Verlag GmbH & Co. KGaA, Weinheim 2013). (i) Schematic of the synthesis process of a NGQDs-WS$_2$/3DCF nanoarchitecture and (j) photographs of a red LED powered by a cable-shaped SIB at various bending angles (reproduced with permission from Ref. [68], © The Royal Society of Chemistry 2018). (k) Schematic of a LSB assembled from a flexible rGO/GC/S cathode and (l) a LED powered by the LSB under different bending conditions, and (m) discharge behaviors of the LSB upon continuous loading to a 50% tensile strain and unloading (reproduced with permission from Ref. [69], © The Royal Society of Chemistry 2018). (n) Schematic illustration of the formation process of a ZIF-L-D-Co$_3$O$_4$/CC and (o) discharge–charge voltage profiles of an all-solid-state Zn-air battery fabricated from the ZIF-L-D-Co$_3$O$_4$/CC under flat and different bending conditions (reproduced with permission from Ref. [70], © Wiley-VCH Verlag GmbH & Co. KGaA, Weinheim 2019).

thin Cu layer (<1 μm) onto an O_2 plasma treated PI membrane, followed by sputtering silicon nanofibrils on the Cu layer of the as-prepared current collector, resulting in the formation of a multilayered silicon electrode (Fig. 2(b)). A pouch cell incorporating this silicon electrode as anode with a Li foil cathode and a $LiFP_6$-EC/diethyl carbonate (DEC) electrolyte delivered a high capacity over 2,000 mAh·g^{-1} during 30 charge –discharge cycles at 0.5 C. Furthermore, at a small bending radius of 1.9 cm, the resultant pouch cell showed a high Coulombic efficiency of 97% after 80 cycles, demonstrating the feasibility of insulating polymers as current collectors for flexible batteries. Nevertheless, this application may be hindered by the additional cost associated with the metallizing process on insulating polymers.

Unlike insulting polymers, conducting polymers such as polyaniline (PANi), polypyrrole (PPy), and polythiophene (PTh) are inherently conductive, and thus can be used directly as current collectors without the need of a metal coating [32]. Furthermore, conducting polymers are electroactive and can act as freestanding electrodes even without the loading of other active materials. In this regard, conducting polymers have been studied either directly as electrodes or as current collectors to load other active materials for flexible batteries. Wang et al. demonstrated this concept by electrochemically preparing highly flexible and freestanding PPy and PPy-$LiFePO_4$ (LFP) composite film electrodes [45]. When tested with a Li metal counter electrode and a $LiPF_6$-EC/DEC electrolyte, both PPy and PPy-LFP film electrodes showed well-defined electrochemical characteristics (Fig. 2(c)). The observed higher capacity of the PPy-LFP composite electrode than that of the PPy electrode (80 vs. 60 mAh·g^{-1}) is attributable to the higher-capacity of the constituent LFP in the composite.

Owing to their excellent flexibility, low cost, and lightweight, polymers have shown distinct advantages for flexible batteries. However, their practical applications are still precluded by the chemical instability and relatively low electrical conductivity of polymers [46]. In this sense, carbonaceous materials appear to play a more important role as current collectors.

2.1.3 *Carbonaceous current collectors*

Carbonaceous materials, such as carbon nanotubes (CNTs) [47– 53], carbon fibers (CFs) [54– 56], carbon papers (CPs) [57– 59], carbon foams [60], carbon clothes (CCs) [61], and graphene materials [62– 64], have been studied as novel current collector materials for flexible batteries due to their high electrical conductivity, flexibility, chemical stability, and mechanical strength. For the electrode preparation, various active materials can be loaded into the carbonaceous substrates through a range of technologies, including vacuum-filtration [65], solution-casting [66], slurry-coating [67], solvothermal method [68], melt-diffusion [69], and MOF-on-MOF (metal organic framework) [70], as discussed below.

Vacuum-filtration has been widely used to prepare composite

paper electrodes due to its facile process and low cost. Noerochim et al. fabricated a freestanding single-walled carbon nanotube/SnO_2 (SWCNT/SnO_2) paper electrode by vacuum filtration for flexible LIBs [65]. Specifically, the SWCNT/SnO_2 hybrid material was prepared from a mixture of SnCl and SWCNTs in diethylene glycol under refluxing, followed by vacuum-filtering the as-synthesized material to obtain the designed paper electrode. A solid-state battery assembled with the SWCNT/SnO_2 paper as anode, a Li foil cathode, and a 1 M $LiPF_6$ containing poly(vinylidene fluoride-co-hexafluorpropylene) (P(VdF-HFP)) gel electrolyte showed an excellent bendability with a bending angle up to 180° (Fig. 2(d)). Importantly, bending did not significantly affect the electrochemical performance of this flexible battery (Fig. 2(e)), demonstrating a good deformability of the carbon-based composite paper electrodes prepared by vacuum filtration.

Solution-casting active materials on pre-prepared carbon substrates has also been studied for fabricating flexible electrodes and batteries. In particular, Zhu et al. reported an all-solid-state flexible LSB with a bilayer electrode [66], which, as shown in Fig. 2(f), was prepared by carbonizing electrospun polyacrylonitrile (PAN) fibers drop-cast with a sulfur/carbon disulfide solution, followed by drop-casting an acetonitrile solution containing bis(trifluoromethane)sulfonimide lithium (LiTFSI), poly(ethylene oxide) (PEO), and 1D ceramic $Li_{0.33}La_{0.557}TiO_3$ (LLTO) nanofiber onto the pre-prepared bilayer substrate. The resultant composite electrode possessed a Young's modulus of 2.0 MPa with a tensile strength of 0.12 MPa and could be easily bent. An all-solid-state flexible LSB incorporating this electrolyte-conatined bilayer electrode as cathode with a Li foil anode displayed a stable cycling performance with a capacity retaining at 415 mAh·g^{-1} and a Coulombic efficiency remaining at 99% after 50 cycles at 0.05 C, showing a good feasibility for fabricating flexible electrodes by solution-casting electrolyte (active) materials on pre-prepared carbon substrates.

Similarly, slurry-coating that is commonly used in LIB industry has been a maneuverable process to prepare flexible electrodes on carbon substrates. With this approach, Wang et al. developed a LIB by simply coating graphite and $LiCoO_2$ (LCO) slurries on CNT films as anode and cathode, respectively [67]. The CNT films were synthesized via a chemical vapor deposition (CVD) method on a wafer, followed by peeling off the resultant composite electrodes from the wafer (Fig. 2(g)). The contact angle of the graphite slurry (graphite, carbon black (CB) and poly(vinylidene fluoride) (PVDF) in N-methyl-2-pyrrolidinone (NMP)) on the CNT film was found to be 19°, much lower than that on a Cu film (48°), confirming the better wetting property of the CNT film than the conventional Cu current collector. As a result, the as-synthesized graphite-CNT film electrode showed a much higher shear strength than the graphite-Cu film electrode (0.12 vs. 0.04 Mpa). As can also be seen in Fig. 2(h), the graphite-CNT film exhibited a Young's modulus of 117 MPa and a tensile strength of 1.08 MPa, much higher than those of a freestanding graphite sheet alone (11 and 0.08 MPa, respectively). When tested in a full battery consisting of the LCO-CNT film cathode, a $LiPF_6$-EC/DEC electrolyte, and a Celgard 2400 separator, the graphite-CNT film and graphite-Cu film anodes delivered their capacities of 335 and 318 mAh·g^{-1} at 0.1 C after 50 cycles, respectively. These results demonstrated the advantages of CNT films for producing superior flexible electrodes over conventional current collectors. Furthermore, the facile slurry process could ensure mass production of flexible electrodes from carbon substrates.

Flexible electrodes have also been prepared by solvothermal method to directly grow active materials onto carbon substrates. Wang et al. used this method to prepare 3D carbon foam-supported WS_2 nanosheets (WS_2/3DCF) as anode for cable-shaped flexible SIBs [68]. As shown in Fig. 2(i), WS_2/3DCF was obtained by a solvothermal reaction between 3DCF and $(NH_4)_2WS_4$, followed by decorating the as-synthesized WS_2/3DCF with nitrogen-doped graphene quantum dots (NGQDs) using electrophoresis. Owing to the 3D porous structure and the NGQDs decoration, the resultant NGQDs-WS_2/3DCF electrode exhibited a high rate capability with a capacity of 268.4 mAh·g^{-1} at 2,000 mA·g^{-1}, and a long lifetime with an extraordinary capacity retention of 97.1% over 1,000 cycles. Furthermore, the NGQDs-WS_2/3DCF anode was coupled with a $Na_{0.44}MnO_2$ (NMO) coated nickel foam (NF) cathode, a glass fiber separator, and a $NaPF_6$-EC/DEC electrolyte to assemble a cable-shaped SIB. Remarkably, the full battery thus fabricated was highly flexible and exhibited stable electrochemical characteristics at various bending angles from 30° to 120°, as shown in Fig. 2(j). These results indicated a new route to enhance the performance of flexible batteries via 3D structure design of carbon-based electrodes.

Melt-diffusion has been demonstrated to be useful for preparing sulfur electrodes for flexible LSBs. Chong et al. used this approach to prepare a flexible cathode consisting of reduced graphene oxide (rGO), graphene crumple and sulfur (rGO/GC/S) for flexible LSBs [69]. Specifically, flower-like graphene oxide crumples (GOCs) were prepared from a graphite oxide solution through a low temperature process, followed by reducing the as-obtained GOCs with hydrazine vapor and then graphitizing at 3,000 °C to produce GCs. GC/S composite was then prepared by heating a mixture of GCs, sulfur powders and carbon disulfide at 155 °C for 12 h. Spinning a mixture containing GC/S and graphite oxide (GO) resulted in a continuous flat GO/GC/S ribbon, which was then reduced using hydrogen iodide vapor to obtain the flexible rGO/GC/S cathode. The cathode thus prepared was incorporated with a Li mesh anode, a polyethylene (PE) film separator, and an electrolyte of 1 M LiTFSI in 1,2-dimethoxyethane (DME)/1,3-dioxolane (DOL) (1:1 by vol.) with 1 wt.% $LiNO_3$ to assemble a flexible LSB (Fig. 2(k)). The rGO/GC/S cathode delivered a capacity of 524 mAh·g^{-1} after 100 cycles at 0.2 C. Significantly, the full battery was mechanically robust and demonstrated stable electrochemical performance against bending (to a minimum bending radius of about 2.0 mm) (Fig. 2(l)) and stretching (to a strain up to 50%) (Fig. 2(m)). This result showed the effectiveness of the melt-diffusion method for preparing flexible electrodes (especially sulfur-based) for flexible batteries.

Apart from the traditional methods, Zhong et al. reported a novel MOF-on-MOF strategy to develop an oxygen catalyst comprising hierarchical Co_3O_4 nanoparticles on CC for flexible Zn-air batteries [70]. As shown in Fig. 2(n), 2D leaf-like microarrays (denoted as ZIF-L) were firstly grown on CC from $Co(NO_3)_2$ and 2-methylimidazole ($C_4H_6N_2$), followed by a further reaction on the as-synthesized ZIF-L/CC to produce ZIF-L-D/CC. Using a facile carbonization-oxidation process, the resultant ZIF-L-D/CC could be converted into hierarchical Co_3O_4 nanoparticles anchored in nitrogen-doped carbon nano-micro arrays on CC (i.e., ZIF-L-D-Co_3O_4/CC). In conjunction with a Zn foil anode and an alkaline poly(vinyl alcohol) (PVA) gel electrolyte, the as-fabricated ZIF-L-D-Co_3O_4/CC cathode was used to assemble an all-solid-state Zn-air battery, which exhibited a high open circuit potential of 1.461 V, capacity of 815 mAh·g_{Zn}^{-1} at 1 mA·cm^{-2}, and energy density of 1,010 Wh·kg_{Zn}^{-1}. Furthermore, this battery showed an excellent stability even upon charge/discharge under serious bending conditions (Fig. 2(o)), demonstrating its outstanding mechanical deformability. This work presented a new approach by using MOF strategy to load active materials on carbon substrates for fabricating flexible electrodes.

As can be seen from the above discussions, metallic, polymeric,

Table 1 Properties of metallic, polymeric, and carbonaceous current collectors

Current collector	Advantages	Disadvantages	Refs.
Metallic	• High electrical conductivity • Good adoptability to current manufacturing processes	• Heavy weight • Low flexibility • Mismatch in volume change with electrode materials • Poor adhesion with electrode materials	[32, 35, 39–41]
Polymeric	• Light weight • High flexibility • Low cost	• Chemical instability • Low electrical conductivity	[42–46]
Carbonaceous	• Light weight • High electrical conductivity • High flexibility • High chemical stability • High mechanical strength	• Complex preparation processes • High cost	[65–70]

and carbonaceous materials have been studied as current collectors for flexible batteries. Table 1 summarizes the major advantages and disadvantages of these materials along with some representative examples discussed in this section. Although different current collector materials possess varied pros and cons, referring to the requirements for an ideal current collector, carbonaceous materials have attracted considerable attention and will continue to play a more and more important role as novel current collector materials for flexible batteries. This has been attributed to the unique properties of carbonaceous materials, including light weight as well as high electrical conductivity, flexibility, chemical stability, and mechanical strength.

2.2 Electrolytes and separators

Much like current collectors, electrolytes and separators are also indispensable components for batteries that greatly influence the performances of batteries. Electrolytes provide ions and electrochemically stable potential windows necessary for charge/discharge of batteries, while separators allow ion transport but prevent electrons from moving through between the anode and cathode [71]. Flexible batteries share the same fundamental property requirements with conventional batteries for electrolytes (high ionic conductivity, high electrochemical stability, and high safety) and separators (high mechanical strength, high thermal stability, high electrical resistivity, and high ionic permeability). Due to their operation under repeated deformations, however, flexible batteries are subjected to a high risk of short circuit, leakage, and even explosion, and hence superior flexibility and deformation stability are required.

Determined by the difference of electrolytes and separators employed, currently researched flexible batteries can be classified into two types: One is based on liquid electrolytes (along with separators), the other on solid state electrolytes (without separators). Liquid electrolytes can be aqueous and non-aqueous, and the latter further include organic aprotic electrolytes and ionic liquid electrolytes [72–74]. Traditional liquid electrolytes, such as $LiFP_6$, $NaClO_4$, and LiTFSI in organic solvents, can be directly used for flexible batteries without any modifications [41, 75, 76]. However, separators are required for liquid electrolytes. Conventional separators, including PP, PE, PVDF, polymethyl methacrylate (PMMA), and PAN as well as their composites, have been employed for flexible batteries [77, 78]. New separators with improved mechanical strength, such as cellulose separators [18, 79–81], ceramic separators [82–84], and ceramic-enhanced PP/PE [13] that have been developed for conventional batteries, have also been used in flexible batteries.

For flexible batteries, the operation under repeated deformations could cause potential evaporation and leakage of the liquid electrolyte. Thus, the development of all-solid-state flexible batteries based on solid state electrolytes has been becoming an attractive and important option. Solid state electrolytes function as not only electrolytes but also separators so that no additional conventional separators are needed, also making the integrations of flexible battery more efficient. Besides, solid state electrolytes possess the potential advantages of nontoxicity, non-flammability, and no leakage, especially suitable for flexible batteries compared to their liquid counterparts [85–89]. Solid state electrolytes currently studied for flexible batteries include gel polymer electrolytes (GPEs), solid polymer electrolytes (SPEs), and composite polymer electrolytes (CPEs), which are discussed in detail below.

2.2.1 *GPEs*

GPEs are composed of liquid electrolytes and polymer matrices, where the polymer matrices serve as supports to provide mechanical strength for electrolytes. By incorporating different electrolytes into polymers matrices, the resultant GPEs can be designed for specific batteries.

Li et al. prepared a quasi-solid GPE to fabricate a flexible battery for storing the energy generated by a triboelectric nanogenerator (TENG) [90]. Specifically, PEO and succinonitrile were dissolved in methylene chloride, followed by the addition of $LiClO_4$, acetone, and then an NMP solution of P(VDF-HFP) to produce a GPE in dry air, which showed a high Li^+ conductivity of 5.67×10^{-4} S·cm^{-1}. For proof of concept, the as-synthesized GPE was used to assemble a flexible pouch cell with a LFP-loaded CC cathode and a Li foil anode to store the pulse form energy harvested by a TENG, providing a stable power output sustainably. The resultant battery showed a good flexibility, a high mechanical strength, and an excellent safety against nail punctures (Figs. 3(a) and 2(b)), demonstrating the advantages of GPEs for fabricating flexible batteries.

Recently, a 3D cross-linked polymer network has been introduced to improve GPE properties. Through a facile one-pot synthesis strategy based on a ring-opening polymerization reaction, Lu et al. reported a novel 3D network GPE membrane for LMBs [85]. In particular, P(VDF-HFP), poly(ethylene glycol) diglycidylether (PEGDE), diglycidyl ether of bisphenol-A (DEBA), and diamino-poly(propylene oxide) (DPPO) were mixed in N,N-dimethylforamide (DMF), followed by spreading the resultant precursor solution on a polytetrafluorothylene plate to produce a 3D cross-linked network polymer membrane. Thereafter, the as-prepared membrane was immersed into a $LiPF_6$-EC/dimethyl carbonate (DMC) liquid electrolyte to incorporate Li salt to obtain the GPE. In the obtained 3D GPE, DEBA was employed as a framework to improve the mechanical strength, PEGDE and DPPO were cross-linked to ensure the fast Li^+ transport, and P(VDF-HFP) was embedded in the network to enhance the flexibility of the GPE membrane. The GPE membrane thus synthesized showed an unprecedented combination of flexibility, ionic conductivity, and efficient suppression of Li dendrite growth for LMBs. A LFP/3D-GPE/Li battery assembled from this GPE

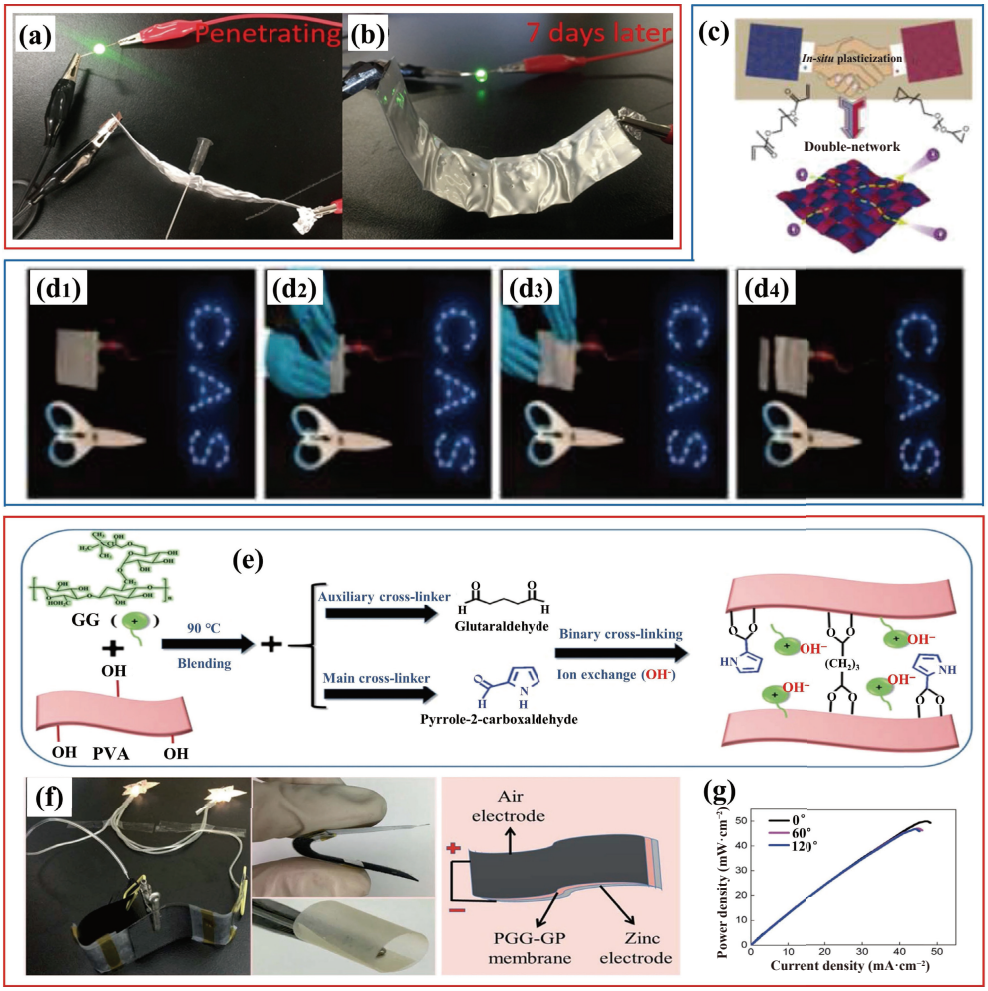

Figure 3 (a) Photograph showing nail puncture test of a flexible battery fabricated from a quasi-solid electrolyte and (b) the flexible battery can still light up a LED even 7 days after the nail puncture test (reproduced with permission from Ref. [90], © Elsevier B.V. 2017). (c) Schematic illustration of an *in-situ* plasticized SPE with double-network (DN-SPE), photographs of a DN-SPE incorporated lithium metal pouch cell lighting up a "CAS" logo consisting of 30 white LED lamps (d1) before deformation, (d2) under deformation, (d3) after recovery, and (d4) after truncation (reproduced with permission from Ref. [17], © Elsevier B.V. 2017). (e) Schematic illustration of the fabrication process of a PGG-GP electrolyte membrane, (f) demonstration and schematic of a flexible ZAB fabricated from the PGG-GP electrolyte, and (g) power density plots of the battery at different bending angles (reproduced with permission from Ref. [96], © The Royal Society of Chemistry 2019).

membrane with a LFP cathode and a Li anode delivered a reversible capacity of 73 mAh·g^{-1} at 20 C, higher than that (52.4 mAh·g^{-1}) of a cell incorporating the same electrodes but with a liquid $LiPF_6$ electrolyte, reflecting the superior properties of 3D GPEs.

More recently, a dual-salt concept has been studied to enhance the ionic conductivity for GPEs. In this context, Fan et al. reported a dual-salt (LiTFSI-$LiPF_6$) GPE with 3D cross-linked polymer network for LMBs [91]. Specifically, poly(ethylene glycol) diacrylate (PEGDA) and ethoxylated trimethylolpropane triacrylate (ETPTA) were first mixed with LiTFSI and $LiPF_6$ in EC:DMC:DEC (1:1:1), followed by adding azodiisobutyronitrile (AIBN) as a thermal initiator. The resultant solution was injected into a cell with a LFP cathode and a Li foil anode, followed by heating at 60 °C to obtain a solid-state LFP/3D-GPE/Li battery. In the as-synthesized GPE, the 3D polymerized network restrained the motion of $TFSI^-$ and PF_6^- and the dual-slat system improved the electrolyte dissociation capacity, making the electrolyte to exhibit a high ionic conductivity of 0.56 mS·cm^{-1} at room temperature. On the other hand, the GPE could built a robust and conductive solid electrolyte interphase (SEI) and ensure a uniform Li^+ distribution and deposition on the lithium metal surface, remarkably suppressing the lithium dendrite growth on the anode. Consequently, this LMB achieved well-defined electrochemical performance and maintained a high capacity retention of 87.93% even after cycling at 0.5 C for 300 cycles.

Moreover, with their environmentally friendly properties, ionic liquids have been introduced to synthesize GPEs with improved thermal stability, safety, electrochemical stability, and ionic conductivity. In this context, Balo et al. introduced ionic liquid 1-ethyl-3-methylimidazolium bis(trifluoromethylsulfonyl)imide (EMIMTFSI) into a PEO and LiTFSI based GPE and investigated the effect of the amount of EMIMTFSI added [92]. With an optimized amount of EMIMTFSI of 12.5 wt.%, the resultant GPE displayed a high thermal stability (i.e., no weight loss up to 310 °C), a large electrochemical stability window (~ 4.6 V), a high lithium transference number (t_{Li+} = 0.39), and a high ionic conductivity (2.08 × 10^{-4} S·cm^{-1} at 30 °C). This clearly indicates a new route to utilize the unique properties of ionic liquids to synthesize high-performance GPEs.

Apart from the organic systems discussed above, GPEs can also be realized with aqueous electrolytes. In this regard, Tan et al. fabricated polyacrylamide (PAM)-based aqueous GPEs to demonstrate flexible MABs [93]. Specifically, a KOH-PAM and a NaCl-PAM GPEs were obtained by immersing a PAM film in a 6 M KOH and a 10 wt.% NaCl solution, respectively. The resultant GPEs possessed a high ionic conductivity of 0.33 S·cm^{-1}. Onto the KOH-PAM GPE, a C-CoPAN900 catalyst was spread to fabricate an air cathode, followed by attaching a Zn foil anode to assemble a zinc-air battery (ZAB). In the same way, an aluminum-air battery

(AAB) was also assembled by using the NaCl-PAM GPE electrolyte and an Al foil anode. Both batteries were highly flexible and showed well-defined electrochemical performance even under bending down to an angle of 60°. These results proved the effectiveness of aqueous GPEs for flexible aqueous batteries.

As can be seen, GPEs can be easily synthesized from various electrolytes and polymers to satisfy the demands for different battery systems. Nevertheless, since there is still a large content of liquids in the electrolytes, GPEs will inevitably inherit the issues of liquid electrolytes as discussed earlier. To this end, electrolytes without any liquids have been researched, as discussed below.

2.2.2 SPEs

SPEs, consisting of specific salts and polymers with solvation capacity, have been investigated to avoid the leakage and to enhance the mechanical strength of electrolytes. However, the ionic conductivity of SPEs is usually low, limiting their practical applications. To overcome this limitation, various modification strategies have been explored [94, 95]. In particular, Duan et al. reported an *in-situ* plasticized double-network SPE (DN-SPE) with enhanced ionic conductivity, thermal stability, and mechanical strength [17]. As shown in Fig. 3(c), a freestanding DN-SPE membrane was synthesized from a mixture containing PEGDA and PEGDE along with LiTFSI salt and benzoyl peroxide (BPO) as the heat initiator. With the self-plasticization of its double network, the DN-SPE thus synthesized was highly bendable and exhibited a high ionic conductivity of $10^{-4.5}$ S·cm^{-1} at room temperature, a high thermal stability (up to 200 °C), and a good capacity to suppress the growth of lithium dendrite. Solid-state pouch type LMBs assembled from the as-synthesized DN-SPE membrane with a LFP cathode and a Li foil anode maintained their electrochemical characteristics well even under stringent bending and truncated conditions (Fig. 3(d)). The unique double-network structure of the DN-SPE improved not only the mechanical strength and thermal stability but also the ionic conductivity of the electrolyte, responsible for its good electrochemical performance under deformations. Similarly, Wang et al. recently presented a binary cross-linked alkaline anion polymer electrolyte membrane for all-solid-state supercapacitors and flexible rechargeable ZABs [96]. As shown in Fig. 3(e), a highly conductive, flexible and thin alkaline anion-exchange membrane (AAEM) composed of poly(vinylalcohol)/guar hydroxypropyltrimonium chloride (PGG-GP) was fabricated from PVA and guar hydroxypropyltrimonium chloride (GG) by employing glutaraldehyde (GA) and pyrrole-2-carboxaldehyde (PCL) as binary cross-linkers. The resultant PGG-GP electrolyte membrane delivered a high hydroxide conductivity of 0.123 S·cm^{-1} at room temperature and showed excellent mechanical strength and flexibility (Fig. 3(f)). The flexible all-solid-state ZABs comprising the PGG-GP polymer electrolyte, a Zn anode, and an IrO_2/Pt/C@CC air cathode (IrO_2/Pt/C ink coating on CC) delivered a peak power density of 50.2 mW·cm^{-2} and could maintain this performance under different bending angles of 0°, 60°, and 120° (Fig. 3(g)). The binary cross-linked structure provided a new approach for enhancing the properties of polymer electrolytes for flexible batteries.

2.2.3 CPEs

Incorporating inorganic fillers, such as TiO_2 [97, 98], SiO_2 [99, 100], and Al_2O_3 [101], into SPEs has been demonstrated to enhance Li-ion conductivity of the resultant CPEs by preventing the reorganization of polymer chains [102–105]. Furthermore, Li-ion conducting fillers have been utilized to enhance the ionic conductivity of CPEs in recent years [66, 106–109]. Of particular interest, Yang et al. employed Li-ion conducting inorganic particles ($Li_{1.3}Al_{0.3}Ti_{1.7}(PO_4)_3$ (LATP)) as the filler to prepare a new CPE membrane [106], which could be readily fabricated from an acetonitrile solution containing LATP, LITFSI, PEO, poly(ethylene glycol) (PEG), and boronized polyethylene glycol (BPEG). The compact inorganic LATP conducting layer in the resultant CPE provided the membrane with good mechanical strength and high bulk ionic conductivity at room temperature and could physically barricade the free growth of lithium dendrite, while BPEG disorganized the crystallinity of the PEO domain and facilitated a "soft contact" between interfaces, leading to a good ionic conductivity, a low polarization, and an improved lithium plating/stripping on the lithium metal anode. A LMB incorporating this CPE membrane with a LFP cathode and a Li metal anode delivered a good capacity of 158.2 mAh·g^{-1} at 0.1 C with a high rate capability (a capacity of 94.2 mAh·g^{-1} at 2 C). Similarly, in the carbon nanofiber (CNF)/S-PEO/LLTO bilayer electrode discussed earlier (Fig. 2(f)) [66], the Li-ion conducting 1D LLTO nanofibers could act as fillers to enhance the ionic conductivity of the electrolyte to reduce the resistance at the electrode/electrolyte interface, improving the performance for the resultant bilayer electrode.

The filler geometry has also been found to play an important role in influencing the ionic conductivity of CPEs. In this regard, Zhai et al. prepared CPEs with vertically-aligned and connected Li-ion conducting $Li_{1+x}Al_xTi_{2-x}(PO_4)_3$ nanoparticles as fillers into a PEO/$LiClO_4$ matrix [107]. Having direct channels of aligned $Li_{1+x}Al_xTi_{2-x}(PO_4)_3$ nanoparticles for lithium-ion transport, the CPEs thus prepared exhibited a high ionic conductivity of 0.52 × 10^{-4} S·cm^{-1}, which was 3.6 times that of the CPE with randomly dispersed $Li_{1+x}Al_xTi_{2-x}(PO_4)_3$ nanoparticles. This proved the importance of the geometry of fillers in enhancing the ionic conductivity of CPEs.

Although liquid electrolytes (along with separators) can be directly used to fabricate flexible batteries, solid state electrolytes (GPEs, SPEs, and CPEs) have been demonstrated to be superior owing to their multiple advantages, including high flexibility, nontoxicity, non-flammability, and no leakage. However, the relatively lower ionic conductivity of solid-state electrolytes with respect to their liquid counterparts inevitably limits their applications. This provides an important research direction for future studies to further enhance the ionic conductivity of solid state electrolytes for flexible batteries. Table 2 compares the major advantages and disadvantages of various electrolytes along with some representative examples discussed in this section.

3 Battery chemistries

Since the early attempts of alkaline batteries [110], polymer batteries [111, 112], and lithium-metal batteries [113], a variety of battery chemistries have been investigated for flexible batteries. Among them, LIB chemistry is the dominant one for flexible batteries in wearable electronics due to its high nominal operating voltage (typically 3.7 V), high energy and power densities, and long cycle life [12, 13]. Because of the high cost and limited resource of lithium, however, SIBs and PIBs are considered as promising alternatives to LIBs due to the relatively low cost and wide availability of sodium and potassium resources [15, 16]. For other applications (e.g., electric vehicles and renewable energy storage systems), the rapidly increasing demand in energy density has been a driving force for the research and development of flexible batteries with high energy densities from, for example, LMBs [17–21], LSBs [23, 24], and MABs [26, 27]. From the capacity (C) and average voltage (V) of the electrode materials

Table 2 Properties of liquid, gel polymer, solid polymer, and composite polymer electrolytes.

Electrolyte	Advantages	Disadvantages	Refs.
Liquid electrolyte	• High ionic conductivity • Low viscosity	• Toxicity, flammability, evaporation, and leakage • Poor electrochemical stability • Need of conventional separators • Strict requirements for packaging	[88, 89, 92]
GPE	• Ease of preparation • Higher ionic conductivity than SPEs and CPEs • High flexibility • Higher thermal stability than liquid electrolytes • Higher mechanical strength than liquid electrolytes • Higher electrochemical stability than liquid electrolytes • No need for conventional separators	• Lower ionic conductivity than liquid electrolytes • Maintaining the safety issues of liquid electrolytes	[89, 92]
SPE	• Nontoxicity, non-flammability, no evaporation, and no leakage • Light weight • High flexibility • High thermal stability • High mechanical strength • High electrochemical stability • No need for conventional separators	• Lower ionic conductivity than GPEs • Complex manufacturing processes	[19, 88]
CPE	• Nontoxicity, non-flammability, no evaporation, and no leakage • Higher ionic conductivity than SPEs • Light weight • High flexibility • High thermal stability • High mechanical strength • High electrochemical stability • No need for conventional separators	• Lower ionic conductivity than liquid electrolytes • Complex manufacturing processes	[104, 107]

[114– 120], the theoretical average voltage ($V_{\text{average}}^{\text{cathode}} - V_{\text{average}}^{\text{anode}}$) and theoretical energy density (E) of a battery can be calculated from the following equation [121, 122]

$$E = \frac{V_{\text{average}}^{\text{cathode}} - V_{\text{average}}^{\text{anode}}}{\frac{1}{C_{\text{cathode}}} + \frac{1}{C_{\text{anode}}}} \quad (1)$$

Figure 4 shows the theoretical energy densities vs. theoretical average voltages for various batteries, along with their metal contents in the earth' s crust. The research and development of these systems in flexible batteries are discussed in detail in the following sections.

3.1 LIBs

Since their commercialization in the 1990s, LIBs have been rapidly developed for a wide range of applications [123]. During the past decade, they have been extensively researched for flexible and wearable electronic devices. It is important to load electrode materials (cathode and anode) onto appropriate current collectors and incorporate the resultant electrodes with appropriate electrolytes and separators for assembling high-performance flexible batteries, as discussed below.

As discussed in Section 2.1, Al and Cu foils are major current collectors for conventional LIBs due to their high electrical conductivity. However, their poor adhesion with electrode materials makes them unsuitable for flexible applications. As pointed out earlier, surface-roughing of metal foils is useful to address this issue [35]. In this context, Park et al. used honeycomb-patterned Cu and Al current collectors (Figs. 5(a) and 5(b)) prepared via a reactive-ion etching (RIE) process to enhance the adhesion with electrode materials for flexible LIBs [41]. Through a slurry process, a multishelled $LiNi_{0.75}Co_{0.11}Mn_{0.14}O_2$ cathode material and a Si nanoparticle-loaded graphite anode material were coated on the Cu and Al current collectors, respectively. A full cell assembled from the as-prepared flexible electrodes with a $LiPF_6$-EC/DEC/FEC electrolyte and a microporous PE separator retained a high capacity at 50% at 20 C vs. 0.1 C. After cycled under continuous bending at 4 C for 200 cycles, the battery

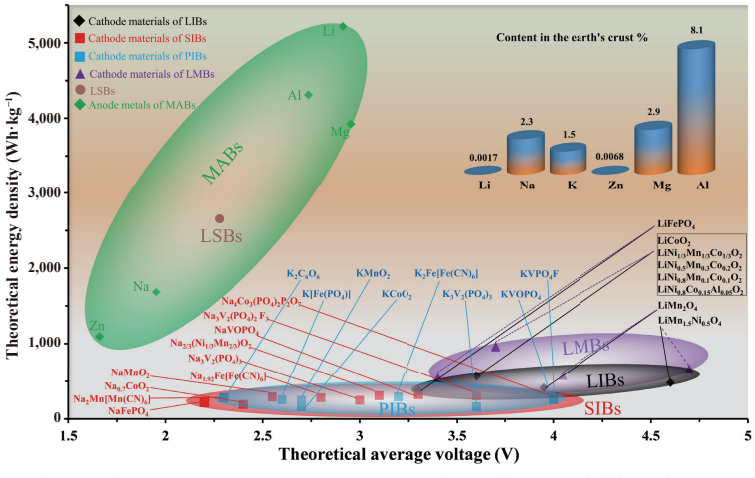

Figure 4 Theoretical average voltages, theoretical energy densities, and metal contents in the earth's crust of different battery systems (graphite and hard carbon are used as the anode for LIBs and SIBs/PIBs, respectively).

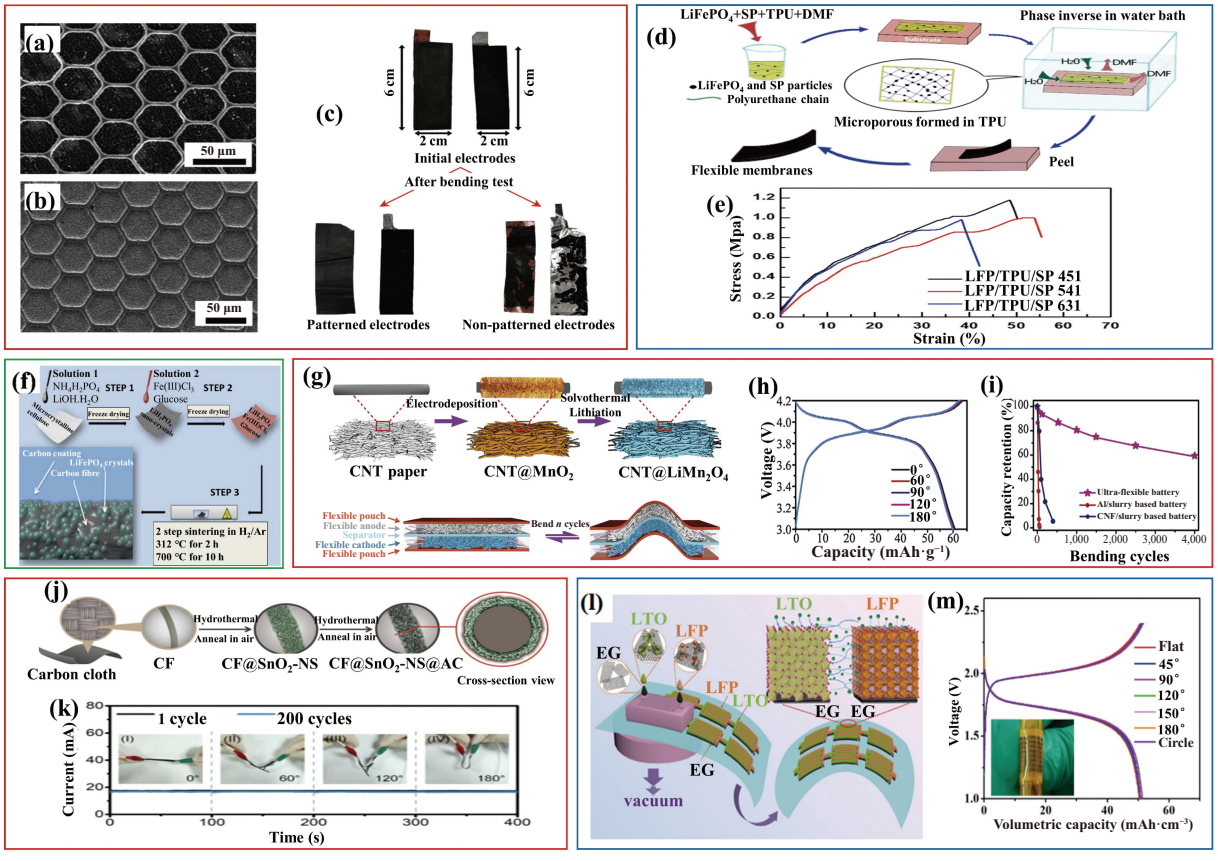

Figure 5 Scanning electron microscopy (SEM) images of honeycomb-patterned (a) Al foil and (b) Cu foil, (c) photographs of electrodes separated from the full cells before and after 100 bending cycles (reproduced with permission from Ref. [41], © American Chemical Society 2014). (d) Schematic illustration of fabrication steps for free-standing flexible LFP/TPU/SP cathodes and (e) stress–strain curves of the LFP/TPU/SP membranes (reproduced with permission from Ref. [125], © Elsevier B. V. 2017). (f) Schematic illustration of the preparation process of a LFP@CP hybrid electrode (reproduced with permission from Ref. [58], © The Royal Society of Chemistry 2016). (g) Schematic illustration of the fabrication of a flexible LIB, (h) charge/discharge curves of the battery with varied bending angles, and (i) capacity retention of different batteries after multiple bending cycles (reproduced with permission from Ref. [77], © Elsevier Ltd. 2017). (j) Formation strategy of a 3D hierarchical flexible CF@SnO_2-NS@AC composite electrode and (k) current–time curves of a battery fabricated from the composite electrode at various bending angles (reproduced with permission from Ref. [130], © Elsevier B.V. 2018). (l) Schematic illustration of the fabrication of LTO//LFP-LIMBs and (m) charge–discharge curves of LTO//LFP-LIMBs measured from flat to 180° and at a highly bending circle state (reproduced with permission from Ref. [131], © Elsevier Ltd. 2018).

showed a capacity retention only 23% lower than that of a control cell without bending. Remarkably, after 100 bending cycles, the electrode materials still adhered to the patterned current collectors while delamination occurred for the nonpatterned ones (Fig. 5(c)), clearly demonstrating the significance of patterned metal current collectors in improving the performance of flexible LIBs.

With their lightweight, low cost, and inherent flexibility, polymers are attractive materials for fabricating composite electrodes for flexible LIBs [124, 125]. In this regard, Bao et al. developed a simple phase separation process for preparing polymer composite membrane electrodes (Fig. 5(d)) [125]. Specifically, a DMF slurry containing LFP, super P (SP) and thermoplastic polyurethane (TPU) was cast onto a polyfluortetraethylene (PTFE) substrate, followed by a phase inversing treatment in a water bath to produce LFP/TPU/SP composite membrane electrodes. These electrodes showed excellent flexibility and mechanical strength with their tensile strength being increased with increasing in the TPU ratio (Fig. 5(e)). Being assembled with a Li metal anode and a $LiPF_6$-EC/DMC electrolyte into a battery, it delivered a reasonable capacity of 153 $mAh·g^{-1}$ at 0.2 C and maintained this capacity up to 93 $mAh·g^{-1}$ even at a high current of 10 C.

Having the advantages of a high electrical conductivity, flexibility, chemical stability and mechanical strength, a large variety of carbonaceous materials have been used for the fabrication of flexible LIBs [126– 129]. Kretschmer et al. used CP to load LFP to prepare a flexible LFP@CP hybrid electrode by using commercial paper towel (PT) as the substrate precursor (Fig. 5(f)) [58]. To start with, these authors impregnated a piece of PT with $NH_4H_2PO_4$ and LiOH, followed by freeze drying. Thereafter, the phosphate and lithium loaded PT was impregnated with $FeCl_3$ and glucose, followed by freeze drying again and then sintering in H_2/Ar to obtain the LFP@CP electrode. With the resultant carbon fiber serving as both the current collector and structure substrate to provide a conductive carbon network for LFP, the LFP@CP electrode thus prepared was highly electroactive. When tested with a Li metal anode and a $LiPF_6$-DMC/DEC/EC electrolyte, this hybrid electrode achieved an initial reversible capacity of 197 $\mu Ah·cm^{-2}$ at 0.1 $mA·cm^{-2}$, which increased to 222 $\mu Ah·cm^{-2}$ after 500 cycles with a superior cycling stability up to 1,000 cycles. This work indicates the usefulness of low-cost precursor materials for preparing efficient carbonaceous current collectors for flexible LIBs.

In another study, Wang et al. used a CNT paper to fabricate a CNT@$LiMn_2O_4$ cathode for flexible LIBs [77]. As shown in Fig. 5(g), MnO_2 was electrochemically deposited onto a CNT paper from a solution containing $MnSO_4$ and H_2SO_4, followed by lithiation via a solvothermal method with LiOH to convert MnO_2 to $LiMn_2O_4$. A LIB incorporating the as-fabricated CNT@$LiMn_2O_4$ as cathode with a graphitized carbon fiber (GCF) anode, a PP membrane separator, and a $LiPF_6$-EC/DEC electrolyte showed highly stable charge/discharge behaviors at different bending angles (Fig. 5(h)). Upon cycling up to 4,000 cycles of bending deformation, this battery still retained a high capacity at 58.8%, which was much

superior over its counterparts fabricated through slurry coating of $LiMn_2O_4$ on an Al foil and a CNF film, respectively (Fig. 5(i)). Indeed, different from the slutty-processed electrodes, the electrochemically prepared CNT@$LiMn_2O_4$ electrode ensured the uniform and tight deposition of $LiMn_2O_4$ on the CNT surface conformably forming a monolithic structure, which could effectively avoid the possible detachment of $LiMn_2O_4$ during bending.

Min et al. used CF textile to prepare an amorphous carbon coated with SnO_2 nanosheets as an anode for flexible LIBs [130]. Briefly, SnO_2 nanosheets (SnO_2-NS) were deposited onto a CF textile through a hydrothermal method from a stannous chloride ($SnCl_2$)-containing solution, followed by coating amorphous carbon (AC) via the carbonization of glucose on the as-synthesized CF@SnO_2-NSs to produce CF@SnO_2-NS@AC (Fig. 5(j)). Due to the tightly woven structure of the CF textile substrate, the resultant composite electrode showed a significant tensile strength of 18.6 MPa with an excellent elongation of 19.7%. A LIB based on this composite electrode as anode and a Li foil cathode, and a $LiPF_6$-EC/DEC electrolyte exhibited a stable current output upon bending up to 180° (Fig. 5(k)) as well as a high specific capacity of 968.6 mAh·g^{-1} after cycling at 85 mA·g^{-1} for 100 cycles. The observed good achievement is attributable to the hierarchical structure and flexibility of the CF textile substrate.

Graphene based materials also exhibited excellent performance both in mechanical strength and electrochemical characteristics in flexible LIBs. In a recent study, Zheng et al. proposed all-solid-state planar integrated lithium ion micro-batteries (LIMBs) based on exfoliated graphene (EG) nanosheets [131]. As shown in Fig. 5(l), an EG dispersion was first filtrated through an interdigital mask attached on a flexible substrate, and then a lithium titanate (LTO)/EG dispersion and a LFP/EG dispersion were filtrated from each side of the mask to establish the anode and cathode film, respectively. Subsequently, an ionogel electrolyte containing LiTFSI, 1-butyl-1-methyl-pyrrolidinium bis(trifluoromethyl-sulfonyl)imide (P_{14}TFSI), and P(VdF-HFP) was drop-cast on the surface of electrode films followed by solidifying to obtain a full battery. The as-fabricated LTO//LFP-LIMB delivered an ultrahigh volumetric energy density of 125.5 mWh·cm^{-3} and a long cycle life (without capacity loss after 3,300 cycles). Importantly, these batteries possessed an excellent mechanical accommodation to deformations, showing no obvious capacity decay under serious bending conditions up to a bending angle of 180° (Fig. 5(m)), and hence tremendous application potential for flexible integrated micro-electronics.

As can be seen from above, flexible LIBs have displayed marvelous achievements and have begun to penetrate into the flexible and wearable electronics market. Along with the rapid developments in the Fifth generation (5G) network, the Internet of Things (IOT), and the electric vehicles, however, the demands of LIBs and hence the consumption of lithium will be greatly accelerated to make the cost and supply of lithium even more serious. Consequently, it is necessary to develop low-cost and earth-abundant SIBs and PIBs as supplements or even replacements to LIBs.

3.2 SIBs/PIBs

With their suitable redox potentials of −2.71 and −2.92 V (vs. SHE) [119, 132], respectively, sodium and potassium can be used to construct metal-ion batteries (i.e., SIBs and PIBs) with the energy storage mechanisms similar to that of LIBs. Moreover, their low cost (for example, 150/ton for sodium vs. 3,000/ton for lithium in 2015) [133] and earth-abundance (Fig. 4) make SIBs and PIBs excellent alternatives to LIBs. Indeed, flexible SIBs and PIBs have been being actively explored in recent years [15, 134].

The structural design and fabrication process of SIBs and PIBs are similar to those of LIBs as systematically discussed above. Therefore, current collectors, electrolytes, and separators of LIBs can also be used for SIBs or PIBs with only Na^+ or K^+ to replace Li^+ for the conduction in the electrolytes.

Up to now, various metal substrates, such as Cu [135, 136] and Ti [137, 138], have been adopted to construct flexible electrode for flexible SIBs due to their high electrical conductivity. For instance, Fan et al. grew additive-free Cu_3P nanowires on Cu substrate to fabricate a flexible anode for SIBs [136]. Specifically, $Cu(OH)_2$ nanowires (NWs) were firstly grown on a Cu foil from a solution containing ammonium peroxodisulfate and sodium hydroxide, followed by phosphidation of the as-prepared $Cu(OH)_2$ NWs under the atmosphere of sodium hypophosphite to obtain Cu_3P NWs (i.e., CPNW). The CPNW anode thus fabricated was used to assemble a pouch-type Na^+ full cell with a $Na_3V_2(PO_4)_3$ (NVP) cathode and a $NaClO_4$-EC/DMC/FEC electrolyte, which displayed a high energy density of 104.5 Wh·kg^{-1}, close to its theoretical values of 188.5 Wh·kg^{-1}, and a good cycle stability with a reversible capacity of 79.9 mAh·g^{-1} after 200 cycles at 600 mA·g^{-1}. Furthermore, the promising potential of the resultant flexible SIBs for portable equipment and wearable products has been successfully demonstrated by connecting them to power a flexible LED screen.

Polymers have also been extensively researched to construct flexible electrodes for SIBs and PIBs due to their excellent flexibility and deformability [15, 134, 139]. However, the inherently high resistivity of polymers unfortunately restricts their applications. To address this issue, compositing polymers with high-conductivity materials has been a useful approach. Indeed, Li et al. proved this concept by combining graphene with poly(dimethylsiloxane) (PDMS) to synthesize a highly porous and conductive "PDMS/rGO sponge" with the use of sugar cubes as a template [139]. This graphene-modified PDMS sponge was further used to load $NaVOPO_4$ and hard carbon (HC) to fabricate flexible cathode and anode, respectively. Incorporating the obtained electrodes with a $NaClO_4$-containing gel electrolyte, the resultant all-component-stretchable SIB exhibited a capacity of 103 mAh·g^{-1} at 0.1 C under flat condition, and more importantly, maintained its high capacities of 96 and 92 mAh·g^{-1} even when stretched at 20% and 50% strains, respectively. These results highlighted the importance of the flexibility of polymers and the feasibility of compositing them with other conductive materials to realize their practical applications. However, this compositing process inevitably implies an extra cost. In this regard, carbonaceous materials possessing not only high flexibility but also inherently high electrical conductivity have thus been considered as promising substrates for constructing flexible SIBs and PIBs.

Like LIBs, a large number of carbonaceous materials have been investigated to fabricate flexible electrodes for SIBs and PIBs, which mainly include CNT, CNF, porous carbon fiber (PCF), graphene, CCs, and carbon textiles (CTs) [75, 78, 134, 140– 150]. Some of these materials were directly explored as anode materials for sodium storage [151, 152]. In this case, heteroatom doping has been an effective strategy to boost their capacities for anode applications [153– 155]. Nevertheless, the majority of the research has been focused on the use of these carbonaceous materials as flexible substrates to load other active materials to fabricate anode and cathode for SIBs and PIBs. In this regard, Chen et al. used PCFs to embed yolk–shell NiS_2 nanoparticles to fabricate flexible NiS_2@PCF anode (Fig. 6(a)) for SIBs [148]. A flexible fiber-shaped SIB based on this kind anode and a Na metal counter electrode, a $NaClO_4$-EC/PC/FEC electrolyte, and a glass microfiber separator (Fig. 6(b)) was able to constantly power a commercial LED and displayed stable charge/discharge

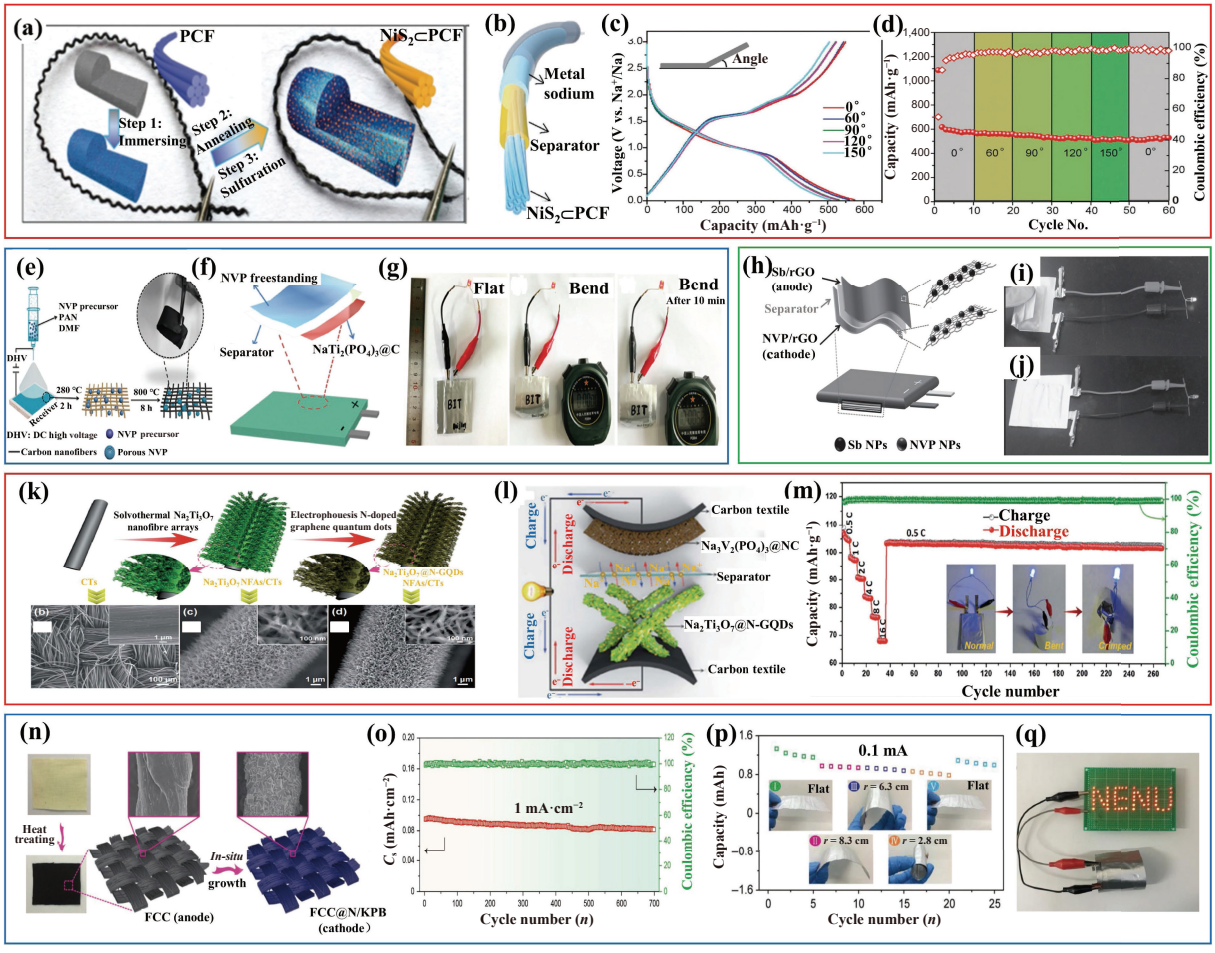

Figure 6 (a) Schematic illustration of the fabrication procedure of a flexible NiS_2⊂PCF anode, (b) illustration of the construction structure of a flexible fiber-shaped SIB, (c) galvanostatic charge/discharge curves of the SIB at 0.1 C under different bending states, and (d) cycling of the SIB at 0.1 C under different bending states (reproduced with permission from Ref. [148], © Wiley-VCH Verlag GmbH & Co. KGaA, Weinheim 2018). (e) Illustration of the preparation procedure for a NVP-loaded CNFs electrode, (f) inside structure of a flexible sodium-ion soft package battery, and (g) bending tests of the battery (reproduced with permission from Ref. [156], © Wiley-VCH Verlag GmbH & Co. KGaA, Weinheim 2018). (h) Schematic illustration for the fabrication of a flexible SIB, (i) digital picture for the bending SIB that lights a LED and (j) digital picture for the free-bending SIB that lights a LED after 30 cycles of bending (reproduced with permission from Ref. [78], © Wiley-VCH Verlag GmbH & Co. KGaA, Weinheim 2015). (k) Fabrication processes of a N-GQD decorated $Na_2Ti_3O_7$ NFAs/carbon textile electrode and the corresponding SEM images, (l) schematic illustration of a $Na_2Ti_3O_7$@N-GQDs/CT//$Na_3V_2(PO_4)_3$@NC/CT full battery, and (m) cycling performance and bending tests of the battery (reproduced with permission from Ref. [75], © The Royal Society of Chemistry 2019). (n) Illustration of the formation process for a FCC anode and a FCC@N/KPB cathode, (o) cycling performance of a FCC//FCC@NPB battery at 1 mA·cm^{-2} for 700 cycles, (p) cycling stability of the FCC//FCC@NPB battery at different bending states, and (q) a FCC//FCC@KPB battery as a power supply for 33 LED bulbs at a bent state (reproduced with permission from Ref. [140], © Wiley-VCH Verlag GmbH & Co. KGaA, Weinheim 2019).

characteristics (showing a small reversible capacity reduction of about 11% at a very high bending angle of 150°) (Fig. 6(c)) with outstanding cycling performance (Fig. 6(d)) under different bending conditions.

Ni et al. used an electrospinning technique to load NVP on CNFs to prepare a flexible freestanding composite cathode (Fig. 6(e)), which was used to assemble a flexible SIB with a $NaTi_2(PO_4)_3$@C (on Cu foil) anode, a $NaClO_4$-PC/FEC electrolyte, and a glass fiber separator (Fig. 6(f)) [156]. The resultant film-shaped battery achieved a high energy density of 123 Wh·kg^{-1} and could successfully power a red LED even at a dramatically bent state for 10 min (Fig. 6(g)).

Zhang et al. used a GO aqueous suspension to develop flexible binder-free composite electrodes, including a NVP/rGO cathode and a Sb/rGO anode [78]. Using these paper-like electrodes, a full SIB was assembled with a $NaClO_4$-EC/DMC/FEC electrolyte, and a glass fiber membrane separator (Fig. 6(h)). When charged/discharged at 100 mA·g^{-1}, this battery achieved a high initial discharge capacity of 481 mAh·g^{-1} and maintained its capacity at 400 mAh·g^{-1} after 100 cycles. Notably, it could power a commercial LED even under a bent state (Fig. 6(i)) or after 30 bending cycles (Fig. 6(j)). Here, the good electrochemical performance of the battery could be attributed to the insertion of active material nanoparticles into the interlayers of rGO films to prevent the restacking of rGO nanosheets, while its good deformable property to the excellent flexibility of graphene.

Kong et al. used a hydrothermal process to directly grow $Na_2Ti_3O_7$ nanofiber arrays on flexible CTs and used electrophoresis to decorate N-doped graphene quantum dot (N-GQD) on the resultant $Na_2Ti_3O_7$ nanofiber arrays on CTs to prepare a novel binder-free 3D hierarchical $Na_2Ti_3O_7$@N-GQDs/CT electrode (Fig. 6(k)) [75]. Using this electrode as anode, a flexible pouch-type SIB was assembled with a NVP@NC/CT cathode, a $NaPF_6$-EC/DMC/FEC electrolyte, and a glass microfiber filter separator (Fig. 6(l)), which showed an excellent rate with a capacity of 76.3 mAh·g^{-1} at 8 C (vs. 104.8 mAh·g^{-1} at 0.5 C) and an outstanding stability with a capacity retention of 97.8% after cycling at 0.5 C for 230 cycles. Moreover, this battery could easily light up a LED even when bent and crimped (Fig. 6(m)). The combination of the high conductivity of the as-prepared 3D hierarchical electrodes and the good flexibility of the CT substrate was responsible for this good achievement.

Guo et al. proposed an facile approach to fabricate flexible Na-ion/K-ion batteries by utilizing a flexible carbon cloth (FCC) directly as anode and as the substrate to fabricate cathodes [140]. Specifically, after the carbonization of a commercially available cotton cloth, the obtained FCC was loaded with prussian blue (PB) to prepare a binder-free and self-supporting FCC@NPB (or FCC@KPB) electrode (Fig. 6(n)). Using the FCC as anode and the as-prepared FCC@NPB (or FCC@KPB) electrode as cathode, along with a glass filter separator and a 1 M $NaClO_4$ (or 1 M KPF_6)-containing electrolyte, a NIB (or KIB) full cell was assembled. Impressively, the FCC//FCC@NPB battery exhibited an excellent electrochemical cycling performance (Fig. 6(o)) and maintained its good electrochemical characteristics at different bending states (Fig. 6(p)). Similarly, the FCC//FCC@KPB battery could work well as a power supply for 33 LED bulbs even at a bent state (Fig. 6(q)).

As discussed above, with their well-defined energy storage mechanisms, flexible metal-ion batteries including LIBs, SIBs, and PIBs have achieved remarkable progresses for flexible and wearable electronics. However, the relatively low energy densities of these batteries would hinder their applications with a high-energy demand. To this end, more energetic systems possessing an energy density beyond LIBs, including LMBs, LSBs, and MABs (Fig. 4), have entered the emerging field of flexible batteries in recent years, as discussed below.

3.3 LMBs

Metallic lithium is considered a core anode material for high-energy batteries due to its high theoretical specific capacity (3,860 $mAh·g^{-1}$) and the lowest redox potential (−3.042 V vs. SHE) among anode materials [157]. Using lithium as an anode, various cathode materials can be incorporated to construct LMBs. However, the relatively easy and most straightforward approach is the use of existing LIB cathode materials to fabricate LMBs that possess energy densities distinctly higher than those of their LIB counterparts (Fig. 4).

Since flexible electrodes are a primary requirement for flexible batteries, the intrinsic flexibility of lithium is favorable for its anode use for LMBs. On the cathode side, the progresses that have been achieved for flexible cathodes of LIBs (as discussed under Section 3.1) are beneficial for LMBs. Therefore, the biggest challenge remained for flexible LMBs would be the safety and cycling stability of lithium anode. Indeed, the practical application of LMBs has been largely hindered by the safety and cycling issues of the lithium anode induced by the growth of lithium dendrites, large volume evolution of hostless lithium, and low Coulombic efficiency during lithium plating/stripping [158, 159]. To this end, use of solid state electrolytes including GPEs [91, 160], SPEs [17, 161, 162], and CPEs [109, 163] has been demonstrated to be efficient to address these issues, and hence to become an important research direction in flexible LMBs.

GPEs are relatively easy to be synthesized and used. Furthermore, properties of GPEs have been continued to be improved in order to satisfy the stringent requirements of flexible LMBs owing to their operation under repeated deformations. In this regard, Zhang et al. developed a 3D cross-linked network GPE and demonstrated its excellent performance for LMBs [160]. Specifically, the GPE was obtained by incorporating LiTFSI into a 3D cross-linked polymer network that was formed through an *in-situ* polymerization between methyl methacrylate (MMA) and ETPTA monomers on electrospun PAN nanofibers with the use of AIBN as thermal initiator. This GPE presented a high ionic conductivity of 0.33 $mS·m^{-1}$. A pouch-type flexible LMB was assembled by using a LFP cast Al foil as cathode, a Li foil as anode, and the as-prepared GPE as electrolyte/separator, which delivered a high initial discharge capacity of 134.8 $mAh·g^{-1}$ at 2 C and retained a high capacity retention of 78.6% after 600 cycles. Moreover, at 50 °C, this battery remained a capacity of 112.3 $mAh·g^{-1}$ at 2 C even after 300 cycles, demonstrating the excellent thermal stability and the ability to restrain the growth of lithium dendrites on the proposed 3D cross-linked network GPE. Mechanically, this flexible LMB showed stable discharge performance to power a LED at different bending conditions (Figs. 7(a)– 7(c)) and still worked well even when truncated for three times (Fig. 7(d)).

Extensive research has also been performed to enhance the properties of SPEs for flexible LMBs. Specifically, cross-linked polymer networking has been proven to be an efficient strategy to improve the dimensional stability and electrochemical properties of SPEs [17, 96, 162]. Moreover, due to the operation of flexible batteries under repeated deformations, an electrolyte capable of self-healing is highly desirable for improving the deformability of the electrolytes, and hence the reliability of flexible batteries [101, 164, 165]. In view of the above discussion, Zhou et al. developed a dual-network strategy to prepare a novel polymer electrolyte with mechanically robust and self-healing properties [162]. The electrolyte was prepared by incorporating LiTFSI into a dual-network structure that was formed from poly(ethylene glycol) methyl ether methacrylate (PEGMA), (2-(3-(6-methyl-4-oxo-1,4-dihydropyrimidin-2-yl)ureido)ethyl methacrylate) (UPyMA), and polyethylene glycol-bis-carbamate dimethacrylate (PEGBCDMA), in which PEGBCDMA acted as the cross-linker. In the resultant dual-network self-healing polymer electrolyte (DN-SHPE), the dynamic ureido-pyrimidinone (UPy) dimers were the first network that provided the electrolyte with good self-healing capability and ensured the reliability and lifetime of the polymer lithium batteries, while the crosslinked PEGBCDMA served as the second network that enhanced the dimensional stability, thermal stability, and mechanical strength of the electrolyte. As a result, the DN-SHPE showed a wide electrochemical window of 5.2 V and a stable thermal stability up to 350 °C. Remarkably, when a DN-SHPE was cut into two pieces, the two bisected segments could be brought entirely into contact after heated at 60 °C for 2 h (Fig. 7(e)), and afterwards the self-healed sample could be stretched without showing cracks in the initially damaged interface (Fig. 7(f)). This clearly demonstrates the self-healing capability for the DN-SHPE. When a DN-SHPE was assembled with a LFP cathode and a Li metal anode, the resultant flexible LMB delivered a good capacity of 137.9 $mAh·g^{-1}$ at 0.1 C and could power a LED lamp even under bending and folding conditions. This work highlighted the significance of introducing self-healing capability into polymer electrolytes to ensure the stable operation of LMBs under deformations.

With the contribution of inorganic fillers in polymer matrices, CPEs possess improved ionic conductivity compared with GPEs and SPEs and have thus attracted considerable attention for the fabrication of solid state batteries, including LMBs [108, 131]. In this context, He et al. incorporated $Li_{6.25}Al_{0.25}La_3Zr_2O_{12}$ (LLZO) powder as filler with LiFSI, poly(ethylene carbonate) (PEC), and P(VdF-HFP) to develop a garnet CPE for all-solid-state flexible LMBs [108]. The as-prepared CPE membrane displayed a wide electrochemical stability window of 0–5.5 V vs. Li/Li^+ at 55 °C. Due to the heat-resistant property of the garnet matrix, this electrolyte showed a superior thermal stability over a conventional Celgard separator (Figs. 7(g) and 7(h)). An all-solid-state flexible pouch cell incorporating this electrolyte with a LFP cathode and a Li metal anode exhibited a good discharge capacity of 121.4 $mAh·g^{-1}$ at 1 C (at 55 °C) with a high capacity retention of 96.3% after 100 cycles, indicating the effective suppression of lithium dendrite growth by the CPE. Impressively, this battery showed an excellent bendability to light up a LED even in a bent state

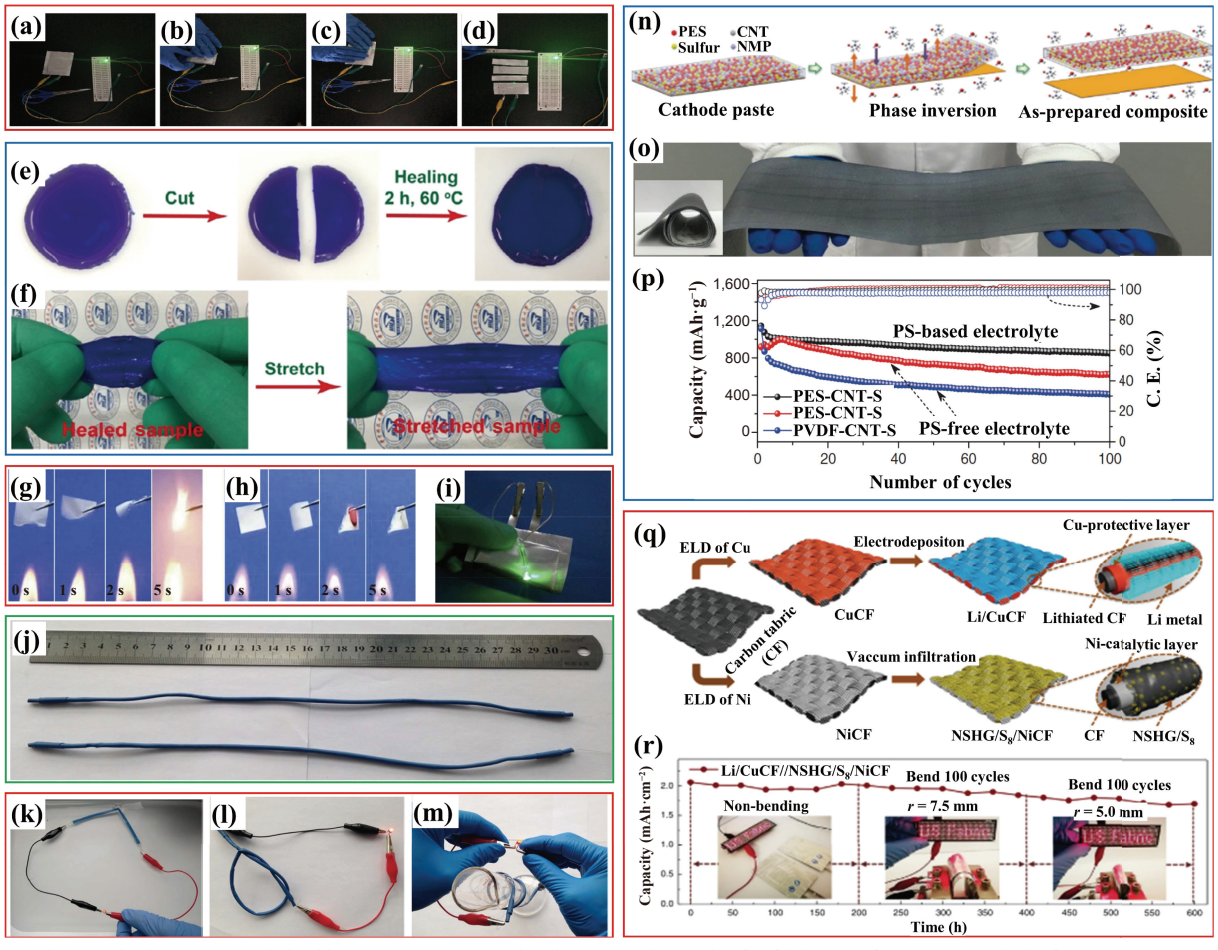

Figure 7 Photographs showing a LED lighted by a LFP//GPE//Li pouch cell (a) at initial state, (b) after folding, (c) after recovery, and (d) after truncation (reproduced with permission from Ref. [160], © Elsevier Ltd. 2019). (e) Optical images showing the self-healing process of a DN-SHPE sample and (f) illustration of the stretchability of the DN-SHPE sample (reproduced with permission from Ref. [162], © Wiley-VCH Verlag GmbH & Co. KGaA, Weinheim 2018). Flammability test of (g) a Celgard separator and (h) a LLZO-PEC-P(VdF-HFP)-LiFSI CPE membrane, (i) photograph of a soft-packaged flexible battery assembled from the CPE membrane in bent state lighting a green LED lamp at 55 °C (reproduced with permission from Ref. [108], © Elsevier B.V. 2018). (j) Optical image of fiber-shaped lithium sulfur batteries with length of 30 cm, photographs displaying a red LED lit up by the battery under (k) bending at 90°, (l) knotting, and (m) twisting (reproduced with permission from Ref. [171], © Elsevier Ltd. 2017). (n) Schematic diagram of the fabrication of a PES-CNT-S composite with a phase inversion method, (o) digital photographs of the as-prepared PES-CNT-S composite and (inset) rolled composite, and (p) cycle performance of half-cell using PES-CNT-S and PVDF-CNT-S cathodes with PS-free electrolyte and PS-modified electrolyte at 0.25 C (reproduced with permission from Ref. [172], © Wiley-VCH Verlag GmbH & Co. KGaA, Weinheim 2018). (q) Schematic of the fabrication process and design principle for a Li/CuCF and a NSHG/S_8/NiCF electrodes and (r) bending test of a Li-S full battery fabricated from the electrodes (reproduced with permission from Ref. [76], © Chang, J. et al. 2018).

(Fig. 7(i)).

3.4 LSBs

Keeping the metallic lithium anode as for LMBs as discussed above, use of a sulfur cathode to replace LIB cathodes will result in LSBs with a higher energy density. Indeed, owing to the high theoretical specific capacities of lithium and sulfur (1,675 mAh·g^{-1}), LSBs possess a high theoretical energy density up to 2,600 Wh·kg^{-1} [166], which is three to five times that of LIBs, as illustrated in Fig. 4. Moreover, LSBs have been considered as one of the next-generation higher-energy battery systems due to multiple advantages of the sulfur, including its low cost, environmental friendliness, and abundant resources [167]. However, the drawbacks associated with the sulfur cathode, such as its low electrical conductivity (5×10^{-30} S·cm^{-1}) [168] and discharge product (Li_2S, 9.21×10^{-9} S·cm^{-1}) [169], the dissolution of lithium polysulfide (PS) formed during the electrochemical process in organic liquid electrolytes, and the large volumetric expansion of sulfur (80%) during lithiation, have hindered the practical applications of LSBs [168]. These are also important factors that should be taken into consideration when developing flexible LSBs [170], as elucidated in the following paragraphs.

As for the battery systems already discussed above, metal current collectors have also been employed for fabricating flexible LSBs. Liu et al. used industrial stainless steel fibers (SSFs) to load sulfur to prepare a composite cathode for fiber-shaped LSBs [171]. Specifically, a rGO/S composite was synthesized by a hydrothermal method from an aqueous suspension containing GO and $Na_2S_2O_3$, followed by loading the as-obtained rGO/S composite (with its ethyl alcohol dispersion) into HF etched SSFs via capillary driven self-assembly. The HF etched SSFs featured a porous fibrous structure that allowed the imbibition of rGO/S composite by a facile capillary action. The sulfur component was well reserved by the rGO nanosheets and the highly conductive SSF current collector, which could overcome the insulting and volume change issues of sulfur to ensure a good electrochemical performance for the resultant sulfur composite electrode. As a result, a fiber-shaped LSB assembled by intertwining this hybrid fiber as cathode with a lithium wire anode, a Celgard 2400 separator, and a LITFSI-DOL/DME electrolyte delivered a capacity of 335 mAh·g^{-1} at 167.5 mA·g^{-1} and retained this high capacity even after 100 cycles. With a long length of up to 30 cm, the battery was still mechanically robust and highly flexible (Fig. 7(j)). It could successfully power a LED under bending

(Fig. 7(k)), knotting (Fig. 7(l)), and twisting (Fig. 7(m)) conditions, demonstrating its great potential for a series of sophisticated applications for flexible and wearable electronics.

Constructing electrodes with polymers is another approach to fabricate flexible LSBs. In this context, Wahyudi et al. introduced a new polymeric binder of PES for fabricating flexible freestanding sulfur composite electrodes and used a polysulfide-modified electrolyte to improve the stability of LSBs [172]. In a typical "phase-inversion" process, a slurry containing CNTs, sulfur, and PES in NMP was casted on a substrate (e.g., Al foil) first, followed by phase inversion in water and peeling off the resultant PES-CNT-S composite electrode from the substrate (Fig. 7(n)). Due to the exchange between NMP and water, numerous porous structures could be produced for this composite electrode. Moreover, the PES-CNT-S composite was highly flexible and could be produced in a large scale (Fig. 7(o)). For comparison, conventional PVDF binder was used to prepare a PVDF-CNT-S electrode as a counterpart. When tested in a LSB with a Li foil counter electrode and a conventional LiTFSI/$LiNO_3$-DOL/DME electrolyte, the PES-CNT-S cathode showed a much higher capacity retention of 68% at the 100th cycle (at 0.25 C) than that of 37% only for the conventional PVDF-CNT-S cathode (Fig. 7(p)), which was confirmed to be due to the higher hydrophilicity and stronger affinity properties of the new PES binder than the conventional PVDF, effectively trapping the soluble polysulfides within the electrode. Moreover, when 0.05 M Li_2S_8 was introduced into the electrolyte, the PES-CNT-S cathode showed a further enhanced initial capacity of 1,141 mAh·g^{-1} and maintained a capacity retention of 75% and a Coulombic efficiency of 100% after 100 cycles in the resultant polysulfide-modified electrolyte (Fig. 7(p)). The improved battery performance with the so-called polysulfide-modified electrolyte has been ascribed to the strong hydrophilicity of polysulfide [173, 174] and its ability to buffer the dissolution of sulfur in the electrolyte [175]. Therefore, this work demonstrated the importance of not only using a new polymer binder to fabricate large-sized flexible sulfur composite electrodes but also incorporating a polysulfide-modified electrolyte to improve the stability of LSBs.

Moreover, the use of conducting polymers has been demonstrated to be especially useful for fabricating high-performance sulfur composite electrodes. Xiao et al. combined poly(3,4-ethylenedioxythiophene)/poly(styrenesulfonate) (PEDOT:PSS) with nanosulfur and graphene to fabricate flexible and binder-free sulfur composite cathodes by vacuum filtration [176]. Specifically, a nano-S-graphene-PEDOT:PSS (SGP) composite was prepared from an aqueous mixture containing $Na_2S_2O_3$, GO, hydrochloric acid, PEDOT:PSS, and sodium ascorbate, followed by dispersing the as-synthesized composite in water and filtering the resultant dispersion to produce a SGP composite membrane electrode. The obtained flexible electrode showed an electrical conductivity of 36.5 S·cm^{-1} under flat state and maintained a high value of 35.9 S·cm^{-1} even after being bent under 180° for 100 cycles, indicating its excellent electrical and mechanical properties. In this SGP composite, nanosulfur was homogenously coated by graphene and PEDOT:PSS in a sandwich structure, which not only provided a highly conductive network and intimate contacts between nanosulfur and graphene/PEDOT:PSS for effective charge transportation, but also offered synergistic physical restriction and chemical confinement to dissoluble intermediate lithium polysulfides during electrochemical processes. As a result, when assembled into a LSB with a lithium anode, a Celgard 2400 separator, and a LiTFSI/$LiNO_3$-DOL/DMC electrolyte, the SGP electrode exhibited a very high reversible volumetric capacity of 1,432 Ah·L^{-1} at 0.1 C and 1,038 Ah·L^{-1} at 1 C and an excellent cycling stability with a capacity retention of 80% after 500 cycles at 1 C. Furthermore, when the battery was subjected to a folding test with a series of folding angles (45°, 90°, 135°, and 180°), its areal capacity (3.3 mAh·cm^{-2}) only slightly dropped to 3.15 mAh·cm^{-2}. This work showed the significance of conducting polymers in fabricating mechanically strong and electrically conductive sulfur composites with a hierarchical structure able to stabilize the electrochemical performance for flexible LSBs.

Same as for other battery systems, carbonaceous materials, such as CNTs [177], CFs [76], graphene [63], and carbon foams [178], have attracted more attention than metals and polymers for the development of flexible sulfur cathodes and LSBs. In this regard, Chang et al. used CFs as substrate to fabricate a flexible high-energy LSB [76]. As shown in Fig. 7(q), with a polymer-assisted metal deposition (PAMD) method, copper and nickel were deposited on CFs to produce Cu-coated CF (CuCF) and Ni-coated CF (NiCF), respectively. Thereafter, the CuCF was loaded with lithium via an electrodeposition method to produce a Li/CuCF electrode, while the NiCF was loaded with a composite consisting of nitrogen and sulfur heavily co-doped graphene (NSHG) (obtained by a hydrothermal method) and S_8@super P (obtained by grinding S_8 powder with super P) via a vacuum infiltration method to produce a NSHG/S_8/NiCF electrode. A flexible LSB was assembled by incorporating the Li/CuCF as anode and NSHG/S_8/NiCF as cathode with a microporous PP membrane separator and a LiTFSI/$LiNO_3$-DOL/DME electrolyte, which showed a high energy density of 288 Wh·kg^{-1} (360 Wh·L^{-1}) and a high capacity retention of 99.92% per cycle over 260 cycles. The high energy density of this battery could be specifically attributable to the minimized loading of lithium on the anode. Usually, lithium foil is directly used as anode in most LSBs reported so far, which implies an excessive amount of lithium (about 1,500% –15,000%) of the anode over the sulfur cathode and thus a low energy density for the resultant batteries [179–183]. With a thin layer of lithium on CFs as anode in the present work (Fig. 7(q)), the excessive amount of lithium of the anode in comparison to the cathode was decreased sharply to 100%, significantly reducing the mass and enhancing the energy density for the battery [76]. Moreover, the resultant battery was highly flexible and exhibited excellent capability to sustain mechanical bending, powering a LED screen with stable brightness during repeated bending at small radii of curvatures of 7.5 and 5 mm (Fig. 7(r)). The inherent flexibility of carbon fabrics and their uniform metallic coatings were the key for this achievement.

With its excellent electrical conductivity, strong mechanical strength, and tunable surface properties and microstructures, graphene has been utilized to fabricate flexible sulfur composite cathodes with enhanced electrochemical characteristics and mitigated shuttling of polysulfides [184–186]. In this context, Liu et al. developed a blade coating technique to prepare flexible large-sized sulfur composite films with graphene [63]. Briefly, a hydrogel containing GO and S nanoparticles was blade-coated on a glass substrate first, followed by chemical reduction with HI to produce porous composite films incorporating sulfur on reduced graphene oxide (rGO@S). The unique porous cross-linked structure of rGO@S endowed the resultant composite films with high mechanical strength and excellent electrochemical performance. A LSB based on the rGO@S composite film as cathode with a lithium foil anode, a Celgard 2300 membrane separator, and a LiTFSI/$LiNO_3$-DOL/DME electrolyte delivered a high discharge capacity of 1,381 mAh·g^{-1} at 0.1 C and maintained a capacity retention up to 70% after 150 cycles at 0.2 C. Furthermore, this battery was highly flexible and could power a LED even under bending and folding conditions. In another

study, Wu et al. employed vacuum-filtration to produce freestanding graphene-based porous carbon (GPC)-sulfur films at a large scale [187]. Typically, GO was first processed to graphene-based microporous carbon (GMC) via a hydrothermal process, followed by ground milling the as-prepared GMC with sulfur to produce a GPC-sulfur composite. Using vacuum-filtration, the GPC-sulfur composite could be easily processed into large-sized film electrodes that displayed a high electrical conductivity of 325 $S \cdot m^{-1}$ even with a thick thickness of 100 μm. A soft-packaged LSB assembled with the GPC-sulfur film as cathode, a lithium foil anode, a glass fiber membrane separator, and a LiTFSI/$LiNO_3$-DOL/DME electrolyte exhibited a discharge capacity of 815 $mAh \cdot g^{-1}$ at 0.5 C and maintained this performance under bending conditions. The excellent electrical and mechanical properties of graphene and the hierarchical structure of the resultant GPC-sulfur composite were responsible for this achievement.

Moreover, 3D carbonaceous materials, such as carbon aerogel, carbon foam, graphene foam (GF), and graphene sponge, are also excellent substrates for fabricating flexible sulfur cathodes. In this regard, Xiang et al. used a 3D carbon foam to fabricate flexible multifunctional hybrid electrodes for LSBs [178]. Specifically, an aqueous mixture composed of melamine foam (MF), CNTs, and magnesium nitrate was treated with NH_3 gas to form $Mg(OH)_2$ on CNTs and MF, followed by calcinating the resultant composite into a hybrid foam of nitrogen-doped carbon foam (CF@CNTs) decorated with ultrafine MgO nanoparticles. A film rolled from the as-prepared foam was immersed into an S/CS_2 solution to load sulfur to obtain a CF@CNTs/MgO-S composite film electrode. The 3D CF matrix of the resultant composite ensured the flexibility of the free-standing electrode without binders. CNTs on CF skeletons established an interconnected 3D conductive network and offered sufficient active sites to achieve an ultrahigh sulfur loading of 14.4 $mg \cdot cm^{-2}$. As a result, the CF@CNTs/MgO-S composite film showed an excellent flexibility and mechanical strength with no crack when the film was rolled, folded, kneaded, and compressed. Due to a high nitrogen content of MF (41.87 wt.%), however, its calcinated product (i.e., CF) could be in-situ doped with nitrogen up to 5.2 wt.%, which could act as surface anchoring sites for polysulfides. Meanwhile, the MgO nanoparticles in the composite could enable a strong chemisorption toward polysulfide species. Together, these effects could suppress the dissolution of polysulfides to ensure a good electrochemical stability for the as-prepared CF@CNTs/MgO-S composite electrode. In fact, when tested in a coin cell with a Li metal anode, a Celgard 2400 separator, and a LiTFSI/$LiNO_3$-DOL/DME electrolyte, this composite cathode delivered a very high initial areal capacity of 10.4 $mAh \cdot cm^{-2}$ at 0.1 C and retained it at 8.8 $mAh \cdot cm^{-2}$ after cycling for 50 cycles. With the same components as for the coin cell, a soft-packaged full pouch cell was assembled, which was used to successfully power 23 LEDs even subjected to bending to 180°, showing its great flexibility and deformability. This work demonstrated the excellent potential of 3D carbon structures for fabricating high-performance flexible sulfur electrodes and LSBs.

3.5 MABs

MABs are composed of a metal anode, an air cathode, a metal-ion conducting electrolyte, and a separator (separator can be abandoned when a solid state electrolyte is used) [188, 189]. Due to the high theoretical capacities of metal anode materials and air cathode (3,350 $mAh \cdot g^{-1}$) [118], MABs possess very high theoretical energy densities (e.g., 5,220, 4,310, and 3,923 $Wh \cdot kg^{-1}$ for Li-O_2, Al-O_2, and Mg-O_2 batteries, respectively) (Fig. 4) and have been considered as promising candidates for high-energy flexible batteries to power flexible and wearable electronic devices.

As for other flexible battery systems, all components of flexible MABs should be flexible and deformable. Therefore, the development of flexible metal anodes and air cathodes is a key for flexible MABs. Furthermore, metal foils are inherently flexible and can be directly used as anodes, achieving good flexibility. On the other hand, it is important to maintain well-defined electrocatalytic activity for air cathodes in flexible MABs. Similar to those in conventional MABs [190], flexible air cathodes can be realized either by growing/casting oxygen reduction reaction (ORR)/oxygen evolution reaction (OER) catalysts on flexible current collectors, such as metal foams [191] and carbonaceous materials [192– 194] or by directly using metal-free carbon electrocatalysts as the cathodes [195– 197]. On the other hand, liquid electrolytes employed in conventional MABs can be used for flexible MABs. However, considering the leakage and safety issues of liquid electrolytes (especially under deformed conditions of batteries), use of solid state electrolytes would be desirable for the fabrication of safer and more stable flexible MABs [96, 190, 191].

Owing to their high electrical conductivity, 3D porous structure, and mechanical flexibility, metal foams have been used as current collectors and substrates to fabricate flexible air cathodes for flexible MABs. However, electrocatalysts directly grown on metal foams are usually disordered and densely packed with "prohibited zones", prohibiting the activity of the catalysts [198, 199]. To minimize the "prohibited zones", Jiang et al. constructed an ordered multidimensional array air cathode consisting of 1D CNTs and 2D carbon nanoridges decorated with 0D cobalt nanoparticles (referred as MPZ-CC@CNT) on NF for flexible Zn-air batteries (FZABs) [191]. As shown in Fig. 8(a), Zn-hexamine (Zn-HMT) was first seeded and sprouted into a well-aligned array on the skeleton of a NF substrate via a hydrothermal process from a methanol solution containing NF, $Zn(NO_3)_2$ and hexamine. Then, the Zn-HMT with smooth surface was partially converted into surface-roughed ZnCo-HMT coordination frameworks via a cation-exchange process in an ethanol solution containing cobalt nitrate. Finally, a CVD process using acetonitrile as carbon and nitrogen sources was performed during the pyrolysis of ZnCo-HMT, in which N-doped CNTs were grown on cobalt particles, resulting in multidimensional MPZ-CC@CNT on NF. Rechargeable FZABs based on this NF supported MPZ-CC@CNT as cathode with a Zn foil anode and an alkaline gel electrolyte containing KOH and $Zn(CH_3COO)_3$ in PVA (Fig. 8(b)) delivered a high energy density of 946 $Wh \cdot kg^{-1}$ and showed a small voltage fading rate of 0.006 mV per cycle over 1,800 cycles at a current density of 50 $mA \cdot cm^{-2}$. More importantly, the charge/discharge polarization curves of the batteries remained virtually unchanged at different bending angles (0°, 90°, and 120°) (Fig. 8(c)), indicating the potential applications of the proposed FZABs for flexible electronics.

Compared with metal foams, carbonaceous materials are lighter, more flexible, and more porous, making them more suitable as current collectors and substrates for loading catalysts to construct flexible air cathodes for flexible MABs. Indeed, the use of carbonaceous materials for flexible MABs has gained substantial research efforts in recent years. In particular, Yoon et al. grew brush-like Co_4N nanorods on CNF papers as air cathodes for LABs [192]. Briefly, a hydrothermal process was used to grow Co(OH)F nanorods on electrospun CNF papers, followed by a nitridation step to convert the as-prepared Co(OH)F/CNF to Co_4N/CNF (Fig. 8(d)). The resultant Co_4N/CNF electrodes were highly flexible due to the good flexibility of the CNF substrate. The intimate electrical contact between the Co_4N nanorods and the underneath CNF (Fig. 8(e)) would efficiently enhance the charge transport, while mesopores in-between the nanorods and

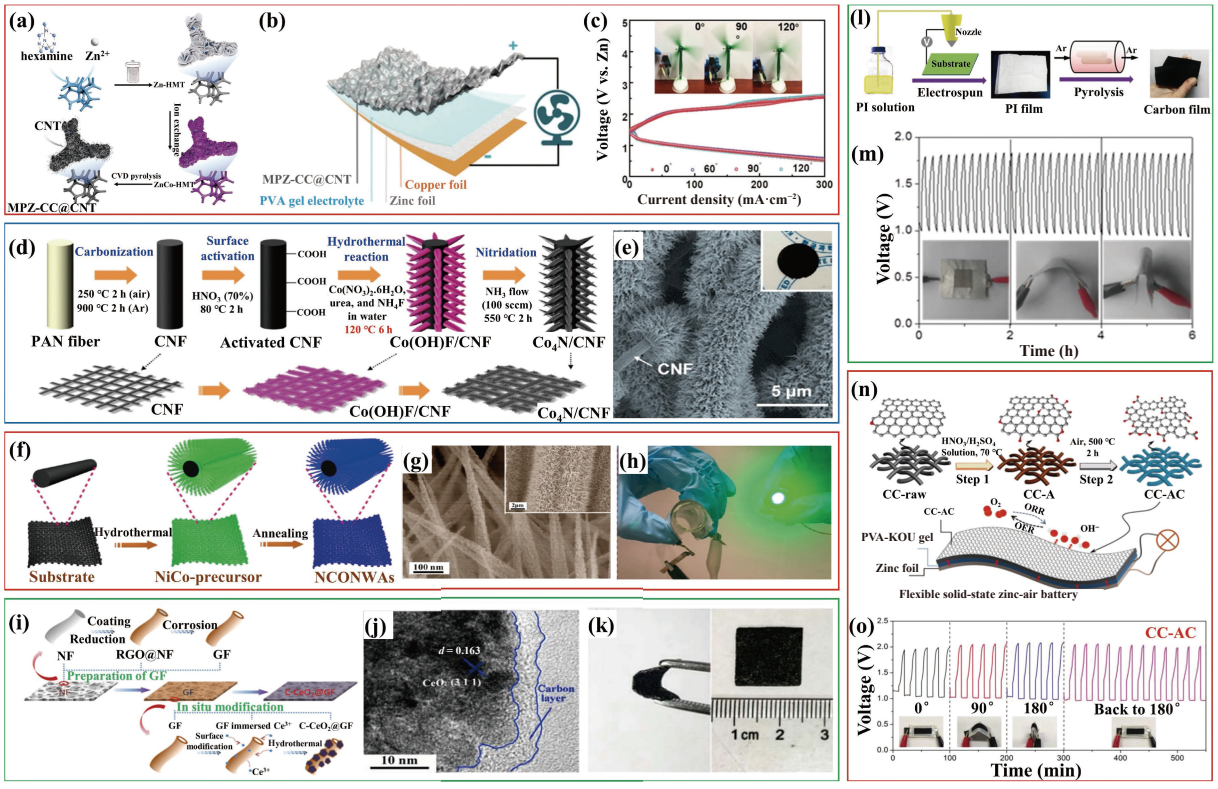

Figure 8 (a) Schematic of the preparation process of a NF supported MPZ-CC@CNT air electrode, (b) illustration of a quasi-solid-state and rechargeable FZAB fabricated from the MPZ-CC@CNT air electrode, and (c) polarization curves between charge/discharge of the FZAB under various bending conditions (reproduced with permission from Ref. [191], © Wiley-VCH Verlag GmbH & Co. KGaA, Weinheim 2019). (d) Schematic of the fabrication procedure of a Co_4N/CNF electrode and (e) SEM image showing the brush-like structure of the Co_4N/CNF (reproduced with permission from Ref. [192], © American Chemical Society 2018). (f) Schematic illustration of the formation of a NCONWAs cathode, (g) SEM images of the NCONWAs cathode, and (h) photograph demonstrating the flexibility of the as-fabricated bendable Li-Air battery assembled using the NCONWAs cathode (reproduced with permission from Ref. [194], © American Chemical Society 2016). (i) Schematic of the formation of a flexible cathode with well dispersed C-CeO_2 on graphene foam, (j) TEM morphology of the C-CeO_2@GF cathode with core–shell structure, and (k) digital photograph of the flexible C-CeO_2@GF cathode showing its bendability (reproduced with permission from Ref. [200], © Wiley-VCH Verlag GmbH & Co. KGaA, Weinheim 2017). (l) Schematic representation of the fabrication procedure toward a NCNF, (m) galvanostatic discharge–charge cycling curve at 2 mA·cm^{-2} for an all-solid-state rechargeable ZAB with the NCNF as catalyst, applying bending strain every 2 h (reproduced with permission from Ref. [202], © Wiley-VCH Verlag GmbH & Co. KGaA, Weinheim 2016). (n) Illustration of a two-step activation method for the fabrication of a CC-AC air electrode for ZABs and the possible surface chemical structure of the CC-AC (grey and red balls represent carbon and oxygen atoms, respectively), and (o) galvanostatic discharge–charge cycling curves of a ZAB using CC-AC as the cathode at 1 mA·cm^{-2}, demonstrating its stable performance under different folding conditions (reproduced with permission from Ref. [203], © Wiley-VCH Verlag GmbH & Co. KGaA, Weinheim 2019).

macropores in-between the bundles of nanorods would increase the electrochemical reaction active sites for ORR/OER. As a result, a flexible LAB assembled from the Co_4N/CNF as cathode with a lithium foil anode, a glass fiber separator, an electrolyte containing 1 M LiTFSI in tetra(ethylene) glycol dimethyl ether (TEGDME), and a gas diffusion layer exhibited a stable charge/discharge performance for over 100 cycles with a small potential gap of ~ 1.23 V at 700 mAh·g^{-1} when charged/discharged with a limited capacity of 1,000 mAh·g^{-1}. Importantly, this battery was bendable up to 180° without significant degradation in its electrochemical characteristics. Similarly, Xue et al. prepared hierarchically porous nickel cobaltate nanoneedle arrays on CTs as air electrodes for LABs [194]. Specifically, the nickel cobaltate nanoneedle arrays (NCONWAs) were grown on CTs by a hydrothermal process from a solution containing urea, $Co(NO_3)_2$, and $Ni(NO_3)_2$, followed by a low-temperature calcination at 300 °C (Fig. 8(f)). A LAB was fabricated by incorporating the as-prepared NCONWAs on CTs as binder-free cathode with a Li foil anode, a glass fiber separator, and a LiTFSI-TEGDME electrolyte, which displayed a high specific capacity of 4,221 mAh·g^{-1} at 200 mA·g^{-1}, an excellent rate capability with an almost 100% capacity retention at 1,000 mAh·g^{-1}, and an outstanding cycling stability with no capacity decay over 200 cycles at 1,000 mA·g^{-1}. The observed excellent performance was attributed to the high electrocatalytic activity of the NCONWAs catalyst and the excellent oxygen diffusion and electrolyte infiltration associated with the mesoporous structure of the air cathode (Fig. 8(g)). Furthermore, the as-assembled LAB could power a LED all the time whether it was flat or bent (Fig. 8(h)), demonstrating its good bendability.

In another study, Jiang et al. prepared CeO_2 microspheres on 3D interconnected GF as cathode for flexible LABs [200]. As shown in Fig. 8(i), GO prepared through a modified Hummers' method [201] was firstly filled into a porous NF template, followed by a hydrothermal process with hydrazine monohydrate to reduce GO to rGO on the NF. The use of hydrochloric acid to remove the NF template from the as-fabricated rGO@NF resulted in a GF. Subsequently, carbon-coated CeO_2 microspheres were synthesized through a hydrothermal treatment with a mixture of PVP and $CeCl_3·7H_2O$ and deposited on the GF. In the resultant C-CeO_2@GF electrode, CeO_2 microspheres were tightly wrapped with carbon layers (Fig. 8(j)), which could improve the electrical conductivity of CeO_2 catalysts, and hence facilitate their charge transfer during ORR and OER processes. Also, the carbon layers could protect CeO_2 catalysts and ensure their structural stability during charge and discharge processes. Furthermore, with the 3D interconnected porous structure of the GF substrate, the C-CeO_2@GF electrode was highly flexible and mechanically strong, which could be folded and flexed without failure (Fig. 8(k)). As a result, when tested in a coin cell with a Li foil anode, an electrolyte containing 1 M LiTFSI in dimethyl sulfoxide (DMSO), and a glass

fiber separator, this C-CeO_2@GF cathode showed a large discharge capacity of 3,250 mAh·g^{-1} at 200 mA·g^{-1} and a small increase in potential gap between charge and discharge even after cycled for 80 times. A flexible pouch-type LAB fabricated with the same components as for the coin cell showed a discharge platform at 2.65 V and a charge platform at 4.14 V, which were maintained even after bending to 90° for 100 cycles. Further bending to 1,000 cycles only caused a small increase in both charge and discharge overpotentials for this battery, demonstrating the great potential of the proposed flexible LABs for the practical applications of flexible electronics.

Along with the recent development of carbon-based metal-free electrocatalysts (C-MFECs) [195– 197], carbonaceous materials without metal catalysts but doped with heteroatoms, such as N, S or O, are becoming promising ORR and OER bifunctional catalysts for rechargeable MABs. In the absence of traditional metal catalysts, the electrocatalytic sites of these carbonaceous materials have been determined to be their doped heteroatoms, which are active toward ORR and OER, and thus can be directly used to fabricate flexible air cathodes for MABs. With their multiple advantages of low cost, abundant resources, high electrocatalytic activity, and excellent flexibility, these meta-free carbon electrocatalysts will play a more and more important role for flexible MABs. In this regard, Liu et al. prepared high-surface-area and nitrogen/oxygen doped nanoporous carbon fiber films (NCNFs) as bifunctional catalytic air cathodes for flexible ZABs [202]. As shown in Fig. 8(l), the NCNFs were prepared by high-temperature pyrolysis of electrospun PI film under Ar atmosphere. The obtained NCNFs were highly flexible and mechanically strong, having a tensile strength of 1.89 MPa and a tensile modulus of 0.31 GPa attributable to the polar interactions associated with the constituent oxygen, nitrogen, and/or hydrogen atoms along the polymer backbone of PI before and after the carbonization. They also possessed a high electrical conductivity (147 S·m^{-1}) and a large specific surface area (1,249 m^2·g^{-1}). Importantly, owing to their nitrogen doping (for ORR activity) and both nitrogen and oxygen dopings (for OER activity), the NCNFs showed excellent bifunctional electrocatalytic activities toward ORR (onset potential = 0.97 V vs. RHE; limiting current density = 4.7 mA·cm^{-2}) and OER (onset potential = 1.43 V vs. RHE, potential = 1.84 V @ 10 mA·cm^{-2}) in 0.1 M KOH. Moreover, an all-solid-state ZAB was assembled by incorporating the NCNF as air cathode with a KOH and zinc acetate containing PVA gel electrolyte and a Zn plate anode, which achieved a high energy density of 378 Wh·kg^{-1} and exhibited stable charge (1.78 V)/discharge (1.0 V) performance for 6 h under a large bending strain (Fig. 8(m)). Further bending/folding back for 48 cycles did not cause obvious structural and morphological changes for this battery.

In another study, Kordek et al. presented a facile two-step method, mild acid oxidation followed by air calcination, to directly activate commercial CC as air cathodes for flexible ZABs (Fig. 8(n)) [203]. The activated CC (CC-AC) thus prepared exhibited superior bifunctional catalytic activities with a strong cathodic ORR peak (0.6–0.9 V vs. RHE) and a strong anodic OER signal (1.5–1.8 V vs. RHE) in 1.0 M KOH. The remarkable electrocatalytic activity and durability of CC-AC were ascribed to the following main factors: The –COOH groups in the defective graphene structure of CC-AC were electrocatalytic active sites for both ORR and OER; the high electrochemically active surface areas (ECSA) of CC-AC, due to its nanoporous surface, provided abundant active sites; the high hydrophilicity of CC-AC increased the affinity of electrolyte species on electrocatalyst surface; the *in-situ* generated compact electrocatalytic layer of CC-AC prevented catalyst delamination during oxygen evolution. For proof-of-concept, a bendable ZAB incorporating this CC-AC as cathode with a Zn foil anode and a KOH/ZnAC-PVA GPE achieved a high open circuit voltage of 1.37 V, a remarkable peak power density of 52.3 mW·cm^{-3} at 77.5 mA·cm^{-3}, and a good cycling performance with a small charge –discharge voltage gap of 0.98 V. Furthermore, under serious folding conditions, this batterymaintaineditscharge/dischargecurvesalmostunchanged (Fig. 8(o)), indicating its excellent bendability. These works provided great potential for the design and fabrication of self-supported metal-free carbon electrocatalyst electrodes for flexible MABs.

Based on the diversities in energy storage reactions and mechanisms, a variety of battery chemistries have been utilized to develop flexible batteries. Among them, LIBs have been predominant due to their high nominal operating voltage, high energy and power densities, and long cycle life. Furthermore, the high cost and limited resource of lithium have triggered the research and development of SIBs and PIBs as promising alternatives to LIBs largely owing to the relatively low cost and wide availability of sodium and potassium resources. Moreover, the relatively low energy densities of these metal-ion batteries would hinder their applications with a high-energy demand, which has in turn spurred the entry of more energetic systems possessing an energy density beyond LIBs, including LMBs, LSBs, and MABs, into the emerging field of flexible batteries in recent years. Through proper structural design and engineering of the electrodes, flexible batteries with various geometries can be developed to meet the application demands for different flexible and wearable electronic devices, to be discussed as follows.

4 Battery device configurations

Structural designing and engineering play an important role in determining both the flexibility and electrochemical performance of flexible batteries [11, 204]. Depending on the difference in device configurations, flexible batteries have been realized and classified into three groups, including 1D fiber-shaped [28], 2D film-shaped [29], and 3D structural batteries [30], generating a large variety of options to satisfy the application requirements for different mechanical deformation circumstances, such as bending, folding, stretching, compressing, and twisting. Recent progresses in research and development of flexible batteries from 1D to 3D configurations are reviewed in the following sections.

4.1 1D batteries

1D batteries are characteristic of a fiber-shaped (or wire-like, cable-type) configuration and represent an important group of flexible batteries [205, 206]. Based on their variations in electrode structure, device configuration, and fabrication process, 1D fiber-shaped batteries can be further divided into four categories, namely solid-helix electrode batteries (SHEBs), hollow-helix electrode batteries (HHEBs), parallel electrode batteries (PEBs), and coaxial electrode batteries (CEBs).

4.1.1 SHEBs

A SHEB is constructed by wrapping a solid central axis with helical electrodes, forming a "solid-axis center spring-components around" structure, in which the elasticity of the central axis is essential to ensure the flexibility of batteries. In this regard. Weng et al. fabricated a LIB in the structure of SHFB as shown in Fig. 9(a) [207]. First, a $LiMn_2O_4$ (LMO)-deposited CNT sheet and a sandwich-structural CNT sheet/Si-deposited CNT/CNT sheet were scrolled into cathode and anode yarns, respectively (Fig. 9(b)). Thereafter, the LIB was assembled by winding the

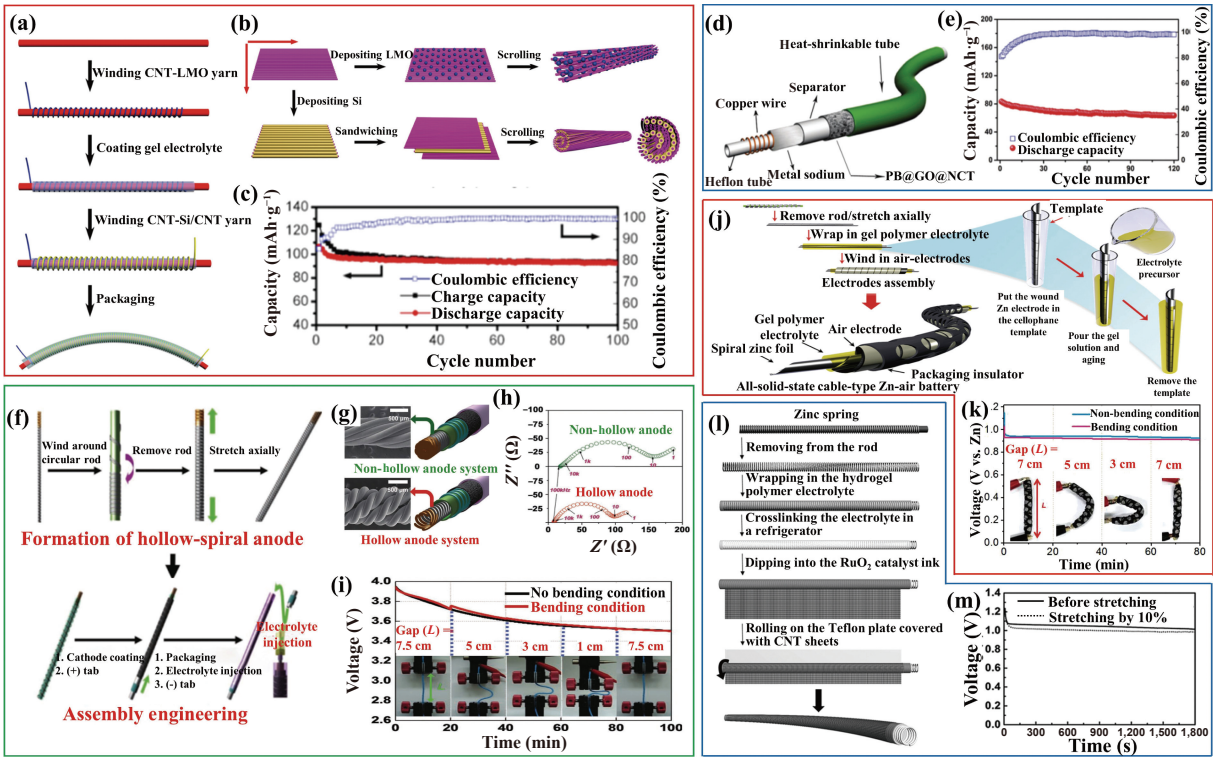

Figure 9 (a) Schematic illustration of the fabrication of a fiber-shaped LIB, (b) schematic illustration of the synthesis of composite yarns, and (c) cycling performance of the as-prepared LIB (reproduced with permission from Ref. [207], © American Chemical Society 2014). (d) Schematic illustration of a flexible fiber-shaped SIB and (e) cycling performance of the SIB at 100 mA·g^{-1} (reproduced with permission from Ref. [208], © Wiley-VCH Verlag GmbH & Co. KGaA, Weinheim 2017). (f) Schematic diagram showing fabrication of a cable battery, (g) images and (h) AC impedance spectra of cable batteries with non-hollow anode and hollow anode, (i) discharge characteristics with variations in bending strain every 20 min. The discharge rate was 0.1 C and the grip speed of the testing machine was 100 mm·min^{-1}. Reproduced with permission from Ref. [28], © Wiley-VCH Verlag GmbH & Co. KGaA, Weinheim 2012. (j) Schematic illustration of an all-solid-state cable-type flexible ZAB assembly and (k) discharge curves of the ZAB by applying bending strain every 20 min at a discharge current density of 0.1 mA·cm^{-2} (reproduced with permission from Ref. [209], © Wiley-VCH Verlag GmbH & Co. KGaA, Weinheim 2015). (l) Schematic illustration to the fabrication of a fiber-shaped Zn-air battery and (m) discharge curves of the battery with a length of 10 cm at a current density of 1 A·g^{-1} before and after stretching by 10% (reproduced with permission from Ref. [210], © Wiley-VCH Verlag GmbH & Co. KGaA, Weinheim 2015).

CNT-LMO helical cathode yarn, a $LiClO_4$-P(VdF-HFP) GPE, and the CNT-Si/CNT helical anode yarn successively around a cotton fiber. The resultant CNT-LMO||GPE||CNT-Si fiber-shaped battery delivered a specific discharge capacity of 106.5 mAh·g^{-1} (based on cathode) at the first cycle at 1 C and maintained a high capacity retention of 87% after 100 cycles (Fig. 9(c)). This remarkable stability was largely attributed to the alleviated volume change of Si during charge/discharge enabled by the CNT scaffolds on the CNT-Si/CNT composite anode. Significantly, this fiber-shaped LIB was highly flexible and could be woven into an energy storage textile with a promising energy density of 4.5 mWh·cm^{-2}, demonstrating its great potential for portable and wearable electronics.

Similarly, Zhu et al. demonstrated a SIB of SHEBs [208]. Specifically, a Ni-coated activated cotton textile (NCT) was firstly deposited with a Prussian blue@graphene oxide (PB@GO) composite suspension to produce a PB@GO@NCT electrode. The proposed SIB was fabricated by intertwining a Teflon tub with a copper helical wire (as anode current collector), a sodium foil anode, a Celgard 2400 separator, and a $NaPF_6$ electrolyte-wetted PB@GO@NTC cathode (Fig. 9(d)). The obtained Na||$NaPF_6$||PB@GO@NTC fiber-shaped battery delivered a high initial discharge capacity of 87 mAh·g^{-1} at 50 mA·g^{-1} with an energy density of 260 Wh·kg^{-1}. When tested at 100 mA·g^{-1} for 120 cycles, this battery showed a nearly constant capacity of 63 mAh·g^{-1} corresponding to a high retention of 76% (Fig. 9(e)). Moreover, upon bending to 60° and 90° for hundreds of times, the battery did not show a significant difference in its discharge capacity at 100 mA·g^{-1}. These results demonstrated the effectiveness of the SHEB configuration in ensuring good electrochemical and mechanical performance for fiber-shaped batteries. However, the presence of an insulting and inactive central axis in SHEBs would introduce unnecessary internal resistance, weight, and volume, inevitably lowering energy density and power density for the batteries. To this end, use of a hollow central axis will be advantageous.

4.1.2 *HHEBs*

Different from a SHEB characteristic of a solid substrate as the central axis, a HHEB refers to a " hollow-axis center spring-components around" configuration, in which the springs are electrodes and the inside of the helix is hollow or filled with electrolytes. Figure 9(f) illustrates a typical LIB of HHEBs reported by Kwon et al. [28]. Specifically, Ni-Sn alloy-coated Cu wires (as anode current collector) were firstly twisted into bundles, followed by winding the as-fabricated bundles around a circular rod to obtain a stretchable hollow-helix anode. Thereafter, this anode was wound by a PET nonwoven separator and then an Al wire (as cathode current collector), followed by coating with a LCO slurry to complete the cell assembly. Finally, a $LiPF_6$-EC/PC/VC electrolyte was injected into the hollow space at the center of the cell to obtain the proposed battery. For comparison, a counterpart battery was also assembled by twisting 12 Ni-Sn-coated Cu wires into a rope as a non-hollow anode (Fig. 9(g)). As a result, the hollow anode battery showed a potential plateau at 3.5 V and delivered a stable capacity of 1 mAh·cm^{-1}, which was much higher than that of the non-hollow anode battery (about 0.3 mAh·cm^{-1}). The more efficient electrolyte permeability to the separator and electrode materials of the hollow-helix battery, evidenced by its

lower Ohmic resistance (real impedance at 100 kHz) and interfacial resistance (estimated diameter of the semicircle) (Fig. 9(h)), should be responsible for this achievement. Furthermore, the hollow-helix battery showed an almost unchanged discharge curve while the grip distance was varied in the range from 7.5 to 1.0 cm (Fig. 9(i)), indicating its excellent electrochemical and deformable properties.

With the HHEB configuration, Park et al. demonstrated a flexible ZAB [209]. As shown in Fig. 9(j), the ZAB was constructed by using a hollow spiral Zn foil as anode, which was wrapped by a KOH GPE and then a Fe/N/C catalyst containing air cathode. Especially, with a cellophane template during the assembly process, the central hollow space of the Zn foil anode could be completely filled with electrolyte. As a result, the resultant battery showed well-defined electrochemical performance with a high voltage plateau of 0.92 V and a long discharge duration of 9 h. Notably, when bent from the initial length of 7 to 3 cm, the battery did not display significant change during its discharge at 0.1 $mA·cm^{-2}$ (Fig. 9(k)), indicating its excellent bendability. Similarly, Xu et al. assembled another fiber-shaped ZAB of HHEBs by using aligned and cross-stacked CNT sheets as a current collector/gas diffusion layer (Fig. 9(l)) [210]. First, a Zn spring was dipped into a KOH-PVA/PEO hydrogel polymer electrolyte solution and kept in a refrigerator to crosslink the electrolyte. The electrolyte-filled spring was further dipped into a RuO_2 containing ethanol suspension to form a catalyst layer on the surrounding surface of the hydrogel polymer electrolyte. Finally, the modified Zn spring was rolled on a Teflon plate covered with CNT sheets to form the battery. Again, due to the filling of electrolyte in the hollow space of the central axis, and hence the efficient electrolyte permeability in the system, the as-assembled ZAB reached a high discharging current density of 1 $A·g^{-1}$ at the voltage plateau of 1.0 V with a high energy density of 6 $Ah·L^{-1}$ and a high power density of 5.7 $Wh·L^{-1}$, respectively. Moreover, no obvious difference in discharge voltage was observed for this battery upon bending to 120° for 100 cycles or stretching by 10% (Fig. 9(m)), indicating its excellent bendability and stretchability.

As can be seen, without a solid substrate in the central axis, HHEBs can easily release the internal stress caused by deformations, and hence have better bendability and especially stretchability than SHEBs. Furthermore, with the electrolyte filled inside the central hollow space of the helix, HHEBs have improved contact area, enhanced electrolyte permeability, and reduced resistance, and thus superior electrochemical performance over SHEBs.

4.1.3 PEBs

A PEB is constructed by simply arranging its two electrodes in parallel with each other inside a packaging component. In this context, Lin et al. developed a LIB in the structure of PEB [211]. First, Si nanoparticles were deposited on a multi-walled carbon nanotube (MWCNT) sheet by an electron beam evaporation technology (to achieve a high Si loading up to 38.1%), followed by twisting the as-prepared MWCNT/Si composite sheet into a fiber (Fig. 10(a)). Thereafter, a LIB was constructed by simply arranging this MWCNT/Si fiber as anode in parallel with a Li wire cathode along with a $LiPF_6$-EC/DC/DMC electrolyte (Fig. 10(b)). The resultant battery displayed a remarkable capacity of 1,042 $mAh·g^{-1}$ at 3.0 $A·g^{-1}$ (vs. 1,670 $mAh·g^{-1}$ at 1 $A·g^{-1}$) and a slight capacity decrease of 6% at 2.0 $A·g^{-1}$ after bending for 100 cycles, demonstrating its excellent rate performance and flexibility. These achievements were attributed to the high electrical conductivity and excellent flexibility of the MWCNT sheet used in the composite anode.

With the same PEB configuration, Wang et al. [212] demonstrated a flexible Zn battery by arranging a MnO_2@CNT fiber cathode (prepared by electrochemical depositing MnO_2 onto a CNT fiber) in parallel with a Zn wire anode along with a $ZnCl_2$-PVA GPE in between (Fig. 10(c)). The as-prepared solid-state fiber-shaped Zn battery delivered a capacity of 290 $mAh·g^{-1}$ corresponding to a high energy density of 360 $Wh·kg^{-1}$. Moreover, this battery could be bent into any degrees (or bent to 180° for 100 cycles) without sacrificing electrochemical performance, demonstrating its excellent bendability.

More recently, this PEB structure has been realized with a relatively new dual-ion battery by Song et al. [213]. Specifically, an Al wire was electrically etched to attain an omnidirectional porous Al wire as anode, while another was coated with graphite from a slurry to fabricate a graphite/Al cathode. The two as-prepared fiber electrodes, along with a separator soaked with a liquid $LiPF_6$-EMC/VC electrolyte, were inserted into a heat-shrinkable tube to assemble a PEB (Fig. 10(d)). Upon charging, Li^+ in the electrolyte transported to the Al anode to form Al-Li alloys and PF_6^- intercalated into the graphite layer of the cathode, and reversibly, upon discharging, Li^+ and PF_6^- returned back to the electrolyte, establishing a dual-ion mechanism for the resultant fiber-shaped battery. This battery demonstrated excellent cycling stability with a discharge capacity of 130.3 $mAh·g^{-1}$ after 200 cycles at 1 C (versus that of the initial value of 145.7 $mAh·g^{-1}$) and delivered a high energy density of 173.33 $Wh·kg^{-1}$ (10.4 $mWh·cm^{-3}$) based on the total mass (volume) of the two electrodes. Moreover, when bent to different angles from 0° to 360° or knotted, the battery still showed a stable potential output of 3.86 V and could be used to power wearable devices such as a watch (Fig. 10(e)).

With their simple configuration, PEBs can be easily scaled up for practical applications, for example, for wearable electronics [214]. However, the non-uniform electric field formed in the radial direction (across the diameters of the two parallel electrodes) implies a limited effective electrode area of PEBs. In addition, the amount of electrolyte used in PEBs is usually much more than just enough for wrapping the two electrodes. These factors would deteriorate the electrochemical performance of PEBs. Therefore, arranging the two electrodes in a more efficient configuration, such as with a coaxial structure, has been studied, as discussed below.

4.1.4 CEBs

Unlike the parallel design of a PEB, the two electrodes in a CEB are arranged in a coaxial (i.e., solid-in-hollow) configuration, where a solid fiber electrode as the core is wrapped with an outer electrode in the shape of either rolled film or coil. In this way, the electric field formed between the two electrodes is uniform in both the axial and the radial directions, maximizing the effective electrode area and lowering the internal resistance of the device. Also, this design allows the intimate contact between multiple components, and thus is able to minimize the amount of electrolyte necessary in the device. This would ensure better-defined electrochemical characteristics for CEBs.

With the configuration of CEB, Yadav et al. designed and fabricated the first microsized fibrous LIBs, as shown in Fig. 10(f) [215]. Specifically, a LFP cathode layer was firstly deposited onto a CF current collector via an electrophoretic deposition process, followed by coating a SPE layer of LiTFSI-PEO on the as-prepared cathode layer electrode. Thereafter, the resultant CF/LFP/SPE fiber (as the core) was coated with a LTO anode layer using the electrophoretic deposition process similar to that for the cathode, followed by coating a carbon layer composed of CB, PEO and MWCNT as the anode current collector to complete the battery assembly. The resultant fiber-shaped LIB had a final thickness of around 22 μm (Fig. 10(g)) and possessed the cross-sectional

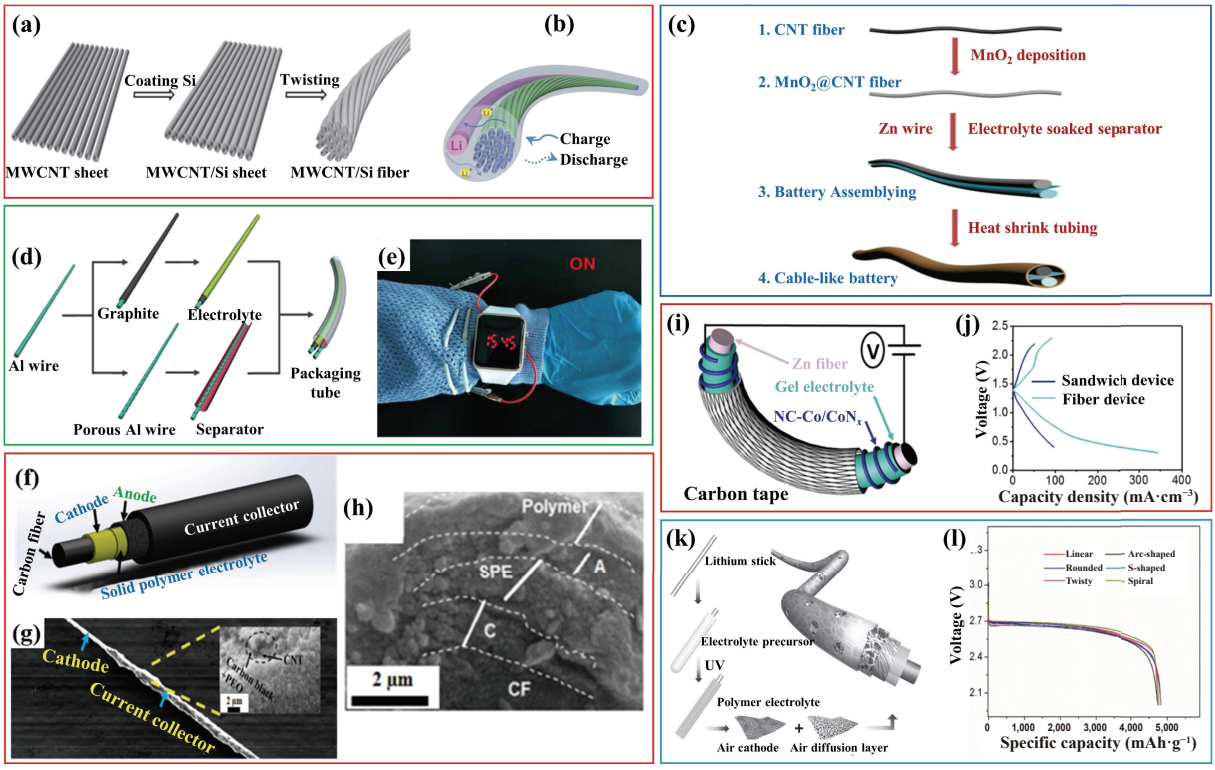

Figure 10 (a) Schematic illustration to the preparation of an aligned MWCNT/Si composite fiber and (b) schematic illustration of a LIB based on the composite fiber (reproduced with permission from Ref. [211], © Wiley-VCH Verlag GmbH & Co. KGaA, Weinheim 2014). (c) Schematic of the preparation of a Zn-MnO_2 cable battery (reproduced with permission from Ref. [212], © American Chemical Society 2018). (d) Schematic illustration of the fabrication of a fiber-shaped dual-ion battery and (e) illustration of the battery in a wearable watch (reproduced with permission from Ref. [213], © Elsevier Ltd. 2019). (f) Schematic of a microsized fiber-shaped LIB, (g) SEM images of the battery fiber, and (h) SEM image of the cross-section of the battery fiber (reproduced with permission from Ref. [215], © American Chemical Society 2019). (i) Schematic representation of a fiber-shaped solid-state Zn-air battery and (j) discharge and charge polarization curves of a fiber-shaped and a sandwich-type Zn-air batteries (reproduced with permission from Ref. [216], © Elsevier B.V. 2018). (k) Schematic representation of the fabrication of a cable-type Li-O_2 battery and (l) discharge curves of the battery at various bended and twisted conditions (reproduced with permission from Ref. [217], © Wiley-VCH Verlag GmbH & Co. KGaA, Weinheim 2016).

structure typical of a CEB (Fig. 10(h)). As a result, this battery showed a high rate capability with a discharge areal capacity of 3.1 μAh·cm^{-2} at 26 μA·cm^{-2} vs. that of 4.2 μAh·cm^{-2} at 13 μA·cm^{-2} Moreover, the battery maintained its good galvanostatic discharge performance during bending tests, indicating its potential applications for flexible and wearable devices.

Furthermore, Guan et al. developed a solid-state flexible ZAB of CEBs by using a Zn microwire as anode, NC-Co/CoN_x nanoarrays on carbon microfiber as cathode, and a GPE in between (Fig. 10(i)) [216]. The NC-Co/CoN_x cathode was prepared by uniformly growing Co decorated nitrogen-doped carbon (NC-Co) nanoarrays from an aqueous mixture containing $C_4H_6N_2$ and $Co(NO_3)_2$ on a carbon microfiber, followed by partially converting Co to CoN_x under Ar/NH_3. Thereafter, the proposed fiber-shaped ZAB was constructed by coating the Zn microwire anode with a KOH and ZnO containing GPE, followed by wrapping the NC-Co/CoN_x fiber cathode around the GPE surface and finally sealing the resultant device with a piece of carbon tape. For comparison, a sandwich-type ZAB was fabricated by attaching a Zn foil as anode and NC-Co/CoN_x nanoarrays on CC as cathode on the two sides of a GPE membrane, respectively. Compared with the conventional sandwich-type ZAB, the fiber-shaped ZAB achieved a similar open circuit potential (1.4 V) but a narrower voltage gap between charge and discharge curves (Fig. 10(j)), exhibiting its enhanced reaction reversibility. Furthermore, the fiber-shaped ZAB delivered a higher maximum discharge current density (344 vs. 96.6 mA·cm^{-3}) and a higher power density (104.0 vs. 41.5 mW·cm^{-3}) than its sandwich-type counterpart, demonstrating its enhanced electrochemical properties. The uniform electric field formed between the two electrodes and the intimate contact between multiple components of the CEB structure should be responsible for these enhancements. Significantly, when two such fiber-shaped ZABs were connected in series, they could power a LED under flat and bent states, showing the excellent flexibility of the battery. Indeed, the advantages of the fiber-shaped structure over sandwich-like one in enhancing the electrochemical performance (especially volumetric) and flexibility for batteries have been emphasized previously [210].

Moreover, the CEB configuration has been demonstrated by Liu et al. with a higher-energy system of LABs [217]. As shown in Fig. 10(k), a lithium stick was first coated with a $LiCF_3SO_3$-HMPP/ETPTA/P(VdF-HFP) GPE, followed by warping the as-formed GPE membrane with a SP loaded CT as the air cathode and then a NF as the air diffusion layer. As a result, when tested at 100 mA·g^{-1} with a capacity limitation of 500 mAh·g^{-1}, the resultant LAB showed a discharge voltage at above 2.0 V for more than 90 cycles, corroborating its good cycling performance. Surprisingly, this fiber-shaped battery showed almost unchanged discharge –charge curves under different bending and twisting conditions (Fig. 10(l)) or upon bending-stretching between 16 and 8 cm for 4,000 cycles, exhibiting its excellent deformability.

As discussed above, based on their differences in electrode structure, device configuration, and fabrication process, 1D fiber-shaped batteries have been realized in various configurations, including SHEBs, HHEBs, PEBs, and CEBs with varied pros and cons. However, fiber-shaped batteries share a common problem, in which their internal resistance would increase upon the increase in length of the fiber electrodes. Batteries with film-shaped

electrodes would be able to solve this issue, as discussed below.

4.2 2D batteries

Macroscopically, all 2D batteries have a film-shaped appearance in common. Depending on their variations in electrode and cell structures, however, these batteries can be classified into four categories, namely unit-film batteries (UFBs), grid-pattern batteries (GPBs), island-pattern batteries (IPBs), and coplanar-electrode batteries (CPEBs). These 2D batteries can be fabricated to possess a high bendability, stretchability, and even transparency.

4.2.1 UFBs

A UFB is usually fabricated by stacking all component layers (including anode, cathode, electrolyte, separator, and protective encapsulation/packaging materials) into a sandwich structure. Compared with fiber-shaped batteries, UFBs are easier to fabricate and more adoptable to the existing battery manufacturing technologies. In this context, UFBs have gain considerable research efforts [65, 69, 76]. Furthermore, owing to their mature manufacturing technologies, LIBs have been frequently used to fabricate flexible UFBs. Koo et al. developed a LIB of UFBs by sandwiching a solid-state lithium phosphorus oxynitride (LiPON) electrolyte between a LCO (on Ni alloy current collector) cathode and a Li metal anode along with PDMS as the protective encapsulation multilayers (Fig. 11(a)), displaying a specific capacity of 99 μAh·cm^{-2} at a bending radius of 3.1 mm, very close to the value for the nonbending state (106 μAh·cm^{-2}) [29]. In another study, Hu et al. used a slurry coating process to coat LCO and LTO onto CNT films, respectively, and used the resultant LCO/CNT cathode and LTO/CNT anode to assemble a LIB with a $LiPF_6$-EC/DEC electrolyte and a paper separator (Fig. 11(c)) [218]. Also with the slurry coating process, Kammoun et al. prepared a Graphite@Cu anode and a LCO@Al cathode film electrodes, respectively, and incorporated the as-prepared electrodes into a LIB with a solid-state graphene-oxide embedded $LiClO_4$-PEO electrolyte (Fig. 11(e)) [219]. These thin-film LIBs were highly flexible and showed well-defined electrochemical performance and good sustainability under bending conditions (Figs. 11(b), 11(d), and 11(f)).

Beyond LIBs, UFBs were also demonstrated with higher-energy systems. In this regard, Guo et al. fabricated a flexible LAB by stacking a rGO coated CP as air cathode, a molten Li loaded rGO film as anode, and a GPE containing LiTFSI, LiI, and SiO_2 nanoparticles in a typical sandwich structure, as shown in Fig. 11(g) [220]. When charged/discharged at 100 mA·g^{-1} with a fixed capacity of 1,000 mAh·g^{-1}, the LAB thus constructed could steadily run for 100 cycles with a small average voltage gap of ~ 1.45 V and almost unchanged voltage curves after bending to 0°, 45°, 90°, 135°, 180° and 360°, respectively (Fig. 11(h)), demonstrating the good stability of the proposed LAB of UFBs under mechanical deformations.

4.2.2 GPBs

As shown in Fig. 11(i), a GPB is constructed by confining electrode materials and metal current collectors beneath inside a grid trench with a certain pattern on a transparent substrate to fabricate electrodes, followed by incorporating two of such grid-patterned electrodes to sandwich a transparent electrolyte. Flexibility of GPBs stems from the use of highly flexible transparent substrates. More importantly, by adjusting the feature dimension and areal portion of the grid trenches of the electrode, it is possible to endow GPBs with a unique function of transparency. Indeed, flexible and transparent batteries have been attracting more and more attentions for the development of

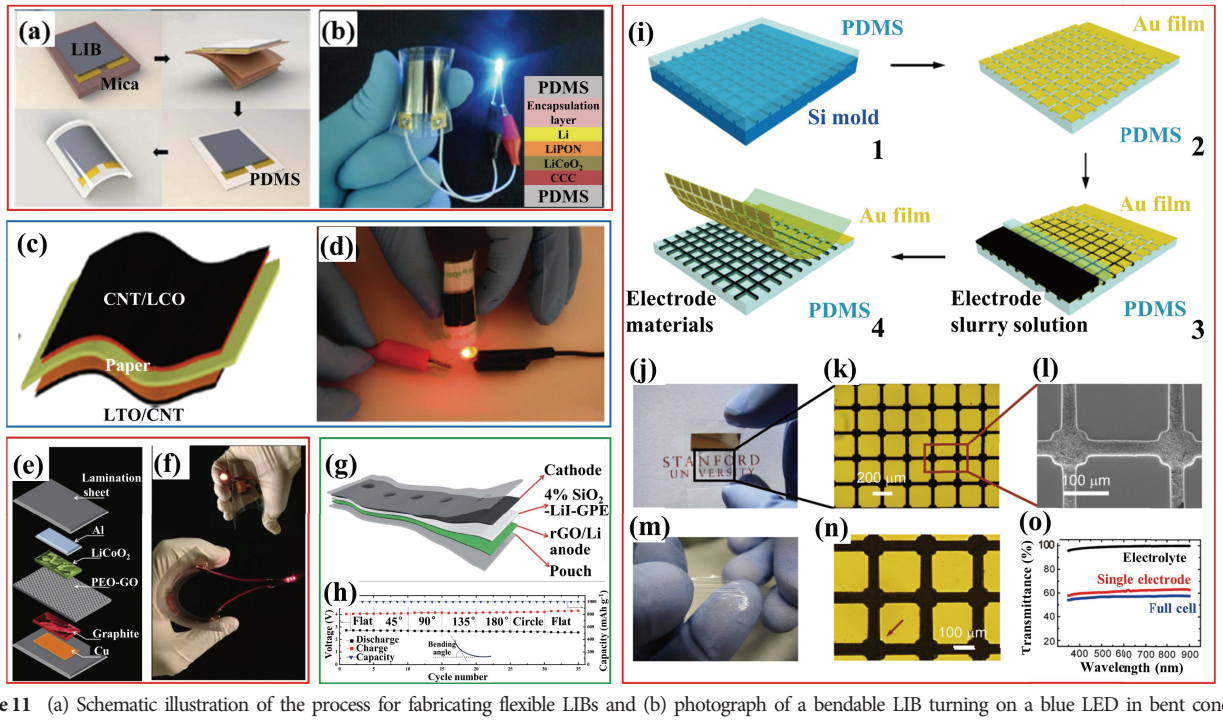

Figure 11 (a) Schematic illustration of the process for fabricating flexible LIBs and (b) photograph of a bendable LIB turning on a blue LED in bent condition (reproduced with permission from Ref. [29], © American Chemical Society 2012). (c) Schematic of a paper Li-ion battery and (d) a bent battery lights an LED device (reproduced with permission from Ref. [218], © American Chemical Society 2010). (e) Schematics of the configuration and materials of a flexible LIB and (f) the LIB powers an LED upon bending (reproduced with permission from Ref. [219], © The Royal Society of Chemistry 2015). (g) Schematic illustration of a flexible belt-shaped Li-air battery and (h) cycling performance of the battery at a current density of 100 mA·g^{-1} and a fixed capacity of 1,000 mAh·g^{-1} under different bending conditions (reproduced with permission from Ref. [220], © The Royal Society of Chemistry 2018). (i) Schematic illustration of the fabrication of a transparent battery, (j) image of the transparent and flexible battery electrode, (k) magnified optical image and (l) SEM image of the battery electrode, (m) optical microscopic image of gel electrolyte, (n) optical microscopic image of the full battery, and (o) UV–VIS spectra of gel electrolyte, a single electrode, and a full battery (reproduced with permission from Ref. [224], © National Academy of Sciences 2011).

transparent and semi-transparent flexible electronics, such as optical circuits, cellphones, displays, and touch panels [221–223]. Since most of the electrode materials in conventional batteries are not transparent, GPBs thus represent a promising strategy to make these opaque materials into transparent batteries for the emerging technologies of transparent flexible electronics. In this regard, Yang et al. used this GPB strategy to demonstrate the first transparent flexible battery, as illustrated in Fig. 11(i) [224]. Specifically, a PDMS precursor was first spin-coated onto a photolithography-patterned silicon mold to create grid trenches on the PDMS substrate thus formed, followed by evaporating a 100 nm-thick gold film onto PDMS as the current collector. Using a microfluidics-assisted method, electrode material slurries containing active material (LMO or LTO), SP conductive additive, and styrene-butadiene-rubber (SBR) binder were filled into the grid trenches of the PDMS substrates to form a LMO cathode and a LTO anode, respectively. Finally, the proposed GPB was assembled by sandwiching a $LiClO_4$-P(VdF-HFP) GPE with the LMO cathode and the LTO anode and sealing the resultant cell inside a highly transparent poly(vinyl chloride) (PVC) thermoplastic bag. The battery thus assembled delivered an energy density of 10 $Wh{\cdot}L^{-1}$ based on all components. More importantly, the grid-patterned electrode materials were indistinguishable from the transparent substrates (Fig. 11(j)) due to the small size of these "material lines" (Figs. 11(k) and 11(l)) being less than the resolution of human eyes (50–100 μm). Also, the GPE used was highly transparent (transmittance: 99%, Figs. 11(m) and 11(o)), the areal portion of trenches was low (35%, corresponding to a high transparency of 65%, Fig. 11(o)), and the mismatch between the well-aligned cathode and anode was small (3–5 μm, Fig. 11(n)). These factors made the resultant battery transparent, having a transmittance up to 57% (Fig. 11(o)). On the other hand, due to the high flexibility of PDMS and the presence of SP particles in electrode materials that could bridge cracked Au pieces if formed upon the bending of the battery, the as-prepared electrodes showed a sheet resistance less than 100 $\Omega{\cdot}sq^{-1}$ even after bending with a radius of 2 cm for 100 cycles (comparing to a value of 60 $\Omega{\cdot}sq^{-1}$ under the flat state), indicating the good bendability of the battery. In fact, the GPB thus fabricated could light up a LED and showed negligible capacity degradation under bending conditions.

4.2.3 IPBs

The concept of IPBs can be dated back to the year of 2004 when Wagner et al. proposed a stretchable electronic system, in which replicated cells are interconnected with flexible and stretchable metallization in a certain pattern on a stretchable substrate, as shown in Fig. 12(a) [225]. In this design, the cells (like islands) were made sufficiently rigid to protect them from breaking and were electrically connected by stretchable metal interconnects on a stretchable substrate (like the sea), enabling the entire system to accommodate mechanical deformations without loading severe stress on individual cells. Therefore, the system thus constructed is characteristic of excellent stretchability.

Xu et al. made this concept into reality along with a further improved structure called "self-similar" serpentine (Figs. 12(b)–12(d)) [226]. Specifically, using a slurry coating method, LCO and LTO were coated on current collector pads (Al for cathode and Cu for anode) on flexible Si wafer substrates to make the cathode and anode, respectively (Fig. 12(c)). Incorporating the cathode and anode thus fabricated to sandwich a $LiClO_4$-PEO GPE resulted in a typical IPB, which delivered a capacity density of ~ 1.1 $mAh{\cdot}cm^{-2}$ at 0.5 C. More importantly, all individual cells on the flexible silicone substrates were electrically connected by metal interconnects (Al for cathode and Cu for anode), forming a self-similar serpentine structure at two levels, i.e., smaller serpentines of the first level joining together to form a larger serpentine at the second level (Fig. 12(d)). When the system was stretched, the second level serpentine expanded along the stretching direction, and the first level serpentines began to expand after the collapse of the second level serpentine. Such a two-level expansion of serpentines offered a great opportunity to release the stress on individual cells and thus an excellent stretchability for the battery. Consequently, the resultant IPB possessed a reversible stretchability up to 300%, much higher than that of film-stacked batteries (e.g., 150% for a film-stacked battery based on a CNT/Li($Ni_{1/3}Co_{1/3}Mn_{1/3}$)O_2 (NCM) film cathode and a CNT/LTO film anode [227]). The IPB maintained its capacity density of ~ 1.1 $mAh{\cdot}cm^{-2}$ at 0.5 C even under a 300% uniaxial strain state and could work properly to power a LED while biaxially stretched to 300%, folded, twisted, or mounted on the human elbow (Figs. 12(e)–12(h)).

4.2.4 Coplanar-electrode batteries (CPEBs)

Unlike the sandwich structure of UFBs, GPBs and IPBs, a CPEB is constructed by a coplanar configuration in which anodes and cathodes are interdigitatedly positioned on a same plane. In the absence of the large thickness of a stacked sandwich structure, CPEBs can be fabricated in a thin-film manner to enhance the bending tolerance of batteries. This thin-structure design, further, enables CPEBs to have the capability of increasing their cell voltage by in series-connecting multiple single cells. In this context, Kim et al. have developed a LIB of CPEBs (Fig. 12(i)) [228]. Specifically, via slurry casting, a graphite anode on Cu foil and a $LiNi_{0.8}Co_{0.15}Al_{0.05}O_2$ (NCA) cathode on Al foil were fabricated, respectively, followed by punching off the cathode and anode thus fabricated into fork-shaped patterns. Subsequently, the patterned cathode and anode were coplanar cross-attached onto a PP/Al/Nylon pouch with barriers between the electrodes, followed by inserting the formed cell into a sealing tap. The assembly process was finalized by injecting a $LiPF_6$-P(VdF-HFP) GPE into the pouch, followed by a vacuum sealing process to obtain a thin film LIB (Fig. 12(j)). By so doing, the resultant LIB had a very thin thickness of 0.5 mm only. Also, for demonstration, two single cells (3.7 V each) were connected in series to achieve a high voltage of 7.4 V for the prototype LIB (Fig. 12(i)). More importantly, the barriers between electrodes could efficiently release the stress under bending to avoid the disruptions on electrode materials to ensure a good bendability for the battery. In fact, the as-assembled coplanar LIB displayed a stable discharge performance to power six LEDs even after being bent in the end-to-end distance between 45 and 10 mm for 5,000 cycles.

As discussed above, by changing the electrode structure and cell configuration, 2D film-shaped batteries have been developed with varied function features. Particularly, among all 2D batteries, UFBs are the easiest to fabricate and most adoptable to the existing battery manufacturing technologies. They have a low resistance as well as high energy/power densities and have been used for some applications, such as wearable smart watches and roll-up displays. However, the thick stacked structure of UFBs indicates their difficulty in releasing the stress under mechanical deformations, and thus limiting their bendability and especially stretchability [34]. GPBs are bendable and transparent and can provide power for flexible transparent electronics. However, an acceptable light transmittance of GPBs will require a relatively low areal portion of trenches for electrodes, unfortunately sacrificing their energy and power densities. IPBs are highly stretchable and are good power sources for flexible electronics. However, like GPBs, IPBs have low energy and power densities largely due to their low mass loadings of active materials. Use of higher-capacity electrode materials

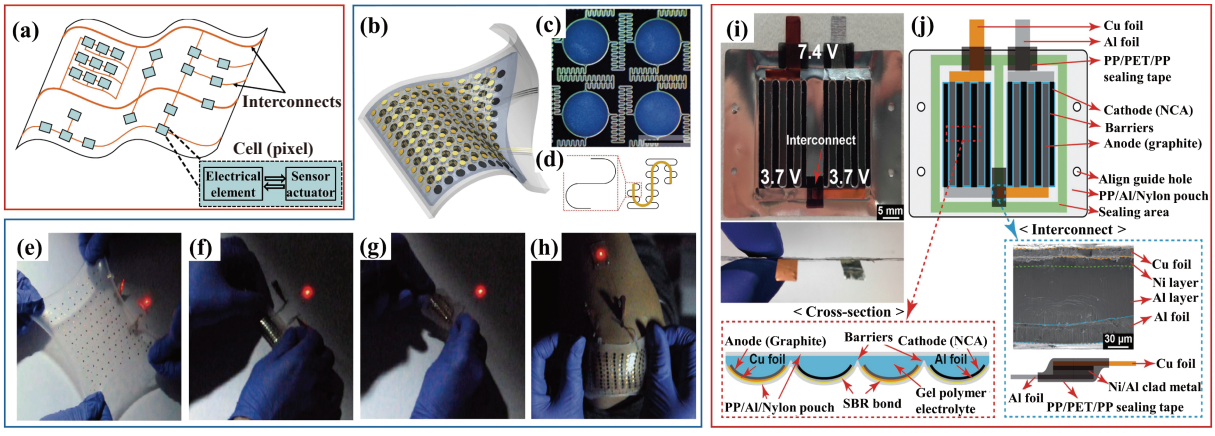

Figure 12 (a) Concept of a stretchable electronic system (reproduced with permission from Ref. [225], © Elsevier B.V. 2004). (b) Schematic illustration of an IPB, (c) optical image of Al electrode pads and self-similar interconnects on a Si wafer, (d) schematic illustration of "self-similar" serpentine geometries used for the interconnects (yellow: 1st level serpentine; black: 2nd level serpentine), and a stretchable IPB lighting up a LED while (e) biaxially stretched to 300%, (f) folded, (g) twisted, and (h) mounted on the human elbow (reproduced with permission from Ref. [226], © Xu, S. et al. 2013). (i) Top-viewed and cross-sectional photographs of a coplanar flexible battery in which two of 3.7 V cells are connected in series and (j) schematic illustration of the coplanar flexible battery (reproduced with permission from Ref. [228], © American Chemical Society 2015).

and/or higher-energy battery systems would be able to overcome the low energy/power issues of GPBs and IPBs. CPEBs have an excellent bendability and can be integrated with flexible thin electronics, such as smart cards and medical patches. However, compared with sandwich-type batteries, the limited rate of CPEBs due to a long distance between cathode and anode needs to be addressed to strengthen their practical application capabilities. The use of 2D batteries as building blocks to construct 3D structural flexible batteries has been demonstrated to be efficient to further enhance the deformability, and hence suitability of batteries for practical applications.

4.3 3D batteries

3D batteries have been devised with various configurations, such as serpentine patterns [229], spine-like structures [30], and origami and kirigami structures [230, 231]. Li et al. used stiff materials to make compliant thin film patterns as platforms for stretchable electronics [229]. This concept can be well illustrated by a piece of paper cut into a serpentine (Fig. 13(a)). When the paper was stretched at two ends, the initial planar serpentine could elongate by twisting out of plane to accommodate the elongation (Fig. 13(b)). In fact, it has been shown that serpentine metal interconnects on elastomeric substrates can sustain more than 200 cycles of elongation by 25% [232]. These studies offered a scheme that could be used to incorporate stiff UFBs through appropriate patterning to fabricate 3D stretchable batteries.

Inspired by the animal spine with robust mechanical strength and high flexibility, Qian et al. fabricated a spine-like flexible LIB via a scalable process (Fig. 13(c)) [30]. Specifically, a sandwich-structure LIB assembled with a LCO/Al foil cathode, a graphite/Cu foil anode, a Celgard 2500 separator, and a $LiPF_6$-EC/DEC electrolyte was first cut into designed straps, followed by wrapping the as-prepared cell straps to form a spine-like battery. In this integrated design, the cell energy density was determined by the longitudinal percentage of vertebral stacks compared to the whole length. In fact, a high energy density over 85% of a conventional prismatic cell was achieved for the spine-like battery. More importantly, with the spine structure of the battery, the major function of the thick and rigid segments corresponding to the vertebras was storing energy, while that of the thin, unwound, and flexible parts was serving as marrow to interconnect all vertebra-like stacks together to provide flexibility for the entire system, ensuring an excellent deformability for the battery. During a cycling test at 0.2 C for 100 cycles, flexing and twisting were applied between flat states on the battery (Fig. 13(d)), i.e., 10,000 times of flexing with a bending diameter of 20 mm and 1,000 times of twisting with a twisting angle of 90°. At the end of these tests, the battery displayed a discharge capacity retention over 94.3% (initial capacity: 151.4 $mAh \cdot g^{-1}$) with a Coulombic efficiency above 99.9%, demonstrating its excellent bendability and twistability.

Origami and kirigami are interesting structures that have been exploited to fabricate flexible batteries with high linear and areal deformabilities. In this regard, Song et al. incorporated an origami design to demonstrate foldable, bendable and twistable LIBs [230]. In order to ensure the stable electrochemical characteristics of batteries under mechanical deformations, flexible CNT-coated paper was utilized as the current collector to load LCO and LTO to fabricate the cathode and anode, respectively. Film-shaped batteries based on these electrodes were assembled with a $LiFP_6$-EC/DMC/DEC electrolyte and a Celgard 2500 separator, followed by folding the as-assembled batteries into the origami patterns, as shown in Fig. 13(e), in which many identical parallelogram faces were connected by "mountain" and "valley" creases. The angles between adjacent "mountain" and "valley" creases made the Miura-ori either almost completely compressible in one direction (lower left of Fig. 13(e), referred to as "45° Miura folding") or collapsible in two directions (lower right of Fig. 13(e), referred to as "90° Miura folding"). Therefore, when folded or stretched, the pre-defined creases and collapses of the resultant origami LIBs could accommodate the deformation changes, that is, the stain only occurred at the creases while the base or substrate material at parallelograms maintained strain free. Consequently, the origami LIBs could deliver a stable power output even in a linearly deformed (1,300%), twisted (10.8° per cm), or bent (0.83 cm) state (Figs. 13(f)– 13(h)). Furthermore, the same research group demonstrated stretchable LIBs using the concept of kirigami [231]. Specifically, as illustrated in Fig. 13(i), the batteries were prepared by folding and cutting a planar battery (consisting of a LCO/Al foil cathode, a graphite/Cu foil anode, a Celgard 2500 separator, and a $LiPF_6$-EC/DMC/DEC electrolyte) according to different kirigami patterns. In these structures, fracture due to cutting and folding was suppressed by plastic rolling, which provided kirigami LIBs with excellent electrochemical and mechanical characteristics. As a result, the resultant kirigami batteries achieved a great stretchability over 150% and showed a stable discharge plateau of 3.7 V under both compacted and stretched states. Using the LIB with cut-N-twist pattern as an example (Fig. 13(i)(2)), it showed a

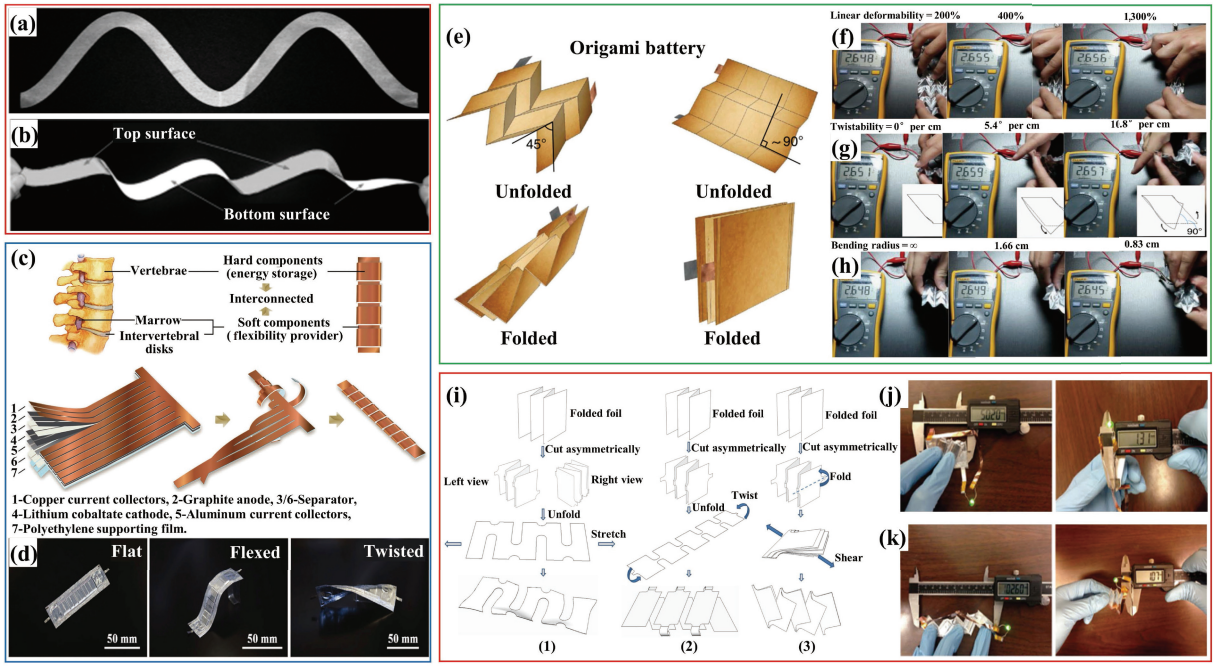

Figure 13 (a) A paper serpentine and (b) the serpentine structure offers stretchability (reproduced with permission from Ref. [229], © Materials Research Society 2005). (c) Schematic representation of the fabrication of a spine-like battery and (d) optical images of the battery in the state of flat, flexed, and twisted (reproduced with permission from Ref. [30], © Wiley-VCH Verlag GmbH & Co. KGaA, Weinheim 2018). (e) Two examples of origami LIBs using Miura folding, photos of an origami LIB while it is in the state of (f) linear deformed, (g) twisted, and (h) bent (reproduced with permission from Ref. [230], © Song, Z. et al. 2014). (i) Illustrations of three kirigami patterns: (1) zigzag-cut pattern, (2) cut-N-twist pattern, and (3) cut-N-shear pattern, photographs of a LIB with cut-N-twist pattern at its (j) most compact state and (k) most stretched state (reproduced with permission from Ref. [231], © Song, Z. et al. 2015).

capacity retention over 85% after charged/discharged at 1/3 C for 100 cycles while experienced mixed states of both compact and stretched (Figs. 13(j) and 13(k)).

As can be seen from above discussions, through their diversities in electrode structures and device fabrication processes, flexible batteries can be devised into multiple dimensions from 1D fiber-shaped, 2D film-shaped, to 3D structures. Particularly, 1D batteries have been realized in various configurations of SHEBs, HHEBs, PEBs, and CEBs with varied pros and cons. 2D batteries have been fabricated in UFBs, GPBs, IPBs, and CPEBs with different function strengths on bendability, stretchability, and even transparency. With appropriate configurations, 2D film-shaped batteries can be further assembled into 3D batteries. Since only a small portion is against deformation while the majority remaining strain free in the resultant structures, 3D batteries possess further enhanced mechanical deformability and thus greater practical application capability for flexible and wearable electronics. Overall, flexible batteries in multiple dimensions from 1D to 3D have gained considerable achievements in recent years and have been exploited for practical applications, as discussed in detail below.

5 Applications of flexible batteries

Though still in their early stage, flexible batteries have shown great potential for various practical applications and have begun to be integrated into prototype flexible and wearable electronic products, such as Philips fluid flexible smartphone, Samsung flexible prototype display windows, and the incoming Apple flexible i-phones [9]. Flexible batteries are indispensable power sources for various objects with varied motion modes, such as moving [231, 233–240] and rolling [241, 242]. Indeed, along with the extraordinary progresses accomplished in battery chemistries/materials, constituent components, and device configurations as discussed in earlier sections, many application concepts and even prototypes have been demonstrated with flexible batteries for marketing. To this end, this section will elaborate the applications of flexible batteries in accordance with their configurations from 1D, 2D, to 3D.

5.1 Applications of 1D batteries

With their unique fiber-shaped structures, 1D batteries are promising flexible power sources for wearable electronics. In this emerging field, while LIBs play the predominant role, other battery systems have also been attracting considerable attention in recent years. Though having various specific configurations (as detailed in Section 4.1), fiber-shaped 1D batteries can be either knitted/integrated with existing cloths/fabrics or directly woven into textiles without any additional substrates [205].

In the first approach, fiber-shaped 1D batteries are readily knitted/integrated with existing flexible cloths/fabrics (as substrates) to fabricate power textiles. In this regard, Liu et al. [233] incorporated a frequently studied couple of materials (i.e., LTO and LFP) with PEO to prepare hybrid fibers as the anode and cathode, respectively, and incorporated the as-prepared fiber electrodes with a mixed lithium salt-containing PEO/PEG GPE to assemble fiber-shaped LIBs in the configuration of PEBs. For application demonstration, the resultant LIB stripes were successfully knitted with fabrics to make a power textile (Fig. 14(a)). In a more recent study, Zhang et al. [234] reported newly-developed aqueous LIBs of PEBs based on a PI/CNT hybrid fiber anode, a LMO/CNT hybrid fiber cathode, and an aqueous Li_2SO_4 electrolyte, possessing a high energy density of 48.93 $Wh{\cdot}kg^{-1}$ and a high power density of 10,217.74 $W{\cdot}kg^{-1}$, and knitted the fiber-shaped LIBs thus assembled with fabrics to fabricate a flexible energy textile (Fig. 14(b)(1)). The resultant energy textile showed excellent electrochemical performance and mechanical stability under bending, folding, and twisting conditions (Figs. 14(b)(2)– 14(b)(5)), demonstrating its great potential for wearable applications. Beyond LIBs, higher-energy systems have also been exploited for fiber-shaped battery-integrated power textiles. In this regard, Fang et al. [235] integrated a fabric with cable-shaped LSBs of PEBs assembled from a Li wire anode, a

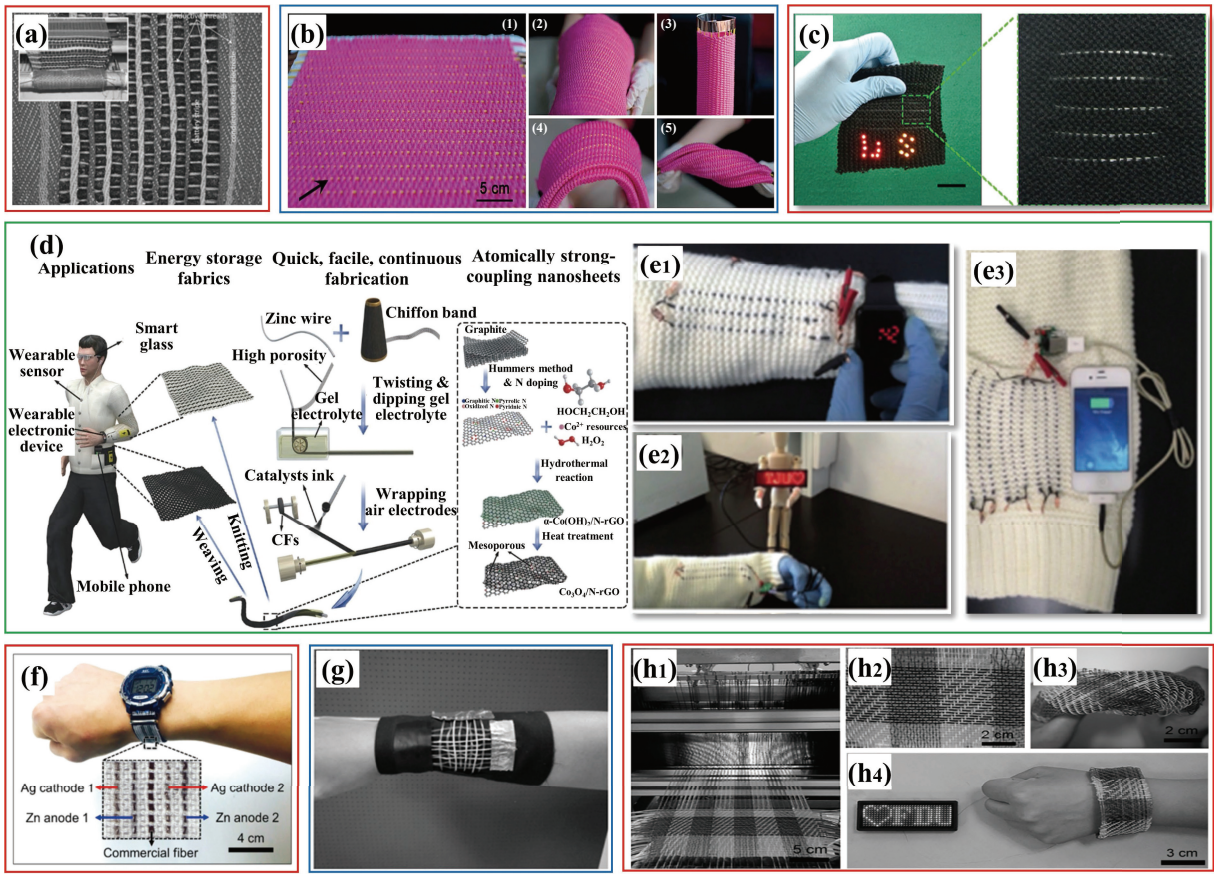

Figure 14 (a) A fabric knitted with LIB stripes (reproduced with permission from Ref. [233], © The Electrochemical Society 2012). (b) An energy textile woven with flexible LIBs under bending, folding, and twisting ((1) to (5) correspond to the states before and after different deformations) (reproduced with permission from Ref. [234], © The Royal Society of Chemistry 2016). (c) A fabric integrated with cable-shaped lithium sulfur batteries (reproduced with permission from Ref. [235], © Wiley-VCH Verlag GmbH & Co. KGaA, Weinheim 2016). (d) Schematic representation of the fabrication process of a flexible fiber-shaped ZAB and (e) the ZABs knitted with a cloth as power source (reproduced with permission from Ref. [236], © Wiley-VCH Verlag GmbH & Co. KGaA, Weinheim 2018). (f) A photograph of two serial connected Ag-Zn yarn batteries woven in a textile watch strap (reproduced with permission from Ref. [237], © Lee, J. M. et al. 2018). (g) Fiber-shaped LIBs woven into a textile (reproduced with permission from Ref. [238], © Wiley-VCH Verlag GmbH & Co. KGaA, Weinheim 2014). (h1) A photograph showing the process of fiber-shaped Si-O_2 batteries being woven into a textile, and photographs of the textile (h2) before and (h3) after twisting and (h4) lighting up an LED screen under deformations (reproduced with permission from Ref. [239], © Wiley-VCH Verlag GmbH & Co. KGaA, Weinheim 2017).

sulfur-loaded carbon nanostructured hybrid fiber cathode, and a LiTFSI/$LiNO_3$-DOL/DME electrolyte to fabricate a stretchable power textile (Fig. 14(c)). Li et al. fabricated fiber-shaped ZABs in the structure of SHEB by using a Zn wire as core anode, which was wrapped with a chiffon band separator and a KOH-PVA GPE and finally wound by Co_3O_4/N-rGO coated CFs as air cathode [236]. The resultant ZABs showed a high volumetric energy density of 36.1 mWh·cm^{-3}, maintained their stable performance when charged/discharged under various deformations (bending, recovering, and knotting), and could be knitted and woven into textiles for wearable devices, as shown in Fig. 14(d). Indeed, three in-series-connected ZABs (15 cm in length) were successfully knitted into a cloth to power a watch (Fig. 14(e1)) or a LED screen (Fig. 14(e2)), and three in-parallel-connected ZAB sets (each set contained three ZABs in-series) were knitted to charge an Iphone 4S (Fig. 14(e3)). More recently, Lee et al. [237] developed silver-zinc batteries of SHEBs based on a Zn nanoparticles/CNT hybrid yarn abode, an Ag nanofiber/CNT hybrid yarn cathode, and a KOH-PVA GPE and successfully integrated the resultant yarn batteries into a textile watch strap (Fig. 14(f)).

Unlike the aforementioned integration process, the second approach is to directly weave fiber-shaped 1D batteries into power textiles without a substrate. To this end, Ren et al. [238] prepared stretchable fiber-shaped LIBs of PEBs from an aligned MWCNT/$LiTi_2O_5$ composite yarn anode, a MWCNT/LMO composite yarn cathode, and a LiTFSI-PEO GPE. The LIBs thus assembled delivered an energy density of 27 Wh·kg^{-1} (17.7 mWh·cm^{-3}) and a power density of 880 W·kg^{-1} (0.56 W·cm^{-3}) and maintained their capacity at 97% after 1,000 bending cycles. When fabricated into a spring structure, these batteries could keep 84% of their capacity even after stretching at a strain of 100% for 200 cycles. More importantly, these fiber-shaped LIBs were successfully woven into lightweight, flexible, and stretchable battery textiles (Fig. 14(g)), demonstrating their excellent potential for large-scale flexible applications. In a more recent study, Zhang et al. [239] developed silicon-oxygen batteries (SOBs) in the configuration of CEB by wrapping a GPE-coated lithiated silicon/CNT hybrid fiber inner anode with a bare CNT sheet outer cathode. The resultant fiber-shaped batteries had a high energy density of 512 Wh·kg^{-1} and could work efficiently even after bending (i.e., changing the distance between two ends of the battery fiber from the original length of 8 to 1 cm) for 20,000 cycles. As a result of their ultrathin diameter of 500 μm, SOB fibers thus prepared were successfully woven into flexible battery textiles (Fig. 14(h1)), which exhibited great mechanical deformabilities including bendability, foldability, and twistability (Figs. 14(h2) and 14(h3)) and could light up a commercial LED screen under deformations (Fig. 14(h4)). This work provided a promising strategy for the development of high-energy-density wearable power textiles.

As can be seen, fiber-shaped 1D batteries can be knitted/integrated with existing cloths/fabrics or directly woven

into textiles without a substrate. The resultant power textiles by the former approach have robust mechanical strengths but relatively low energy densities due to the presence of inactive substrates in the system, while those by the latter approach have the opposite properties. Thus, to fabricate a power textile for a specific application, a good balance between its power supply and mechanical property should be carefully evaluated prior to the selection of a suitable knitting/weaving method. Moreover, the diversities of a vast of battery materials/systems allow the fabrication of fiber-shaped 1D batteries with appropriate properties to meet the application demands for various wearable electronics.

5.2 Applications of 2D and 3D batteries

While fiber-shaped 1D batteries are promising for wearable applications, film-shaped 2D and 3D structural batteries have found more suitability for large-scale flexible electronics, such as displays, touch panels and even robots. To this end, the diverse device configurations and versatile deformable properties of 2D and 3D batteries (as discussed in Sections 4.2 and 4.3, respectively) have provided them with great opportunities for practical applications.

In this context, Tajima et al. developed a flexible film-shaped LIB to power a wrist-wearable display [241]. With the configuration of UFB, the LIB was fabricated from a LFP coated Al foil cathode, a graphite coated Cu foil anode, a plastic film separator, and a Li salt containing organic electrolyte, followed by sealing the as-assembled battery with an embossed Al laminate film (providing strong resistance to deformations). The obtained thin film battery was successfully served as a power source to power a flexible organic LED panel and a flexible printed circuit of a wrist-wearable display as shown in Fig. 15(a). The battery was thin (2.1 mm), flexible, and robust, which could bear severe bending up to 10,000 cycles without obvious changes in electrochemical characteristics and mechanical properties, showing its brilliant suitability for flexible electronic systems. In another demonstration study, Kim et al. fabricated large-scale flexible battery modules via IPBs strategy (Fig. 15(b)) [242]. Specifically, the flexible electrodes used were prepared by casting LTO and LFP slurries on Ni-coated polyester textiles as anode and cathode, respectively. The single LIBs based on these electrodes were fabricated in a sandwich structure with a $LiPF_6$-EC/DMC electrolyte and a polyurethane separator, possessing a cell voltage of 1.8 V and a capacity of 25 mAh. Connecting the as-assembled batteries via a IPBs strategy resulted in a battery module, whose overall voltage and capacity could be tuned by modulating the connections to meet the requirement for a designed application, for example, to power a rollable display or an outdoor tent as shown in Fig. 15(b). Importantly, due to the inherent flexibility of the textile electrodes and the IPBs strategy employed, the obtained batteries and battery modules could efficiently release the stress generated from folding and rolling, able to provide a stable power for their applications. This work clearly demonstrated the effectiveness of flexible electrodes and IPBs design in fabricating flexible power sources for the practical applications of flexible electronics.

With their further enhanced mechanical deformability compared to 2D batteries, 3D batteries are practically useful to provide power for flexible and wearable electronics. In this regard, during its application demonstration, the 3D kirigami battery developed by Song et al. [231], as shown in Fig. 13(i), has been successfully integrated to power a Samsung Gear 2 smart watch (Fig. 15(c)). Importantly, due to its great stretchability enabled by the kirigami design, the battery could be stably discharged at 48 mA for one hour even under stretched states, showing its great potential for the practical applications for wearable electronics.

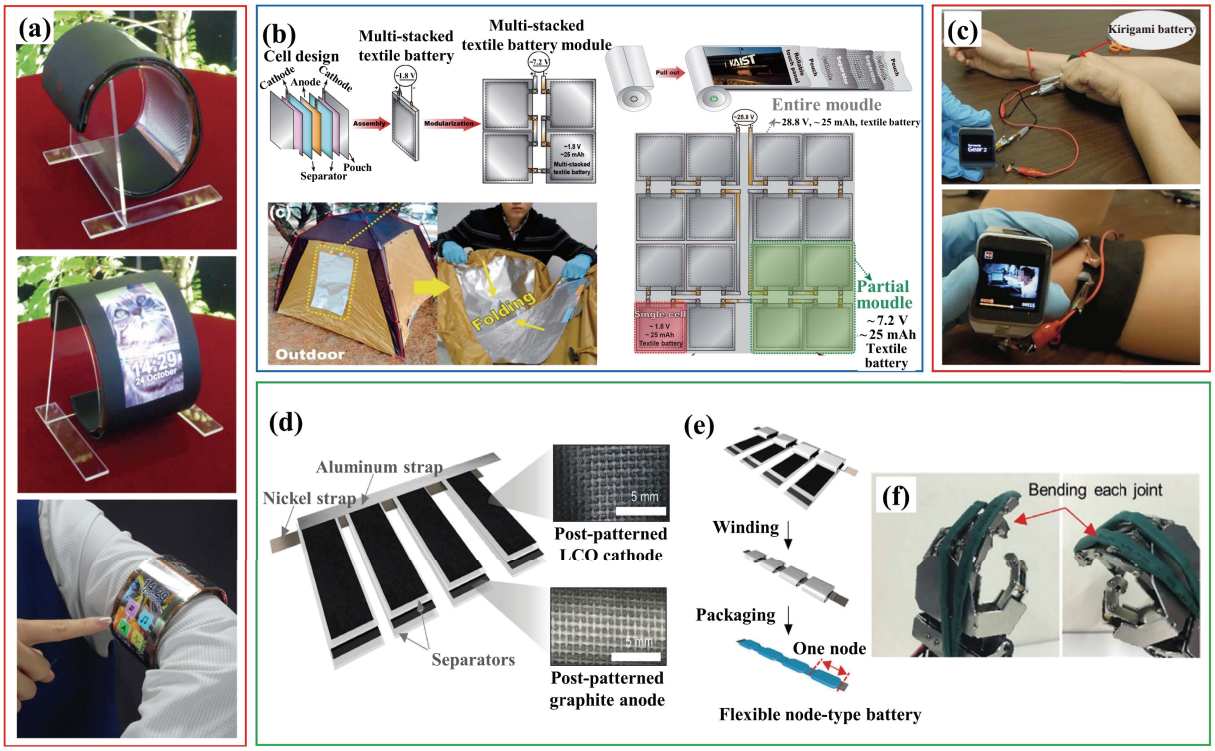

Figure 15 (a) A prototype wrist-wearable display powered by a flexible LIB (reproduced with permission from Ref. [241], © Society for Information Display 2014). (b) Schematic illustration of the fabrication process of flexible textile batteries and battery modules as well as their applications for a rollable display and an outdoor tent (reproduced with permission from Ref. [242], © The Royal Society of Chemistry 2014). (c) A kirigami battery powering a Samsung Gear 2 smart watch (reproduced with permission from Ref. [231], © Song, Z. et al. 2015). (d) Schematic of node-type LIBs components, showing digital photographs of the postpatterned LCO and graphite electrodes, (e) cell assembly process, showing that each planar electrode can be wound and packaged as a node cell, and (f) Node-type LIBs embedded on each joint of a robotic hand (reproduced with permission from Ref. [240], © Wiley-VCH Verlag GmbH & Co. KGaA, Weinheim 2017).

Moreover, under some circumstances, such as robots, it is necessary for batteries to be able to sustain deformations in multiple directions. 3D flexible batteries are particularly promising power sources to satisfy this stringent requirement. In this context, Park et al. demonstrated a new class of 3D flexible node-type LIBs by winding postpatterned electrodes on metal straps [240]. Specifically, the graphite/Cu foil anode and LCO/Al foil cathode prepared from a conventional slurry coating process were further subjected to a unique imprinting/patterning process (Fig. 15(d)). Thereafter, the postpatterned anode and cathode thus prepared were welded and wound on the Ni strap and Al strap, respectively, to construct node cells with a stacked structure consisting of PE separator, anode, PE separator, and cathode (Fig. 15(e)), followed by impregnating the resultant cells with a $LiPF_6$-EC/DMC/DEC electrolyte. In this novel design, the node-type LIBs were composed of energy-storage sections and deformable sections, which is similar to an island bridge design reported previously [31]. As a result, owing to the electrode postpatterning and thus the enhanced adhesion between the metal current collector and the coating layer, the node-type LIBs achieved a high linear capacity (6.9 $mAh \cdot cm^{-1}$ at 0.5 C), a high rate capability (capacity retained at 60% at 5 C), and an enhanced cycling stability (capacity retained at 79% after 200 cycles at 1 C). More importantly, the unique segmental design consisting of the energy-storage sections and the deformable sections of these batteries ensured their excellent flexibility, showing stable electrochemical performance even after 3,000 flexing cycles. Moreover, for a practical application, the node-type LIBs could be embedded in a humanoid robotic hand, which allowed the integrated batteries to be flexed along with the bending motion of joints (Fig. 15(f)), demonstrating the excellent multi-directional deformability of 3D batteries.

As discussed above, flexible batteries have demonstrated great potential for practical applications and have been integrated into prototype flexible and wearable electronic products. The multiple dimensions of flexible batteries from 1D to 3D provide them with great opportunities for various applications. While 1D batteries are promising for wearable electronics, 2D and 3D batteries are more attractive for large-scale flexible applications. Moreover, 3D batteries are especially useful for applications under multi-directional deformations.

6 Conclusion and outlook

In the past decade, we have witnessed the tremendous progresses in the research and development of flexible batteries for flexible and wearable electronic devices. In order for flexible batteries to have both high electrochemical performances (including high energy, high power, great safety, and long cycle life) and excellent mechanical deformabilities (such as bendability, foldability, stretchability, compressibility, and twistability), four pivotal aspects of the battery, namely battery constituent components, battery chemistry systems, battery device configurations, and practical applications, should be thoroughly considered. Aiming at this goal, in the present review, we have systematically and comprehensively discussed the fundamentals and recent advancements of flexible batteries.

First, it is of great importance to have high flexibility and deformability for the four essential constituent components (cathode, anode, electrolyte, and separator) of flexible batteries to ensure their stable power supply under mechanical deformations. Specifically, for the fabrication of flexible electrodes, an ideal current collector should have the properties of high flexibility, high electrical conductivity, low weight, and strong surface adhesion with electrode materials. Among the three frequently studied current collector materials (metals, polymers and carbonaceous materials), carbonaceous materials have shown distinct superiorities to meet these requirements and will play a more important role in the future development of flexible electrodes and batteries. Due to the potential evaporation and leakage of liquid electrolytes, development of flexible solid state electrolytes (GPEs, SPEs, and CPEs) possessing the properties of nontoxicity, non-flammability, and no leakage has become a significant strategy to ensure the sustainability and safety of flexible batteries under deformations. Nevertheless, the relatively lower ionic conductivity of solid state electrolytes compared to their liquid counterparts needs to be further enhanced, which indeed stands for an important future research direction for solid state electrolytes.

Second, in addition to the predominant role of LIBs, a large variety of battery chemistry systems have been extensively researched and developed into the emerging field of flexible batteries. The introduction of SIBs and PIBs as potential alternatives to LIBs is determined by the lower cost and richer abundance of sodium and potassium resources than lithium, while that of LMBs, LSBs, and MABs is spurred by their higher energy. Nevertheless, in spite of their high-energy advantage, LMBs, LSBs, and MABs remain some challenges. In particular, the practical applications of flexible LMBs and LSBs have been significantly hindered by the safety and cycling issues of lithium anode induced by the growth of lithium dendrites, large volume evolution of hostless lithium, and low Coulombic efficiency of lithium plating/stripping. Solid state electrolytes have gained considerable research interests to address these issues and will continue to be an important research direction for flexible LMBs and LSBs. Moreover, another challenge remained for LSBs is associated with the shortcomings of sulfur cathode including the low electrical conductivities of sulfur and its discharge product, the dissolution of lithium polysulfides, and the large volumetric expansion of sulfur during lithiation. With their excellent properties of high electrical conductivity, flexibility, chemical stability, and mechanical strength, carboneous materials have been demonstrated to be efficient in compositing with sulfur to develop flexible electrodes to address these issues. In flexible MABs, the achievement of good flexibility and well-defined electrocatalytic activity for air cathodes is an important task and also a challenge. Among many substrate materials studied, a new family of carbonaceous materials without metal catalysts but doped with heteroatoms have become promising ORR/OER bifunctional catalysts for rechargeable MABs. Along with their advantages of low cost, abundant resources, high electrocatalytic activity, and excellent flexibility, these meta-free carbon electrocatalysts will play a more and more important role for flexible MABs.

Third, device configuration has a significant impact on both mechanical and electrochemical properties of flexible batteries. Based on their difference in electrode structure and device fabrication process, flexible batteries can be devised in multiple dimensions from 1D fiber-shaped, 2D film-shaped, to 3D structural, generating a large variety of opportunities for various deformation circumstances. Specifically, 1D batteries have been realized in a range of configurations of SHEBs, HHEBs, PEBs, and CEBs with varied pros and cons. With their unique fiber-shaped structures, 1D batteries are promising flexible power sources for wearable electronics by either knitting with existing cloths/fabrics or directly weaving into textiles without any additional substrates. The resultant power textiles by the former approach have robust mechanical strengths but relatively low energy densities due to the presence of inactive substrates in the system, while those by the latter approach have the opposite properties. Therefore, to fabricate a power textile for a specific application, the knitting/weaving methods to be selected should be carefully

evaluated to ensure a good balance between its power supply and mechanical property. Moreover, 1D batteries share a common issue, that is, their internal resistance would increase upon the increase in length of their fiber electrodes. To this end, highly electrical conductive yet flexible current collectors/substrates, such as carboneous materials, are efficient for the fabrication of conductive and flexible fiber electrodes with a reasonably long length for high-performance fiber-shaped batteries. 2D batteries have been fabricated in UFBs, GPBs, IPBs, and CPEBs with different function strengths on bendability, stretchability, and even transparency. UFBs have the advantages of easy fabrication and adoptability to the existing battery manufacturing process but show limited deformability due to their thick stacked structure. In contrast, GPBs are highly bendable (and transparent) and IPBs are highly stretchable. Nevertheless, because of their low mass loadings of active materials, GPBs and IPBs have low energy and power densities, to which use of high-capacity electrode materials and/or high-energy battery systems implies a good strategy for future GPBs and IPBs. CPEBs possess an excellent bendability but a limited rate performance. Thus, a future challenge for CPEBs lies in shortening the distance between cathode and anode (to boost the rate) while maintaining their unique coplanar configuration (to ensure high bendability). Unlike the fibered-structures of 1D batteries, the film-shaped structures of 2D batteries make them more suitable for applications in flexible electronics. Moreover, 2D batteries have been successfully employed as building blocks to construct 3D batteries. In the resultant 3D structures, since only a small portion is against deformation while the majority remaining strain free, 3D batteries possess further enhanced mechanical deformability and hence greater capability for practical applications in flexible and wearable electronics.

Finally, although still being in their early years and having many issues to be addressed prior to their entry into marketplace, flexible batteries have shown great potential for practical applications and have been integrated into prototype flexible and wearable electronic products. Indeed, the multiple dimensions from 1D to 3D of flexible batteries provide them with versatile opportunities to meet the demands for various deformation scenarios. Specifically, while 1D batteries are promising for wearable applications, 2D and 3D batteries have more suitability for large-scale flexible electronics, and further, 3D batteries are specifically useful for those application circumstances where multi-directional deformations usually exist.

Therefore, through the extraordinary advancements accomplished in the past and the extensive research under development on the pivotal aspects of battery chemistries/materials, constituent components, and device configurations, high-performance flexible batteries possessing both well-defined electrochemical characteristics and excellent mechanical deformatities as well as their prosperous applications as flexible power sources for flexible and wearable electronic devices would be anticipated in the near future.

Acknowledgements

The authors thank our colleagues for their contributions to the work cited. We are also grateful for financial support from The Special Significant Science and Technology Program of Yunnan Province (No. 2016HE001-2016HE002).

References

[1] Li, W. G.; Guo, J. H.; Fan, D. L. 3D graphite-polymer flexible strain sensors with ultrasensitivity and durability for real-time human vital sign monitoring and musical instrument education. *Adv. Mater. Technol.* **2017**, *2*, 1700070.

[2] Lee, J.; Kwon, H.; Seo, J.; Shin, S.; Koo, J. H.; Pang, C.; Son, S.; Kim, J. H.; Jang, Y. H.; Kim, D. E. et al. Conductive fiber-based ultrasensitive textile pressure sensor for wearable electronics. *Adv. Mater.* **2015**, *27*, 2433–2439.

[3] Xie, K. Y.; Wei, B. Q. Materials and structures for stretchable energy storage and conversion devices. *Adv. Mater.* **2014**, *26*, 3592–3617.

[4] Zhai, Q. F.; Xiang, F. W.; Cheng, F.; Sun, Y. J.; Yang, X. P; Lu, W.; Dai, L. M. Recent advances in flexible/stretchable batteries and integrated devices. *Energy Storage Mater.* **2020**, *33*, 116–138.

[5] He, Y. H.; Matthews, B.; Wang, J. Y.; Song, L.; Wang, X.; Wu, G. Innovation and challenges in materials design for flexible rechargeable batteries: From 1D to 3D. *J. Mater. Chem. A* **2018**, *6*, 735–753.

[6] Kong, L.; Tang, C.; Peng, H. J.; Huang, J. Q.; Zhang, Q. Advanced energy materials for flexible batteries in energy storage: A review. *SmartMat* **2020**, *1*, e1007.

[7] Zeng, L. C.; Qiu, L.; Cheng, H. M. Towards the practical use of flexible lithium ion batteries. *Energy Storage Mater.* **2019**, *23*, 434–438.

[8] Yang, Y. A mini-review: Emerging all-solid-state energy storage electrode materials for flexible devices. *Nanoscale* **2020**, *12*, 3560–3573.

[9] Bocchetta, P.; Frattini, D.; Ghosh, S.; Mohan, A. M. V.; Kumar, Y.; Kwon, Y. Soft materials for wearable/flexible electrochemical energy conversion, storage, and biosensor devices. *Materials* **2020**, *13*, 2733.

[10] Lin, L. Y.; Ning, H. M.; Song, S. F.; Xu, C. H.; Hu, N. Flexible electrochemical energy storage: The role of composite materials. *Compos. Sci. Technol.* **2020**, *192*, 108102.

[11] Qian, G. Y.; Liao, X. B.; Zhu, Y. X.; Pan, F.; Chen, X.; Yang, Y. Designing flexible lithium-ion batteries by structural engineering. *ACS Energy Lett.* **2019**, *4*, 690–701.

[12] Tao, T.; Lu, S. G.; Chen, Y. A review of advanced flexible lithium-ion batteries. *Adv. Mater. Technol.* **2018**, *3*, 1700375.

[13] Foreman, E.; Zakri, W.; Sanatimoghaddam, M. H.; Modjtahedi, A.; Pathak, S.; Kashkooli, A. G.; Garafolo, N. G.; Farhad, S. A review of inactive materials and components of flexible lithium-ion batteries. *Adv. Sustainable Syst.* **2017**, *1*, 1700061.

[14] Zhao, Y. F.; Guo, J. C. Development of flexible Li-ion batteries for flexible electronics. *InfoMat* **2020**, *2*, 866–878.

[15] Liu, Y.; Sun, Z. H.; Tan, K.; Denis, D. K.; Sun, J. F.; Liang, L. W.; Hou, L. R.; Yuan, C. Z. Recent progress in flexible non-lithium based rechargeable batteries. *J. Mater. Chem. A* **2019**, *7*, 4353–4382.

[16] Zhang, E. J.; Jia, X. X.; Wang, B.; Wang, J.; Yu, X. Z.; Lu, B. G. Carbon dots@rGO paper as freestanding and flexible potassium-ion batteries anode. *Adv. Sci.* **2020**, *7*, 2000470.

[17] Duan, H.; Yin, Y. X.; Zeng, X. X.; Li, J. Y.; Shi, J. L.; Shi, Y.; Wen, R.; Guo, Y. G.; Wan, L. J. *In-situ* plasticized polymer electrolyte with double-network for flexible solid-state lithium-metal batteries. *Energy Storage Mater.* **2018**, *10*, 85–91.

[18] Wang, Z. H.; Pan, R. J.; Sun, R.; Edström, K.; Strømme, M.; Nyholm, L. Nanocellulose structured paper-based lithium metal batteries. *ACS Appl. Energy Mater.* **2018**, *1*, 4341–4350.

[19] Wu, N.; Shi, Y. R.; Lang, S. Y.; Zhou, J. M.; Liang, J. Y.; Wang, W.; Tan, S. J.; Yin, Y. X.; Wen, R.; Guo, Y. G. Self-healable solid polymeric electrolytes for stable and flexible lithium metal batteries. *Angew. Chem., Int. Ed.* **2019**, *58*, 18146–18149.

[20] Wang, C. Y.; Zheng, Z. J.; Feng, Y. Q.; Ye, H.; Cao, F. F.; Guo, Z. P. Topological design of ultrastrong MXene paper hosted Li enables ultrathin and fully flexible lithium metal batteries. *Nano Energy* **2020**, *74*, 104817.

[21] Gong, Y. H.; Fu, K.; Xu, S. M.; Dai, J. Q.; Hamann, T. R.; Zhang, L.; Hitz, G. T.; Fu, Z. Z.; Ma, Z. H.; McOwen, D. W. et al. Lithium-ion conductive ceramic textile: A new architecture for flexible solid-state lithium metal batteries. *Mater. Today* **2018**, *21*, 594–601.

[22] Wang, S. J.; Xiong, P.; Zhang, J. Q.; Wang, G. X. Recent progress on flexible lithium metal batteries: Composite lithium metal anodes and solid-state electrolytes. *Energy Storage Mater.* **2020**, *29*,

310–331.
[23] Wang, Z. S.; Xu, X. J.; Ji, S. M.; Liu, Z. B.; Zhang, D. C.; Shen, J. D.; Liu, J. Recent progress of flexible sulfur cathode based on carbon host for lithium-sulfur batteries. *J. Mater. Sci. Technol.* **2020**, *55*, 56–72.
[24] Peng, H. J.; Huang, J. Q.; Zhang, Q. A review of flexible lithium-sulfur and analogous alkali metal-chalcogen rechargeable batteries. *Chem. Soc. Rev.* **2017**, *46*, 5237–5288.
[25] Gao, Y.; Guo, Q. Y.; Zhang, Q.; Cui, Y.; Zheng, Z. J. Fibrous materials for flexible Li-S battery. *Adv. Energy Mater.* **2021**, *11*, 2002580.
[26] Ye, L.; Hong, Y.; Liao, M.; Wang, B. J.; Wei, D. C.; Peng, H. S.; Ye, L.; Hong, Y.; Liao, M.; Wang, B. et al. Recent advances in flexible fiber-shaped metal-air batteries. *Energy Storage Mater.* **2020**, *28*, 364–374.
[27] Zhou, J. W.; Cheng, J. L.; Wang, B.; Peng, H. S.; Lu, J. Flexible metal–gas batteries: A potential option for next-generation power accessories for wearable electronics. *Energy Environ. Sci.* **2020**, *13*, 1933–1970.
[28] Kwon, Y. H.; Woo, S. W.; Jung, H. R.; Yu, H. K.; Kim, K.; Oh, B. H.; Ahn, S.; Lee, S. Y.; Song, S. W.; Cho, J. et al. Cable-type flexible lithium ion battery based on hollow multi-helix electrodes. *Adv. Mater.* **2012**, *24*, 5192–5197.
[29] Koo, M.; Park, K. I.; Lee, S. H.; Suh, M.; Jeon, D. Y.; Choi, J. W.; Kang, K.; Lee, K. J. Bendable inorganic thin-film battery for fully flexible electronic systems. *Nano Lett.* **2012**, *12*, 4810–4816.
[30] Qian, G. Y.; Zhu, B.; Liao, X. B.; Zhai, H. W.; Srinivasan, A.; Fritz, N. J.; Cheng, Q.; Ning, M. Q.; Qie, B. Y.; Li, Y. et al. Bioinspired, spine-like, flexible, rechargeable lithium-ion batteries with high energy density. *Adv. Mater.* **2018**, *30*, 1704947.
[31] Wen, L.; Li, F.; Cheng, H. M. Carbon nanotubes and graphene for flexible electrochemical energy storage: From materials to devices. *Adv. Mater.* **2016**, *28*, 4306–4337.
[32] Kim, S. W.; Cho, K. Y. Current collectors for flexible lithium ion batteries: A review of materials. *J. Electrochem. Sci. Technol.* **2015**, *6*, 1–6.
[33] Li, Q.; Ardebili, H. Flexible thin-film battery based on solid-like ionic liquid-polymer electrolyte. *J. Power Sources* **2016**, *303*, 17–21.
[34] Gockeln, M.; Glenneberg, J.; Busse, M.; Pokhrel, S.; Mädler, L.; Kun, R. Flame aerosol deposited $Li_4Ti_5O_{12}$ layers for flexible, thin film all-solid-state Li-ion batteries. *Nano Energy* **2018**, *49*, 564–573.
[35] Jeon, H.; Cho, I.; Jo, H.; Kim, K.; Ryou, M. H.; Lee, Y. M. Highly rough copper current collector: Improving adhesion property between a silicon electrode and current collector for flexible lithium-ion batteries. *RSC Adv.* **2017**, *7*, 35681–35686.
[36] Wang, C.; Cao, Y. H.; Luo, Z. P.; Li, G. Z.; Xu, W. L.; Xiong, C. X.; He, G. Q.; Wang, Y. D.; Li, S.; Liu, H. et al. Flexible potassium vanadate nanowires on Ti fabric as a binder-free cathode for high-performance advanced lithium-ion battery. *Chem. Eng. J.* **2017**, *307*, 382–388.
[37] Zhao, J.; Ren, H.; Liang, Q. H.; Yuan, D.; Xi, S. B.; Wu, C.; Manalastas, W. Jr.; Ma, J. M.; Fang, W.; Zheng, Y. et al. High-performance flexible quasi-solid-state zinc-ion batteries with layer-expanded vanadium oxide cathode and zinc/stainless steel mesh composite anode. *Nano Energy* **2019**, *62*, 94–102.
[38] Zhang, Y.; Wang, L.; Guo, Z. Y.; Xu, Y. F.; Wang, Y. G.; Peng, H. S. High-performance lithium-air battery with a coaxial-fiber architecture. *Angew. Chem., Int. Ed.* **2016**, *55*, 4487–4491.
[39] Lee, K. L.; Jung, J. Y.; Lee, S. W.; Moon, H. S.; Park, J. W. Electrochemical characteristics of a-Si thin film anode for Li-ion rechargeable batteries. *J. Power Sources* **2004**, *129*, 270–274.
[40] Kim, Y. L.; Sun, Y. K.; Lee, S. M. Enhanced electrochemical performance of silicon-based anode material by using current collector with modified surface morphology. *Electrochim. Acta* **2008**, *53*, 4500–4504.
[41] Park, M. H.; Noh, M.; Lee, S.; Ko, M.; Chae, S.; Sim, S.; Choi, S.; Kim, H.; Nam, H.; Park, S. et al. Flexible high-energy Li-ion batteries with fast-charging capability. *Nano Lett.* **2014**, *14*, 4083–4089.
[42] Zhao, Z. X.; Wu, H. Q. Monolithic integration of flexible lithium-ion battery on a plastic substrate by printing methods. *Nano Res.* **2019**, *12*, 2477–2484.
[43] Yun, J. H.; Han, G. B.; Lee, Y. M.; Lee, Y. G.; Kim, K. M.; Park, J. K.; Cho, K. Y. Low resistance flexible current collector for lithium secondary battery. *Electrochem. Solid-State Lett.* **2011**, *14*, A116.
[44] Choi, J. Y.; Lee, D. J.; Lee, Y. M.; Lee, Y. G.; Kim, K. M.; Park, J. K.; Cho, K. Y. Silicon nanofibrils on a flexible current collector for bendable lithium-ion battery anodes. *Adv. Funct. Mater.* **2013**, *23*, 2108–2114.
[45] Wang, J. Z.; Chou, S. L.; Chen, J.; Chew, S. Y.; Wang, G. X.; Konstantinov, K.; Wu, J.; Dou, S. X.; Liu, H. K. Paper-like free-standing polypyrrole and polypyrrole-$LiFePO_4$ composite films for flexible and bendable rechargeable battery. *Electrochem. Commun.* **2008**, *10*, 1781–1784.
[46] Nyholm, L.; Nyström, G.; Mihranyan, A.; Strømme, M. Toward flexible polymer and paper-based energy storage devices. *Adv. Mater.* **2011**, *23*, 3751–3769.
[47] Aliahmad, N.; Liu, Y. D.; Xie, J.; Agarwal, M. V_2O_5/graphene hybrid supported on paper current collectors for flexible ultrahigh-capacity electrodes for lithium-ion batteries. *ACS Appl. Mater. Interfaces* **2018**, *10*, 16490–16499.
[48] Yehezkel, S.; Auinat, M.; Sezin, N.; Starosvetsky, D.; Ein-Eli, Y. Bundled and densified carbon nanotubes (CNT) fabrics as flexible ultra-light weight Li-ion battery anode current collectors. *J. Power Sources* **2016**, *312*, 109–115.
[49] Yitzhack, N.; Auinat, M.; Sezin, N.; Ein-Eli, Y. Carbon nanotube tissue as anode current collector for flexible Li-ion batteries-understanding the controlling parameters influencing the electrochemical performance. *APL Mater.* **2018**, *6*, 111102.
[50] Sun, L. M.; Wang, X. H.; Wang, Y. R.; Zhang, Q. Roles of carbon nanotubes in novel energy storage devices. *Carbon* **2017**, *122*, 462–474.
[51] Jia, L. J.; Wang, J.; Chen, Z. J.; Su, Y. P.; Zhao, W.; Wang, D. T.; Wei, Y.; Jiang, K. L.; Wang, J. P.; Wu, Y. et al. High areal capacity flexible sulfur cathode based on multi-functionalized super-aligned carbon nanotubes. *Nano Res.* **2019**, *12*, 1105–1113.
[52] Hori, K.; Yamada, Y.; Momma, T.; Noda, S. High-energy density Li_xSi-S full cell based on 3D current collector of few-wall carbon nanotube sponge. *Carbon* **2020**, *161*, 612–621.
[53] Zhou, Z. Y.; Si, W. P.; Lu, P. Y.; Guo, W. L.; Wang, L.; Zhang, T.; Hou, F.; Liang, J. A flexible CNT@nickel silicate composite film for high-performance sodium storage. *J. Energy Chem.* **2020**, *47*, 29–37.
[54] Lu, H. R.; Hagberg, J.; Lindbergh, G.; Cornell, A. $Li_4Ti_5O_{12}$ flexible, lightweight electrodes based on cellulose nanofibrils as binder and carbon fibers as current collectors for Li-ion batteries. *Nano Energy* **2017**, *39*, 140–150.
[55] Kong, L.; Peng, H. J.; Huang, J. Q.; Zhang, Q. Review of nanostructured current collectors in lithium-sulfur batteries. *Nano Res.* **2017**, *10*, 4027–4054.
[56] Yang, H.; Wang, M.; Liu, X. W.; Jiang, Y.; Yu, Y. MoS_2 embedded in 3D interconnected carbon nanofiber film as a free-standing anode for sodium-ion batteries. *Nano Res.* **2018**, *11*, 3844–3853.
[57] Chen, X.; Zhao, Z.; Zhou, Y.; Shu, Y.; Sajjad, M.; Bi, Q. S.; Ren, Y.; Wang, X.; Zhou, X. W.; Liu, Z. MWCNTs modified α-Fe_2O_3 nanoparticles as anode active materials and carbon nanofiber paper as a flexible current collector for lithium-ion batteries application. *J. Alloys Compd.* **2019**, *776*, 974–983.
[58] Kretschmer, K.; Sun, B.; Xie, X. Q.; Chen, S. Q.; Wang, G. X. A free-standing $LiFePO_4$-carbon paper hybrid cathode for flexible lithium-ion batteries. *Green Chem.* **2016**, *18*, 2691–2698.
[59] Yuan, Z.; Peng, H. J.; Huang, J. Q.; Liu, X. Y.; Wang, D. W.; Cheng, X. B.; Zhang, Q. Hierarchical free-standing carbon-nanotube paper electrodes with ultrahigh sulfur-loading for lithium-sulfur batteries. *Adv. Funct. Mater.* **2014**, *24*, 6105–6112.
[60] Cao, Z. X.; Zhang, J.; Ding, Y. M.; Li, Y. L.; Shi, M. J.; Yue, H. Y.; Qiao, Y.; Yin, Y. H.; Yang, S. T. *In situ* synthesis of flexible elastic N-doped carbon foam as a carbon current collector and interlayer for high-performance lithium sulfur batteries. *J. Mater. Chem. A* **2016**, *4*, 8636–8644.

[61] Yang, L. Y.; Li, H. Z.; Cheng, L. Z.; Li, S. T.; Liu, J.; Min, J.; Zhu, K. J.; Wang, H.; Lei, M. A three-dimensional surface modified carbon cloth designed as flexible current collector for high-performance lithium and sodium batteries. *J. Alloys Compd.* **2017**, *726*, 837–845.
[62] Rana, K.; Singh, J.; Lee, J. T.; Park, J. H.; Ahn, J. H. Highly conductive freestanding graphene films as anode current collectors for flexible lithium-ion batteries. *ACS Appl. Mater. Interfaces* **2014**, *6*, 11158–11166.
[63] Liu, Y.; Yao, M. J.; Zhang, L. L.; Niu, Z. Q. Large-scale fabrication of reduced graphene oxide-sulfur composite films for flexible lithium-sulfur batteries. *J. Energy Chem.* **2019**, *38*, 199–206.
[64] Wu, Z. P.; Wang, Y. L.; Liu, X. B.; Lv, C.; Li, Y. S.; Wei, D.; Liu, Z. F. Carbon-nanomaterial-based flexible batteries for wearable electronics. *Adv. Mater.* **2019**, *31*, 1800716.
[65] Noerochim, L.; Wang, J. Z.; Chou, S. L.; Wexler, D.; Liu, H. K. Free-standing single-walled carbon nanotube/SnO_2 anode paper for flexible lithium-ion batteries. *Carbon* **2012**, *50*, 1289–1297.
[66] Zhu, P.; Yan, C. Y.; Zhu, J. D.; Zang, J.; Li, Y.; Jia, H.; Dong, X.; Du, Z.; Zhang, C. M.; Wu, N. Q. et al. Flexible electrolyte-cathode bilayer framework with stabilized interface for room-temperature all-solid-state lithium-sulfur batteries. *Energy Storage Mater.* **2019**, *17*, 220–225.
[67] Wang, K.; Luo, S.; Wu, Y.; He, X. F.; Zhao, F.; Wang, J. P.; Jiang, K. L.; Fan, S. S. Super-aligned carbon nanotube films as current collectors for lightweight and flexible lithium ion batteries. *Adv. Funct. Mater.* **2013**, *23*, 846–853.
[68] Wang, Y.; Kong, D. Z.; Huang, S. Z.; Shi, Y. M.; Ding, M.; Von Lim, Y.; Xu, T. T.; Chen, F. M.; Li, X. J.; Yang, H. Y. 3D carbon foam-supported WS_2 nanosheets for cable-shaped flexible sodium ion batteries. *J. Mater. Chem. A* **2018**, *6*, 10813–10824.
[69] Chong, W. G.; Xiao, Y. H.; Huang, J. Q.; Yao, S. S.; Cui, J.; Qin, L.; Gao, C.; Kim, J. K. Highly conductive porous graphene/sulfur composite ribbon electrodes for flexible lithium-sulfur batteries. *Nanoscale* **2018**, *10*, 21132–21141.
[70] Zhong, Y. T.; Pan, Z. H.; Wang, X. S.; Yang, J.; Qiu, Y. C.; Xu, S. Y.; Lu, Y. T.; Huang, Q. M.; Li, W. S. Hierarchical Co_3O_4 nano-micro arrays featuring superior activity as cathode in a flexible and rechargeable zinc-air battery. *Adv. Sci.* **2019**, *6*, 1802243.
[71] Wang, Z. F.; Li, H. F.; Tang, Z. J.; Liu, Z. X.; Ruan, Z. H.; Ma, L. T.; Yang, Q.; Wang, D. H.; Zhi, C. Y. Hydrogel electrolytes for flexible aqueous energy storage devices. *Adv. Funct. Mater.* **2018**, *28*, 1804560.
[72] Li, Z.; Borodin, O.; Smith, G. D.; Bedrov, D. Effect of organic solvents on Li^+ ion solvation and transport in ionic liquid electrolytes: A molecular dynamics simulation study. *J. Phys. Chem. B* **2015**, *119*, 3085–3096.
[73] Howlett, P. C.; Brack, N.; Hollenkamp, A. F.; Forsyth, M.; MacFarlane, D. R. Characterization of the lithium surface in *N*-methyl-*N*-alkylpyrrolidinium bis(trifluoromethanesulfonyl)amide room-temperature ionic liquid electrolytes. *J. Electrochem. Soc.* **2006**, *153*, A595–A606.
[74] Kuang, Y. D.; Chen, C. J.; Pastel, G.; Li, Y. J.; Song, J. W.; Mi, R. Y.; Kong, W. Q.; Liu, B. Y.; Jiang, Y. Q.; Yang, K. et al. Conductive cellulose nanofiber enabled thick electrode for compact and flexible energy storage devices. *Adv. Energy Mater.* **2018**, *8*, 1802398.
[75] Kong, D. Z.; Wang, Y.; Huang, S. Z.; Von Lim, Y.; Zhang, J.; Sun, L. F.; Liu, B.; Chen, T. P.; Valdivia y Alvarado, P.; Yang, H. Y. Surface modification of $Na_2Ti_3O_7$ nanofibre arrays using N-doped graphene quantum dots as advanced anodes for sodium-ion batteries with ultra-stable and high-rate capability. *J. Mater. Chem. A* **2019**, *7*, 12751–12762.
[76] Chang, J.; Shang, J.; Sun, Y. M.; Ono, L. K.; Wang, D. R.; Ma, Z. J.; Huang, Q. Y.; Chen, D. D.; Liu, G. Q.; Cui, Y. et al. Flexible and stable high-energy lithium-sulfur full batteries with only 100% oversized lithium. *Nat. Commun.* **2018**, *9*, 4480.
[77] Wang, J.; Zhang, L.; Zhou, Q. W.; Wu, W. L.; Zhu, C.; Liu, Z. Q.; Chang, S. Z.; Pu, J.; Zhang, H. G. Ultra-flexible lithium ion batteries fabricated by electrodeposition and solvothermal synthesis. *Electrochim. Acta* **2017**, *237*, 119–126.
[78] Zhang, W.; Liu, Y. T.; Chen, C. J.; Li, Z.; Huang, Y. H.; Hu, X. L. Flexible and binder-free electrodes of Sb/rGO and $Na_3V_2(PO_4)_3$/rGO nanocomposites for sodium-ion batteries. *Small* **2015**, *11*, 3822–3829.
[79] Pan, R. J.; Cheung, O.; Wang, Z. H.; Tammela, P.; Huo, J. X.; Lindh, J.; Edström, K.; Strømme, M.; Nyholm, L. Mesoporous *Cladophora* cellulose separators for lithium-ion batteries. *J. Power Sources* **2016**, *321*, 185–192.
[80] Pan, R. J.; Wang, Z. H.; Sun, R.; Lindh, J.; Edström, K.; Strømme, M.; Nyholm, L. Thickness difference induced pore structure variations in cellulosic separators for lithium-ion batteries. *Cellulose* **2017**, *24*, 2903–2911.
[81] Leijonmarck, S.; Cornell, A.; Lindbergh, G.; Wågberg, L. Single-paper flexible Li-ion battery cells through a paper-making process based on nano-fibrillated cellulose. *J. Mater. Chem. A* **2013**, *1*, 4671–4677.
[82] Kim, J. H.; Kim, J. H.; Kim, J. M.; Lee, Y. G.; Lee, S. Y. Superlattice crystals-mimic, flexible/functional ceramic membranes: Beyond polymeric battery separators. *Adv. Energy Mater.* **2015**, *5*, 1500954.
[83] Suriyakumar, S.; Raja, M.; Angulakshmi, N.; Nahm, K. S.; Stephan, A. M. A flexible zirconium oxide based-ceramic membrane as a separator for lithium-ion batteries. *RSC Adv.* **2016**, *6*, 92020–92027.
[84] Raja, M.; Angulakshmi, N.; Thomas, S.; Kumar, T. P.; Stephan, A. M. Thin, flexible and thermally stable ceramic membranes as separator for lithium-ion batteries. *J. Membr. Sci.* **2014**, *471*, 103–109.
[85] Lu, Q. W.; He, Y. B.; Yu, Q. P.; Li, B. H.; Kaneti, Y. V.; Yao, Y. W.; Kang, F. Y.; Yang, Q. H. Dendrite-free, high-rate, long-life lithium metal batteries with a 3D cross-linked network polymer electrolyte. *Adv. Mater.* **2017**, *29*, 1604460.
[86] Cheng, X. B.; Zhang, R.; Zhao, C. Z.; Zhang, Q. Toward safe lithium metal anode in rechargeable batteries: A review. *Chem. Rev.* **2017**, *117*, 10403–10473.
[87] Zhao, N. N.; Wu, F.; Xing, Y.; Qu, W. J.; Chen, N.; Shang, Y. X.; Yan, M. X.; Li, Y. J.; Li, L.; Chen, R. J. Flexible hydrogel electrolyte with superior mechanical properties based on poly(vinyl alcohol) and bacterial cellulose for the solid-state zinc-air batteries. *ACS Appl. Mater. Interfaces* **2019**, *11*, 15537–15542.
[88] Zhang, Q. Q.; Liu, K.; Ding, F.; Liu, X. J. Recent advances in solid polymer electrolytes for lithium batteries. *Nano Res.* **2017**, *10*, 4139–4174.
[89] Shen, W.; Li, K.; Lv, Y. Y.; Xu, T.; Wei, D.; Liu, Z. F. Highly-safe and ultra-stable all-flexible gel polymer lithium ion batteries aiming for scalable applications. *Adv. Energy Mater.* **2020**, *10*, 1904281.
[90] Li, S. Q.; Zhang, D.; Meng, X. Y.; Huang, Q. A.; Sun, C. W.; Wang, Z. L. A flexible lithium-ion battery with quasi-solid gel electrolyte for storing pulsed energy generated by triboelectric nanogenerator. *Energy Storage Mater.* **2018**, *12*, 17–22.
[91] Fan, W.; Li, N. W.; Zhang, X. L.; Zhao, S. Y.; Cao, R.; Yin, Y. Y.; Xing, Y.; Wang, J. N.; Guo, Y. G.; Li, C. J. A dual-salt gel polymer electrolyte with 3D cross-linked polymer network for dendrite-free lithium metal batteries. *Adv. Sci.* **2018**, *5*, 1800559.
[92] Balo, L.; Shalu; Gupta, H.; Singh, V. K.; Singh, R. K. Flexible gel polymer electrolyte based on ionic liquid EMIMTFSI for rechargeable battery application. *Electrochim. Acta* **2017**, *230*, 123–131.
[93] Tan, M. J.; Li, B.; Chee, P.; Ge, X. M.; Liu, Z. L.; Zong, Y.; Loh, X. J. Acrylamide-derived freestanding polymer gel electrolyte for flexible metal-air batteries. *J. Power Sources* **2018**, *400*, 566–571.
[94] Nakayama, M.; Wada, S.; Kuroki, S.; Nogami, M. Factors affecting cyclic durability of all-solid-state lithiumpolymer batteries using poly (ethylene oxide)-based solid polymer electrolytes. *Energy Environ. Sci.* **2010**, *3*, 1995–2002.
[95] Tang, C. Y.; Hackenberg, K.; Fu, Q.; Ajayan, P. M.; Ardebili, H. High ion conducting polymer nanocomposite electrolytes using hybrid nanofillers. *Nano Lett.* **2012**, *12*, 1152–1156.
[96] Wang, M.; Xu, N. N.; Fu, J.; Liu, Y. Y.; Qiao, J. L. High-

performance binary cross-linked alkaline anion polymer electrolyte membranes for all-solid-state supercapacitors and flexible rechargeable zinc-air batteries. *J. Mater. Chem. A* **2019**, *7*, 11257–11264.

[97] Cao, J.; Wang, L.; He, X. M.; Fang, M.; Gao, J.; Li, J. J.; Deng, L. F.; Chen, H.; Tian, G. Y.; Wang, J. L. et al. *In situ* prepared nano-crystalline TiO_2–poly(methyl methacrylate) hybrid enhanced composite polymer electrolyte for Li-ion batteries. *J. Mater. Chem. A* **2013**, *1*, 5955–5961.

[98] Cao, J.; Wang, L.; Shang, Y. M.; Fang, M.; Deng, L. F.; Gao, J.; Li, J. J.; Chen, H.; He, X. M. Dispersibility of nano-TiO_2 on performance of composite polymer electrolytes for Li-ion batteries. *Electrochim. Acta* **2013**, *111*, 674–679.

[99] Lee, Y. S.; Ju, S. H.; Kim, J. H.; Hwang, S. S.; Choi, J. M.; Sun, Y. K.; Kim, H.; Scrosati, B.; Kim, D. W. Composite gel polymer electrolytes containing core-shell structured $SiO_2(Li^+)$ particles for lithium-ion polymer batteries. *Electrochem. Commun.* **2012**, *17*, 18–21.

[100] Ju, S. H.; Lee, Y. S.; Sun, Y. K.; Kim, D. W. Unique core–shell structured $SiO_2(Li^+)$ nanoparticles for high-performance composite polymer electrolytes. *J. Mater. Chem. A* **2013**, *1*, 395–401.

[101] Kil, E. H.; Choi, K. H.; Ha, H. J.; Xu, S.; Rogers, J. A.; Kim, M. R.; Lee, Y. G.; Kim, K. M.; Cho, K. Y.; Lee, S. Y. Imprintable, bendable, and shape-conformable polymer electrolytes for versatile-shaped lithium-ion batteries. *Adv. Mater.* **2013**, *25*, 1395–1400.

[102] Kim, J. K.; Lim, Y. J.; Kim, H.; Cho, G. B.; Kim, Y. A hybrid solid electrolyte for flexible solid-state sodium batteries. *Energy Environ. Sci.* **2015**, *8*, 3589–3596.

[103] Wang, T. R.; Zhang, R. Q.; Wu, Y. M.; Zhu, G. N.; Hu, C. C.; Wen, J. Y.; Luo, W. Engineering a flexible and mechanically strong composite electrolyte for solid-state lithium batteries. *J. Energy Chem.* **2020**, *46*, 187–190.

[104] Pan, K. C.; Zhang, L.; Qian, W. W.; Wu, X. K.; Dong, K.; Zhang, H. T.; Zhang, S. J. A flexible ceramic/polymer hybrid solid electrolyte for solid-state lithium metal batteries. *Adv. Mater.* **2020**, *32*, 2000399.

[105] Jiang, T. L.; He, P. G.; Wang, G. X.; Shen, Y.; Nan, C. W.; Fan, L. Z. Solvent-free synthesis of thin, flexible, nonflammable garnet-based composite solid electrolyte for all-solid-state lithium batteries. *Adv. Energy Mater.* **2020**, *10*, 1903376.

[106] Yang, L. Y.; Wang, Z. J.; Feng, Y. C.; Tan, R.; Zuo, Y. X.; Gao, R. T.; Zhao, Y.; Han, L.; Wang, Z. Q.; Pan, F. Flexible composite solid electrolyte facilitating highly stable "soft contacting" Li-electrolyte interface for solid state lithium-ion batteries. *Adv. Energy Mater.* **2017**, *7*, 1701437.

[107] Zhai, H. W.; Xu, P. Y.; Ning, M. Q.; Cheng, Q.; Mandal, J.; Yang, Y. A flexible solid composite electrolyte with vertically aligned and connected ion-conducting nanoparticles for lithium batteries. *Nano Lett.* **2017**, *17*, 3182–3187.

[108] He, Z. J.; Chen, L.; Zhang, B. C.; Liu, Y. C.; Fan, L. Z. Flexible poly(ethylene carbonate)/garnet composite solid electrolyte reinforced by poly(vinylidene fluoride-hexafluoropropylene) for lithium metal batteries. *J. Power Sources* **2018**, *392*, 232–238.

[109] Zhao, C. Z.; Zhang, X. Q.; Cheng, X. B.; Zhang, R.; Xu, R.; Chen, P. Y.; Peng, H. J.; Huang, J. Q.; Zhang, Q. An anion-immobilized composite electrolyte for dendrite-free lithium metal anodes. *Proc. Natl. Acad. Sci. USA* **2017**, *114*, 11069–11074.

[110] Gaikwad, A. M.; Whiting, G. L.; Steingart, D. A.; Arias, A. C. Highly flexible, printed alkaline batteries based on mesh-embedded electrodes. *Adv. Mater.* **2011**, *23*, 3251–3255.

[111] Saunier, J.; Alloin, F.; Sanchez, J. Y.; Caillon, G. Thin and flexible lithium-ion batteries: Investigation of polymer electrolytes. *J. Power Sources* **2003**, 119–121,454-459.

[112] Wang, J. Z.; Too, C. O.; Wallace, G. G. A highly flexible polymer fibre battery. *J. Power Sources* **2005**, *150*, 223–228.

[113] Abouimrane, A.; Abu-Lebdeh, Y.; Alarco, P. J.; Armand, M. Plastic crystal-lithium batteries: An effective ambient temperature all-solid-state power source. *J. Electrochem. Soc.* **2004**, *151*, A1028–A1031.

[114] Berg, E. J.; Villevieille, C.; Streich, D.; Trabesinger, S.; Novák, P. Rechargeable batteries: Grasping for the limits of chemistry. *J. Electrochem. Soc.* **2015**, *162*, A2468–A2475.

[115] Zhao, C. L.; Lu, Y. X.; Li, Y. M.; Jiang, L. W.; Rong, X. H.; Hu, Y. S.; Li, H.; Chen, L. Q. Novel methods for sodium-ion battery materials. *Small Methods* **2017**, *1*, 1600063.

[116] Wang, Q. D.; Zhao, C. L.; Lu, Y. X.; Li, Y. M.; Zheng, Y. H.; Qi, Y. R.; Rong, X. H.; Jiang, L. W.; Qi, X. G.; Shao, Y. J. et al. Advanced nanostructured anode materials for sodium-ion batteries. *Small* **2017**, *13*, 1701835.

[117] Fang, Y. J.; Liu, Q.; Xiao, L. F.; Rong, Y. C.; Liu, Y. D.; Chen, Z. X.; Ai, X. P.; Cao, Y. L.; Yang, H. X.; Xie, J. et al. A fully sodiated $NaVOPO_4$ with layered structure for high-voltage and long-lifespan sodium-ion batteries. *Chem* **2018**, *4*, 1167–1180.

[118] Zu, C. X.; Li, H. Thermodynamic analysis on energy densities of batteries. *Energy Environ. Sci.* **2011**, *4*, 2614–2624.

[119] Xu, Y. S.; Duan, S. Y.; Sun, Y. G.; Bin, D. S.; Tao, X. S.; Zhang, D.; Liu, Y.; Cao, A. M.; Wan, L. J. Recent developments in electrode materials for potassium-ion batteries. *J. Mater. Chem. A* **2019**, *7*, 4334–4352.

[120] Hwang, J. Y.; Myung, S. T.; Sun, Y. K. Recent progress in rechargeable potassium batteries. *Adv. Funct. Mater.* **2018**, *28*, 1802938.

[121] Kasavajjula, U.; Wang, C. S.; Appleby, A. J. Nano- and bulk-silicon-based insertion anodes for lithium-ion secondary cells. *J. Power Sources* **2007**, *163*, 1003–1039.

[122] Placke, T.; Kloepsch, R.; Dühnen, S.; Winter, M. Lithium ion, lithium metal, and alternative rechargeable battery technologies: The odyssey for high energy density. *J. Solid State Electrochem.* **2017**, *21*, 1939–1964.

[123] Goodenough, J. B. Energy storage materials: A perspective. *Energy Storage Mater.* **2015**, *1*, 158–161.

[124] Liu, Y. T.; Zhu, X. D.; Duan, Z. Q.; Xie, X. M. Flexible and robust MoS_2-graphene hybrid paper cross-linked by a polymer ligand: A high-performance anode material for thin film lithium-ion batteries. *Chem. Commun.* **2013**, *49*, 10305–10307.

[125] Bao, J. J.; Zou, B. K.; Cheng, Q.; Huang, Y. P.; Wu, F.; Xu, G. W.; Chen, C. H. Flexible and free-standing $LiFePO_4$/TPU/SP cathode membrane prepared via phase separation process for lithium ion batteries. *J. Membr. Sci.* **2017**, *541*, 633–640.

[126] Zhao, Q. S.; Liu, J. L.; Li, X. X.; Xia, Z. Z.; Zhang, Q. X.; Zhou, M.; Tian, W.; Wang, M.; Hu, H.; Li, Z. T. et al. Graphene oxide-induced synthesis of button-shaped amorphous Fe_2O_3/rGO/CNFs films as flexible anode for high-performance lithium-ion batteries. *Chem. Eng. J.* **2019**, *369*, 215–222.

[127] Ren, J.; Ren, R. P.; Lv, Y. K. A flexible 3D graphene@CNT@MoS_2 hybrid foam anode for high-performance lithium-ion battery. *Chem. Eng. J.* **2018**, *353*, 419–424.

[128] Zhao, F. Y.; Zhao, X.; Peng, B.; Gan, F.; Yao, M. Y.; Tan, W. J.; Dong, J.; Zhang, Q. H. Polyimide-derived carbon nanofiber membranes as anodes for high-performance flexible lithium ion batteries. *Chin. Chem. Lett.* **2018**, *29*, 1692–1697.

[129] Huang, X. Y.; Cai, X.; Xu, D. H.; Chen, W. Y.; Wang, S. J.; Zhou, W. Y.; Meng, Y. Z.; Fang, Y. P.; Yu, X. Y. Hierarchical Fe_2O_3@CNF fabric decorated with MoS_2 nanosheets as a robust anode for flexible lithium-ion batteries exhibiting ultrahigh areal capacity. *J. Mater. Chem. A* **2018**, *6*, 16890–16899.

[130] Min, X.; Sun, B.; Chen, S.; Fang, M. H.; Wu, X. W.; Liu, Y. G.; Abdelkader, A.; Huang, Z. H.; Liu, T.; Xi, K. et al. A textile-based SnO_2 ultra-flexible electrode for lithium-ion batteries. *Energy Storage Mater.* **2019**, *16*, 597–606.

[131] Zheng, S. H.; Wu, Z. S.; Zhou, F.; Wang, X.; Ma, J. M.; Liu, C.; He, Y. B.; Bao, X. H. All-solid-state planar integrated lithium ion micro-batteries with extraordinary flexibility and high-temperature performance. *Nano Energy* **2018**, *51*, 613–620.

[132] Nayak, P. K.; Yang, L. T.; Brehm, W.; Adelhelm, P. From lithium-ion to sodium-ion batteries: Advantages, challenges, and surprises. *Angew. Chem., Int. Ed.* **2018**, *57*, 102–120.

[133] Li, Z.; Ding, J.; Mitlin, D. Tin and tin compounds for sodium ion battery anodes: Phase transformations and performance. *Acc. Chem. Res.* **2015**, *48*, 1657–1665.

[134] Wang, H. G.; Li, W.; Liu, D. P.; Feng, X. L.; Wang, J.; Yang, X. Y.; Zhang, X. B.; Zhu, Y. J.; Zhang, Y. Flexible electrodes for

sodium-ion batteries: Recent progress and perspectives. *Adv. Mater.* **2017**, *29*, 1703012.

[135] Bian, H. D.; Xiao, X. F.; Zeng, S. S.; Yuen, M. F.; Li, Z. B.; Kang, W. P.; Yu, D. Y. W.; Xu, Z. T.; Lu, J.; Li, Y. Y. Mesoporous C-coated SnO_x nanosheets on copper foil as flexible and binder-free anodes for superior sodium-ion batteries. *J. Mater. Chem. A* **2017**, *5*, 2243–2250.

[136] Fan, M. P.; Chen, Y.; Xie, Y. H.; Yang, T. Z.; Shen, X. W.; Xu, N.; Yu, H. Y.; Yan, C. L. Half-cell and full-cell applications of highly stable and binder-free sodium ion batteries based on Cu_3P nanowire anodes. *Adv. Funct. Mater.* **2016**, *26*, 5019–5027.

[137] Fu, S. D.; Ni, J. F.; Xu, Y.; Zhang, Q.; Li, L. Hydrogenation driven conductive $Na_2Ti_3O_7$ nanoarrays as robust binder-free anodes for sodium-ion batteries. *Nano Lett.* **2016**, *16*, 4544–4551.

[138] Yang, T. Z.; Qian, T.; Wang, M. F.; Shen, X. W.; Xu, N.; Sun, Z. Z.; Yan, C. L. A sustainable route from biomass byproduct okara to high content nitrogen-doped carbon sheets for efficient sodium ion batteries. *Adv. Mater.* **2016**, *28*, 539–545.

[139] Li, H. S.; Ding, Y.; Ha, H.; Shi, Y.; Peng, L. L.; Zhang, X. G.; Ellison, C. J.; Yu, G. H. An all-stretchable-component sodium-ion full battery. *Adv. Mater.* **2017**, *29*, 1700898.

[140] Guo, J. Z.; Gu, Z. Y.; Zhao, X. X.; Wang, M. Y.; Yang, X.; Yang, Y.; Li, W. H.; Wu, X. L. Flexible Na/K-ion full batteries from the renewable cotton cloth-derived stable, low-cost, and binder-free anode and cathode. *Adv. Energy Mater.* **2019**, *9*, 1902056.

[141] Zhou, C. S.; Fan, S. X.; Hu, M. X.; Lu, J. M.; Li, J.; Huang, Z. H.; Kang, F. Y.; Lv, R. T. High areal specific capacity of $Ni_3V_2O_8$/carbon cloth hierarchical structures as flexible anodes for sodium-ion batteries. *J. Mater. Chem. A* **2017**, *5*, 15517–15524.

[142] Ren, W. N.; Zhang, H. F.; Guan, C.; Cheng, C. W. Ultrathin MoS_2 nanosheets@metal organic framework-derived N-doped carbon nanowall arrays as sodium ion battery anode with superior cycling life and rate capability. *Adv. Funct. Mater.* **2017**, *27*, 1702116.

[143] Sun, N.; Guan, Y. B.; Liu, Y. T.; Zhu, Q. Z.; Shen, J. R.; Liu, H.; Zhou, S. Q.; Xu, B. Facile synthesis of free-standing, flexible hard carbon anode for high-performance sodium ion batteries using graphene as a multi-functional binder. *Carbon* **2018**, *137*, 475–483.

[144] Kretschmer, K.; Sun, B.; Zhang, J. Q.; Xie, X. Q.; Liu, H.; Wang, G. X. 3D interconnected carbon fiber network-enabled ultralong life $Na_3V_2(PO_4)_3$@carbon paper cathode for sodium-ion batteries. *Small* **2017**, *13*, 1603318.

[145] Ma, X. X.; Chen, L.; Ren, X. H.; Hou, G. M.; Chen, L. N.; Zhang, L.; Liu, B. B.; Ai, Q.; Zhang, L.; Si, P. C. et al. High-performance red phosphorus/carbon nanofibers/graphene free-standing paper anode for sodium ion batteries. *J. Mater. Chem. A* **2018**, *6*, 1574–1581.

[146] Huang, Y.; Fang, C.; Zeng, R.; Liu, Y. J.; Zhang, W.; Wang, Y. J.; Liu, Q. J.; Huang, Y. H. *In situ*-formed hierarchical metal-organic flexible cathode for high-energy sodium-ion batteries. *ChemSusChem* **2017**, *10*, 4704–4708.

[147] Ren, X. L.; Turcheniuk, K.; Lewis, D.; Fu, W. B.; Magasinski, A.; Schauer, M. W.; Yushin, G. Iron phosphate coated flexible carbon nanotube fabric as a multifunctional cathode for Na-ion batteries. *Small* **2018**, *14*, 1703425.

[148] Chen, Q.; Sun, S.; Zhai, T.; Yang, M.; Zhao, X. Y.; Xia, H. Yolk-shell NiS_2 nanoparticle-embedded carbon fibers for flexible fiber-shaped sodium battery. *Adv. Energy Mater.* **2018**, *8*, 1800054.

[149] Yin, H.; Cao, M. L.; Yu, X. X.; Zhao, H.; Shen, Y.; Li, C.; Zhu, M. Q. Self-standing Bi_2O_3 nanoparticles/carbon nanofiber hybrid films as a binder-free anode for flexible sodium-ion batteries. *Mater. Chem. Front.* **2017**, *1*, 1615–1621.

[150] Wang, X. W.; Guo, H. P.; Liang, J.; Zhang, J. F.; Zhang, B.; Wang, J. Z.; Luo, W. B.; Liu, H. K.; Dou, S. X. An integrated free-standing flexible electrode with holey-structured 2D bimetallic phosphide nanosheets for sodium-ion batteries. *Adv. Funct. Mater.* **2018**, *28*, 1801016.

[151] Wang, Y. W.; Xiao, N.; Wang, Z. Y.; Tang, Y. C.; Li, H. Q.; Yu, M. L.; Liu, C.; Zhou, Y.; Qiu, J. S. Ultrastable and high-capacity carbon nanofiber anodes derived from pitch/polyacrylonitrile for flexible sodium-ion batteries. *Carbon* **2018**, *135*, 187–194.

[152] Choe, J. H.; Kim, N. R.; Lee, M. E.; Yoon, H. J.; Song, M. Y.; Jin, H. J.; Yun, Y. S. Flexible graphene stacks for sodium-ion storage. *ChemElectroChem* **2017**, *4*, 716–720.

[153] Deng, X.; Xie, K. Y.; Li, L.; Zhou, W.; Sunarso, J.; Shao, Z. P. Scalable synthesis of self-standing sulfur-doped flexible graphene films as recyclable anode materials for low-cost sodium-ion batteries. *Carbon* **2016**, *107*, 67–73.

[154] An, H. R.; Li, Y.; Gao, Y.; Cao, C.; Han, J. K.; Feng, Y. Y.; Feng, W. Free-standing fluorine and nitrogen co-doped graphene paper as a high-performance electrode for flexible sodium-ion batteries. *Carbon* **2017**, *116*, 338–346.

[155] Wang, S. Q.; Xia, L.; Yu, L.; Zhang, L.; Wang, H. H.; Lou, X. W. Free-standing nitrogen-doped carbon nanofiber films: Integrated electrodes for sodium-ion batteries with ultralong cycle life and superior rate capability. *Adv. Energy Mater.* **2016**, *6*, 1502217.

[156] Ni, Q.; Bai, Y.; Li, Y.; Ling, L. M.; Li, L. M.; Chen, G. H.; Wang, Z. H.; Ren, H. X.; Wu, F.; Wu, C. 3D electronic channels wrapped large-sized $Na_3V_2(PO_4)_3$ as flexible electrode for sodium-ion batteries. *Small* **2018**, *14*, 1702864.

[157] Harry, K. J.; Hallinan, D. T.; Parkinson, D. Y.; MacDowell, A. A.; Balsara, N. P. Detection of subsurface structures underneath dendrites formed on cycled lithium metal electrodes. *Nat. Mater.* **2014**, *13*, 69–73.

[158] Xu, W.; Wang, J. L.; Ding, F.; Chen, X. L.; Nasybulin, E.; Zhang, Y. H.; Zhang, J. G. Lithium metal anodes for rechargeable batteries. *Energy Environ. Sci.* **2014**, *7*, 513–537.

[159] Xu, S. M.; Duan, H.; Shi, J. L.; Zuo, T. T.; Hu, X. C.; Lang, S. Y.; Yan, M.; Liang, J. Y.; Yang, Y. G.; Kong, Q. H. et al. *In situ* fluorinated solid electrolyte interphase towards long-life lithium metal anodes. *Nano Res.* **2020**, *13*, 430–436.

[160] Zhang, X. L.; Zhao, S. Y.; Fan, W.; Wang, J. N.; Li, C. J. Long cycling, thermal stable, dendrites free gel polymer electrolyte for flexible lithium metal batteries. *Electrochim. Acta* **2019**, *301*, 304–311.

[161] Li, D.; Chen, L.; Wang, T. S.; Fan, L. Z. 3D fiber-network-reinforced bicontinuous composite solid electrolyte for dendrite-free lithium metal batteries. *ACS Appl. Mater. Interfaces* **2018**, *10*, 7069–7078.

[162] Zhou, B. H.; Zuo, C.; Xiao, Z. L.; Zhou, X. P.; He, D.; Xie, X. L.; Xue, Z. G. Self-healing polymer electrolytes formed via dual-networks: A new strategy for flexible lithium metal batteries. *Chem.—Eur. J.* **2018**, *24*, 19200–19207.

[163] Zhu, Y. H.; Cao, J.; Chen, H.; Yu, Q. P.; Li, B. H. High electrochemical stability of a 3D cross-linked network PEO@nano-SiO_2 composite polymer electrolyte for lithium metal batteries. *J. Mater. Chem. A* **2019**, *7*, 6832–6839.

[164] Zhao, Y.; Zhang, Y.; Sun, H.; Dong, X. L.; Cao, J. Y.; Wang, L.; Xu, Y. F.; Ren, J.; Hwang, Y.; Son, I. H. et al. A self-healing aqueous lithium-ion battery. *Angew. Chem., Int. Ed.* **2016**, *55*, 14384–14388.

[165] Nam, Y. J.; Cho, S. J.; Oh, D. Y.; Lim, J. M.; Kim, S. Y.; Song, J. H.; Lee, Y. G.; Lee, S. Y.; Jung, Y. S. Bendable and thin sulfide solid electrolyte film: A new electrolyte opportunity for free-standing and stackable high-energy all-solid-state lithium-ion batteries. *Nano Lett.* **2015**, *15*, 3317–3323.

[166] Li, C. M.; Zhang, H.; Otaegui, L.; Singh, G.; Armand, M.; Rodriguez-Martinez, L. M. Estimation of energy density of Li-S batteries with liquid and solid electrolytes. *J. Power Sources* **2016**, *326*, 1–5.

[167] Zheng, D.; Zhang, X. R.; Wang, J. K.; Qu, D. Y.; Yang, X. Q.; Qu, D. Y. Reduction mechanism of sulfur in lithium-sulfur battery: From elemental sulfur to polysulfide. *J. Power Sources* **2016**, *301*, 312–316.

[168] Helen, M.; Reddy, M. A.; Diemant, T.; Golla-Schindler, U.; Behm, R. J.; Kaiser, U.; Fichtner, M. Single step transformation of sulphur to Li_2S_2/Li_2S in Li-S batteries. *Sci. Rep.* **2015**, *5*, 12146.

[169] Choi, S.; Yoon, I.; Nichols, W. T.; Shin, D. Carbon-coated Li_2S cathode for improving the electrochemical properties of an all-solid-state lithium-sulfur battery using Li_2S-P_2S_5 solid electrolyte. *Ceram. Int.* **2018**, *44*, 7450–7453.

[170] Jamesh, M. I. Recent advances on flexible electrodes for Na-ion batteries and Li-S batteries. *J. Energy Chem.* **2019**, *32*, 15–44.
[171] Liu, R. Q.; Liu, Y. J.; Chen, J.; Kang, Q.; Wang, L. L.; Zhou, W. X.; Huang, Z. D.; Lin, X. J.; Li, Y.; Li, P. et al. Flexible wire-shaped lithium-sulfur batteries with fibrous cathodes assembled via capillary action. *Nano Energy* **2017**, *33*, 325–333.
[172] Wahyudi, W.; Cao, Z.; Kumar, P.; Li, M. L.; Wu, Y. Q.; Hedhili, M. N.; Anthopoulos, T. D.; Cavallo, L.; Li, L. J.; Ming, J. Phase inversion strategy to flexible freestanding electrode: Critical coupling of binders and electrolytes for high performance Li-S battery. *Adv. Funct. Mater.* **2018**, *28*, 1802244.
[173] Wei, H.; Ma, J.; Li, B.; Zuo, Y. X.; Xia, D. G. Enhanced cycle performance of lithium-sulfur batteries using a separator modified with a PVDF-C layer. *ACS Appl. Mater. Interfaces* **2014**, *6*, 20276–20281.
[174] Ming, J.; Li, M. L.; Kumar, P.; Lu, A. Y.; Wahyudi, W.; Li, L. J. Redox species-based electrolytes for advanced rechargeable lithium ion batteries. *ACS Energy Lett.* **2016**, *1*, 529–534.
[175] Agostini, M.; Scrosati, B.; Hassoun, J. An advanced lithium-ion sulfur battery for high energy storage. *Adv. Energy Mater.* **2015**, *5*, 1500481.
[176] Xiao, P. T.; Bu, F. X.; Yang, G. H.; Zhang, Y.; Xu, Y. X. Integration of graphene, Nano sulfur, and conducting polymer into compact, flexible lithium-sulfur battery cathodes with ultrahigh volumetric capacity and superior cycling stability for foldable devices. *Adv. Mater.* **2017**, *29*, 1703324.
[177] Chong, W. G.; Huang, J. Q.; Xu, Z. L.; Qin, X. Y.; Wang, X. Y.; Kim, J. K. Lithium-sulfur battery cable made from ultralight, flexible graphene/carbon nanotube/sulfur composite fibers. *Adv. Funct. Mater.* **2017**, *27*, 1604815.
[178] Xiang, M. W.; Wu, H.; Liu, H.; Huang, J.; Zheng, Y. F.; Yang, L.; Jing, P.; Zhang, Y.; Dou, S. X.; Liu, H. K. A flexible 3D multifunctional MgO-decorated carbon foam@CNTs hybrid as self-supported cathode for high-performance lithium-sulfur batteries. *Adv. Funct. Mater.* **2017**, *27*, 1702573.
[179] Zhou, G. M.; Li, L.; Wang, D. W.; Shan, X. Y.; Pei, S. F.; Li, F.; Cheng, H. M. A flexible sulfur-graphene-polypropylene separator integrated electrode for advanced Li-S batteries. *Adv. Mater.* **2015**, *27*, 641–647.
[180] Yuan, Z.; Peng, H. J.; Hou, T. Z.; Huang, J. Q.; Chen, C. M.; Wang, D. W.; Cheng, X. B.; Wei, F.; Zhang, Q. Powering lithium-sulfur battery performance by propelling polysulfide redox at sulfiphilic hosts. *Nano Lett.* **2016**, *16*, 519–527.
[181] Tao, Y. Q.; Wei, Y. J.; Liu, Y.; Wang, J. T.; Qiao, W. M.; Ling, L. C.; Long, D. H. Kinetically-enhanced polysulfide redox reactions by Nb_2O_5 nanocrystals for high-rate lithium–sulfur battery. *Energy Environ. Sci.* **2016**, *9*, 3230–3239.
[182] Sun, Z. H.; Zhang, J. Q.; Yin, L. C.; Hu, G. J.; Fang, R. P.; Cheng, H. M.; Li, F. Conductive porous vanadium nitride/graphene composite as chemical anchor of polysulfides for lithium-sulfur batteries. *Nat. Commun.* **2017**, *8*, 14627.
[183] Sun, Q.; Fang, X.; Weng, W.; Deng, J.; Chen, P. N.; Ren, J.; Guan, G. Z.; Wang, M.; Peng, H. S. An aligned and laminated nanostructured carbon hybrid cathode for high-performance lithium-sulfur batteries. *Angew. Chem., Int. Ed.* **2015**, *54*, 10539–10544.
[184] Zhou, G. M.; Pei, S. F.; Li, L.; Wang, D. W.; Wang, S. G.; Huang, K.; Yin, L. C.; Li, F.; Cheng, H. M. A graphene-pure-sulfur sandwich structure for ultrafast, long-life lithium-sulfur batteries. *Adv. Mater.* **2014**, *26*, 625–631.
[185] Wang, H. L.; Yang, Y.; Liang, Y. Y.; Robinson, J. T.; Li, Y. G.; Jackson, A.; Cui, Y.; Dai, H. J. Graphene-wrapped sulfur particles as a rechargeable lithium-sulfur battery cathode material with high capacity and cycling stability. *Nano Lett.* **2011**, *11*, 2644–2647.
[186] Fang, R. P.; Zhao, S. Y.; Sun, Z. H.; Wang, D. W.; Cheng, H. M.; Li, F. More reliable lithium-sulfur batteries: Status, solutions and prospects. *Adv. Mater.* **2017**, *29*, 1606823.
[187] Wu, C.; Fu, L. J.; Maier, J.; Yu, Y. Free-standing graphene-based porous carbon films with three-dimensional hierarchical architecture for advanced flexible Li–sulfur batteries. *J. Mater. Chem. A* **2015**, *3*, 9438–9445.
[188] Cheng, F. Y.; Chen, J. Metal-air batteries: From oxygenreduction electrochemistry to cathode catalysts. *Chem. Soc. Rev.* **2012**, *41*, 2172–2192.
[189] Xiang, F. W.; Chen, X. H.; Yu, J.; Ma, W. H.; Li, Y. P.; Yang, N. Synthesis of three-dimensionally ordered porous perovskite type $LaMnO_3$ for Al-air battery. *J. Mater. Sci. Technol.* **2018**, *34*, 1532–1537.
[190] Tan, P.; Chen, B.; Xu, H. R.; Zhang, H. C.; Cai, W. Z.; Ni, M.; Liu, M. L.; Shao, Z. P. Flexible Zn-and Li-air batteries: Recent advances, challenges, and future perspectives. *Energy Environ. Sci.* **2017**, *10*, 2056–2080.
[191] Jiang, Y.; Deng, Y. P.; Liang, R. L.; Fu, J.; Luo, D.; Liu, G. H.; Li, J. D.; Zhang, Z.; Hu, Y. F.; Chen, Z. W. Multidimensional ordered bifunctional air electrode enables flash reactants shuttling for high-energy flexible Zn-air batteries. *Adv. Energy Mater.* **2019**, *9*, 1900911.
[192] Yoon, K. R.; Shin, K.; Park, J.; Cho, S. H.; Kim, C.; Jung, J. W.; Cheong, J. Y.; Byon, H. R.; Lee, H. M.; Kim, I. D. Brush-like cobalt nitride anchored carbon nanofiber membrane: Current collector-catalyst integrated cathode for long cycle Li-O_2 batteries. *ACS Nano* **2018**, *12*, 128–139.
[193] Ji, D. X.; Peng, S. J.; Safanama, D.; Yu, H. N.; Li, L. L.; Yang, G. R.; Qin, X. H.; Srinivasan, M.; Adams, S.; Ramakrishna, S. Design of 3-dimensional hierarchical architectures of carbon and highly active transition metals (Fe, Co, Ni) as bifunctional oxygen catalysts for hybrid lithium-air batteries. *Chem. Mater.* **2017**, *29*, 1665–1675.
[194] Xue, H. R.; Wu, S. C.; Tang, J.; Gong, H.; He, P.; He, J. P.; Zhou, H. S. Hierarchical porous nickel cobaltate nanoneedle arrays as flexible carbon-protected cathodes for high-performance lithium-oxygen batteries. *ACS Appl. Mater. Interfaces* **2016**, *8*, 8427–8435.
[195] Gong, K. P.; Du, F.; Xia, Z. H.; Durstock, M.; Dai, L. M. Nitrogen-doped carbon nanotube arrays with high electrocatalytic activity for oxygen reduction. *Science* **2009**, *323*, 760–764.
[196] Geng, D. S.; Ding, N.; Hor, T. S. A.; Liu, Z. L.; Sun, X. L.; Zong, Y. Potential of metal-free "graphene alloy" as electrocatalysts for oxygen reduction reaction. *J. Mater. Chem. A* **2015**, *3*, 1795–1810.
[197] Dai, L. M.; Xue, Y. H.; Qu, L. T.; Choi, H. J.; Baek, J. B. Metal-free catalysts for oxygen reduction reaction. *Chem. Rev.* **2015**, *115*, 4823–4892.
[198] Cao, X. H.; Zheng, B.; Rui, X. H.; Shi, W. H.; Yan, Q. Y.; Zhang, H. Metal oxide-coated three-dimensional graphene prepared by the use of metal-organic frameworks as precursors. *Angew. Chem., Int. Ed.* **2014**, *53*, 1404–1409.
[199] Hu, Y. X.; Wei, J.; Liang, Y.; Zhang, H. C.; Zhang, X. W.; Shen, W.; Wang, H. T. Zeolitic imidazolate framework/graphene oxide hybrid nanosheets as seeds for the growth of ultrathin molecular sieving membranes. *Angew. Chem., Int. Ed.* **2016**, *55*, 2048–2052.
[200] Jiang, Y. X.; Cheng, J. F.; Zou, L.; Li, X. Y.; Huang, Y. Z.; Jia, L. C.; Chi, B.; Pu, J.; Li, J. Graphene foam decorated with ceria microspheres as a flexible cathode for foldable lithium-air batteries. *ChemCatChem* **2017**, *9*, 4231–4237.
[201] Marcano, D. C.; Kosynkin, D. V.; Berlin, J. M.; Sinitskii, A.; Sun, Z. Z.; Slesarev, A.; Alemany, L. B.; Lu, W.; Tour, J. M. Improved synthesis of graphene oxide. *ACS Nano* **2010**, *4*, 4806–4814.
[202] Liu, Q.; Wang, Y. B.; Dai, L. M.; Yao, J. N. Scalable fabrication of nanoporous carbon fiber films as bifunctional catalytic electrodes for flexible Zn-air batteries. *Adv. Mater.* **2016**, *28*, 3000–3006.
[203] Kordek, K.; Jiang, L. X.; Fan, K. C.; Zhu, Z. J.; Xu, L.; Al-Mamun, M.; Dou, Y. H.; Chen, S.; Liu, P. R.; Yin, H. J. et al. Two-step activated carbon cloth with oxygen-rich functional groups as a high-performance additive-free air electrode for flexible zinc-air batteries. *Adv. Energy Mater.* **2019**, *9*, 1802936.
[204] Fu, K. K.; Cheng, J.; Li, T.; Hu, L. B. Flexible batteries: From mechanics to devices. *ACS Energy Lett.* **2016**, *1*, 1065–1079.
[205] Mo, F. N.; Liang, G. J.; Huang, Z. D.; Li, H. F.; Wang, D. H.; Zhi, C. Y. An overview of fiber-shaped batteries with a focus on multifunctionality, scalability, and technical difficulties. *Adv. Mater.* **2020**, *32*, 1902151.
[206] Zhou, Y.; Wang, C. H.; Lu, W.; Dai, L. M. Recent advances in fiber-shaped supercapacitors and lithium-ion batteries. *Adv. Mater.* **2020**, *32*, 1902779.

[207] Weng, W.; Sun, Q.; Zhang, Y.; Lin, H. J.; Ren, J.; Lu, X.; Wang, M.; Peng, H. S. Winding aligned carbon nanotube composite yarns into coaxial fiber full batteries with high performances. *Nano Lett.* **2014**, *14*, 3432–3438.
[208] Zhu, Y. H.; Yuan, S.; Bao, D.; Yin, Y. B.; Zhong, H. X.; Zhang, X. B.; Yan, J. M.; Jiang, Q. Decorating waste cloth via industrial wastewater for tube-type flexible and wearable sodium-ion batteries. *Adv. Mater.* **2017**, *29*, 1603719.
[209] Park, J.; Park, M.; Nam, G.; Lee, J. S.; Cho, J. All-solid-state cable-type flexible zinc-air battery. *Adv. Mater.* **2015**, *27*, 1396–1401.
[210] Xu, Y. F.; Zhang, Y.; Guo, Z. Y.; Ren, J.; Wang, Y. G.; Peng, H. S. Flexible, stretchable, and rechargeable fiber-shaped zinc-air battery based on cross-stacked carbon nanotube sheets. *Angew. Chem., Int. Ed.* **2015**, *54*, 15390–15394.
[211] Lin, H. J.; Weng, W.; Ren, J.; Qiu, L. B.; Zhang, Z. T.; Chen, P. N.; Chen, X. L.; Deng, J.; Wang, Y. G.; Peng, H. S. Twisted aligned carbon nanotube/silicon composite fiber anode for flexible wire-shaped lithium-ion battery. *Adv. Mater.* **2014**, *26*, 1217–1222.
[212] Wang, K.; Zhang, X. H.; Han, J. W.; Zhang, X.; Sun, X. Z.; Li, C.; Liu, W. H.; Li, Q. W.; Ma, Y. W. High-performance cable-type flexible rechargeable Zn battery based on MnO_2@CNT fiber microelectrode. *ACS Appl. Mater. Interfaces* **2018**, *10*, 24573–24582.
[213] Song, C. H.; Li, Y. P.; Li, H.; He, T.; Guan, Q.; Yang, J.; Li, X. L.; Cheng, J. L.; Wang, B. A novel flexible fiber-shaped dual-ion battery with high energy density based on omnidirectional porous Al wire anode. *Nano Energy* **2019**, *60*, 285–293.
[214] Xiao, X.; Li, T. Q.; Yang, P. H.; Gao, Y.; Jin, H. Y.; Ni, W. J.; Zhan, W. H.; Zhang, X. H.; Cao, Y. Z.; Zhong, J. W. et al. Fiber-based all-solid-state flexible supercapacitors for self-powered systems. *ACS Nano* **2012**, *6*, 9200–9206.
[215] Yadav, A.; De, B.; Singh, S. K.; Sinha, P.; Kar, K. K. Facile development strategy of a single carbon-fiber-based all-solid-state flexible lithium-ion battery for wearable electronics. *ACS Appl. Mater. Interfaces* **2019**, *11*, 7974–7980.
[216] Guan, C.; Sumboja, A.; Zang, W. J.; Qian, Y. H.; Zhang, H.; Liu, X. M.; Liu, Z. L.; Zhao, D.; Pennycook, S. J.; Wang, J. Decorating Co/CoN_x nanoparticles in nitrogen-doped carbon nanoarrays for flexible and rechargeable zinc-air batteries. *Energy Storage Mater.* **2019**, *16*, 243–250.
[217] Liu, T.; Liu, Q. C.; Xu, J. J.; Zhang, X. B. Cable-type water-survivable flexible Li-O_2 battery. *Small* **2016**, *12*, 3101–3105.
[218] Hu, L. B.; Wu, H.; La Mantia, F.; Yang, Y.; Cui, Y. Thin, flexible secondary Li-ion paper batteries. *ACS Nano* **2010**, *4*, 5843–5848.
[219] Kammoun, M.; Berg, S.; Ardebili, H. Flexible thin-film battery based on graphene-oxide embedded in solid polymer electrolyte. *Nanoscale* **2015**, *7*, 17516–17522.
[220] Guo, Z. Y.; Li, J. L.; Xia, Y.; Chen, C.; Wang, F. M.; Tamirat, A. G.; Wang, Y. G.; Xia, Y. Y.; Wang, L.; Feng, S. H. A flexible polymer-based Li-air battery using a reduced graphene oxide/Li composite anode. *J. Mater. Chem. A* **2018**, *6*, 6022–6032.
[221] Wu, Z. C.; Chen, Z. H.; Du, X.; Logan, J. M.; Sippel, J.; Nikolou, M.; Kamaras, K.; Reynolds, J. R.; Tanner, D. B.; Hebard, A. F. et al. Transparent, conductive carbon nanotube films. *Science* **2004**, *305*, 1273–1276.
[222] Park, S. I.; Xiong, Y. J.; Kim, R. H.; Elvikis, P.; Meitl, M.; Kim, D. H.; Wu, J.; Yoon, J.; Yu, C. J.; Liu, Z. J. et al. Printed assemblies of inorganic light-emitting diodes for deformable and semitransparent displays. *Science* **2009**, *325*, 977–981.
[223] Bae, S.; Kim, H.; Lee, Y.; Xu, X. F.; Park, J. S.; Zheng, Y.; Balakrishnan, J.; Lei, T.; Kim, H. R.; Song, Y. I. et al. Roll-to-roll production of 30-inch graphene films for transparent electrodes. *Nat. Nanotechnol.* **2010**, *5*, 574–578.
[224] Yang, Y.; Jeong, S.; Hu, L. B.; Wu, H.; Lee, S. W.; Cui, Y. Transparent lithium-ion batteries. *Proc. Natl. Acad. Sci. USA* **2011**, *108*, 13013–13018.
[225] Wagner, S.; Lacour, S. P.; Jones, J.; Hsu, P. H. I.; Sturm, J. C.; Li, T.; Suo, Z. G. Electronic skin: Architecture and components. *Phys. E Low Dimens. Syst. Nanostruct.* **2004**, *25*, 326–334.
[226] Xu, S.; Zhang, Y. H.; Cho, J.; Lee, J.; Huang, X.; Jia, L.; Fan, J. A.; Su, Y.; Su, J.; Zhang, H. G. et al. Stretchable batteries with self-similar serpentine interconnects and integrated wireless recharging systems. *Nat. Commun.* **2013**, *4*, 1543.
[227] Yu, Y.; Luo, Y. F.; Wu, H. C.; Jiang, K. L.; Li, Q. Q.; Fan, S. S.; Li, J.; Wang, J. P. Ultrastretchable carbon nanotube composite electrodes for flexible lithium-ion batteries. *Nanoscale* **2018**, *10*, 19972–19978.
[228] Kim, J. S.; Ko, D.; Yoo, D. J.; Jung, D. S.; Yavuz, C. T.; Kim, N. I.; Choi, I. S.; Song, J. Y.; Choi, J. W. A half millimeter thick coplanar flexible battery with wireless recharging capability. *Nano Lett.* **2015**, *15*, 2350–2357.
[229] Li, T.; Suo, Z. G.; Lacour, S. P.; Wagner, S. Compliant thin film patterns of stiff materials as platforms for stretchable electronics. *J. Mater. Res.* **2005**, *20*, 3274–3277.
[230] Song, Z. M.; Ma, T.; Tang, R.; Cheng, Q.; Wang, X.; Krishnaraju, D.; Panat, R.; Chan, C. K.; Yu, H. Y.; Jiang, H. Q. Origami lithium-ion batteries. *Nat. Commun.* **2014**, *5*, 3140.
[231] Song, Z. M.; Wang, X.; Lv, C.; An, Y. H.; Liang, M. B.; Ma, T.; He, D.; Zheng, Y. J.; Huang, S. Q.; Yu, H. Y. et al. Kirigami-based stretchable lithium-ion batteries. *Sci. Rep.* **2015**, *5*, 10988.
[232] Gray, D. S.; Tien, J.; Chen, C. S. High-conductivity elastomeric electronics. *Adv. Mater.* **2004**, *16*, 393–397.
[233] Liu, Y.; Gorgutsa, S.; Santato, C.; Skorobogatiy, M. Flexible, solid electrolyte-based lithium battery composed of $LiFePO_4$ cathode and $Li_4Ti_5O_{12}$ anode for applications in smart textiles. *J. Electrochem. Soc.* **2012**, *159*, A349–A356.
[234] Zhang, Y.; Wang, Y. H.; Wang, L.; Lo, C. M.; Zhao, Y.; Jiao, Y. D.; Zheng, G. F.; Peng, H. S. A fiber-shaped aqueous lithium ion battery with high power density. *J. Mater. Chem. A* **2016**, *4*, 9002–9008.
[235] Fang, X.; Weng, W.; Ren, J.; Peng, H. S. A cable-shaped lithium sulfur battery. *Adv. Mater.* **2016**, *28*, 491–496.
[236] Li, Y. B.; Zhong, C.; Liu, J.; Zeng, X. Q.; Qu, S. X.; Han, X. P.; Deng, Y. D.; Hu, W. B.; Lu, J. Atomically thin mesoporous Co_3O_4 layers strongly coupled with N-rGO nanosheets as high-performance bifunctional catalysts for 1D knittable zinc-air batteries. *Adv. Mater.* **2018**, *30*, 1703657.
[237] Lee, J. M.; Choi, C.; Kim, J. H.; De Andrade, M. J.; Baughman, R. H.; Kim, S. J. Biscrolled carbon nanotube yarn structured silver-zinc battery. *Sci. Rep.* **2018**, *8*, 11150.
[238] Ren, J.; Zhang, Y.; Bai, W. Y.; Chen, X. L.; Zhang, Z. T.; Fang, X.; Weng, W.; Wang, Y. G.; Peng, H. S. Elastic and wearable wire-shaped lithium-ion battery with high electrochemical performance. *Angew. Chem., Int. Ed.* **2014**, *53*, 7864–7869.
[239] Zhang, Y.; Jiao, Y. D.; Lu, L. J.; Wang, L.; Chen, T. Q.; Peng, H. S. An ultraflexible silicon-oxygen battery fiber with high energy density. *Angew. Chem., Int. Ed.* **2017**, *56*, 13741–13746.
[240] Park, M.; Cha, H.; Lee, Y.; Hong, J.; Kim, S. Y.; Cho, J. Postpatterned electrodes for flexible node-type lithium-ion batteries. *Adv. Mater.* **2017**, *29*, 1605773.
[241] Tajima, R.; Miwa, T.; Oguni, T.; Hitotsuyanagi, A.; Miyake, H.; Katagiri, H.; Goto, Y.; Saito, Y.; Goto, J.; Kaneyasu, M. et al. Truly wearable display comprised of a flexible battery, flexible display panel, and flexible printed circuit. *J. Soc. Inf. Disp.* **2014**, *22*, 237–244.
[242] Kim, J. S.; Lee, Y. H.; Lee, I.; Kim, T. S.; Ryou, M. H.; Choi, J. W. Large area multi-stacked lithium-ion batteries for flexible and rollable applications. *J. Mater. Chem. A* **2014**, *2*, 10862–10868.